Assessing Low-Temperature Geothermal Play Types: Relevant Data and Play Fairway Analysis Methods

Estefanny Davalos-Elizondo, Amanda Kolker, Nicole Taverna, and Emily Holt

National Renewable Energy Laboratory

NREL is a national laboratory of the U.S. Department of Energy
Office of Energy Efficiency & Renewable Energy
Operated by the Alliance for Sustainable Energy, LLC

This report is available at no cost from the National Renewable Energy Laboratory (NREL) at www.nrel.gov/publications.

Contract No. DE-AC36-08GO28308

Technical Report
NREL/TP-5700-87259
September 2023

Assessing Low-Temperature Geothermal Play Types: Relevant Data and Play Fairway Analysis Methods

Estefanny Davalos-Elizondo, Amanda Kolker, Nicole Taverna, and Emily Holt

National Renewable Energy Laboratory

Suggested Citation
Davalos-Elizondo, Estefanny, Amanda Kolker, Nicole Taverna, and Emily Holt. 2023. *Assessing Low-Temperature Geothermal Play Types: Relevant Data and Play Fairway Analysis Methods*. Golden, CO: National Renewable Energy Laboratory. NREL/TP-5700-87259. https://www.nrel.gov/docs/fy23osti/87259.pdf.

NREL is a national laboratory of the U.S. Department of Energy
Office of Energy Efficiency & Renewable Energy
Operated by the Alliance for Sustainable Energy, LLC

This report is available at no cost from the National Renewable Energy Laboratory (NREL) at www.nrel.gov/publications.

Contract No. DE-AC36-08GO28308

Technical Report
NREL/TP-5700-87259
September 2023

National Renewable Energy Laboratory
15013 Denver West Parkway
Golden, CO 80401
303-275-3000 • www.nrel.gov

NOTICE

This work was authored by the National Renewable Energy Laboratory, operated by Alliance for Sustainable Energy, LLC, for the U.S. Department of Energy (DOE) under Contract No. DE-AC36-08GO28308. Funding provided by the U.S. Department of Energy Office of Energy Efficiency and Renewable Energy Geothermal Technologies Office. The views expressed herein do not necessarily represent the views of the DOE or the U.S. Government.

Photos (clockwise) by Dennis Schroeder, NREL 36653; Alaska Center for Energy and Power, NREL 32760; Dennis Schroeder, NREL 48223 and 48223; John W. Lund, NREL 13101; Robb Williamson, NREL 13033

Acknowledgments

This work was authored by the National Renewable Energy Laboratory, operated by Alliance for Sustainable Energy, LLC, for the U.S. Department of Energy (DOE) under Contract No. DE-AC36-08GO28308. Funding provided by the U.S. Department of Energy Office of Energy Efficiency and Renewable Energy Geothermal Technologies Office. The views expressed herein do not necessarily represent the views of the DOE or the U.S. Government.

List of Acronyms

AGS	advanced geothermal systems
BHT	bottom-hole temperature
CAHSB	Central Alaskan Hot Springs Belt
DOE	U.S. Department of Energy
EGS	enhanced geothermal systems
EIA	U.S. Energy Information Administration
GDR	Geothermal Data Repository
GPT	geothermal play type
GTO	Geothermal Technologies Office
HHP	high-heat-producing
LCOH	levelized cost of heat
NREL	National Renewable Energy Laboratory
OBGPT	orogenic belt geothermal play type
PFA	play fairway analysis
RGPT	radiogenic geothermal play type
RSAT	Resource Size Assessment Tool
SBGPT	sedimentary basin geothermal play type
SMU	Southern Methodist University
USGS	U.S. Geological Survey
WSM	World Stress Map
XRF	X-ray fluorescence

Executive Summary

The U.S. Department of Energy (DOE) Geothermal Technologies Office (GTO) supports the Geothermal Heating and Cooling Geospatial Datasets and Analysis project, conducted by the National Renewable Energy Laboratory (NREL). This project is part of a broader effort to demonstrate the multifaceted value of integrating geothermal power and geothermal heating and cooling technologies into national decarbonization strategies and community energy plans. There is a need to establish baseline low-temperature geothermal resource data sets and evaluate methods for deploying these technologies.

This research is focused on collecting baseline data sets, updating conceptual models, and creating play fairway analysis (PFA) methodologies for low-temperature (<150°C) geothermal resources of different geothermal play types (e.g., sedimentary basin, orogenic belts, and radiogenic geothermal play types) that could be used for geothermal heating and cooling, combined heat and power, and other geothermal direct-use applications. Low-temperature geothermal resources are defined as reservoirs—natural or engineered—with temperatures <150°C. While the focus in the NREL effort is on geothermal heating and cooling, resources at the upper end of this temperature range can also be used for small-scale power generation. This project does not include ground-source heat pump technologies because they can be effectively developed almost anywhere.

Low-temperature geothermal resources have not been studied as extensively as medium- to higher-temperature geothermal resources, but there is recent interest in improving understanding of these types of resources because of the potential for geothermal technologies to help decarbonize heating and cooling systems. In addition, enhanced geothermal systems (EGS) and other emerging technologies for exploiting petrothermal resources have opened the possibility of utilizing deep sedimentary basin systems, where porous media provide permeability, and high temperatures can be reached at great depths.

This project takes the approach of classifying low-temperature geothermal resources by geothermal play type (GPT). We defined and characterized three major classes of low-temperature GPT: sedimentary basins, orogenic systems, and radiogenic systems. We develop methodologies for evaluating and analyzing the potential for these resources building off the PFA approach to de-risking geothermal exploration and characterization.

The proposed PFA approach for low-temperature geothermal resources includes: (1) identifying relevant data (e.g., data sets such as bottom-hole temperatures from oil and gas wells, heat flow data, Quaternary faults and stress field data, and geophysical data); (2) grouping and weighting relevant data sets into PFA criteria (e.g., geological, risk, and economic criteria); (3) performing uncertainty quantification; (4) developing favorability or common risk maps for low-temperature geothermal resources to identify potential locations for more focused data collection; and (5) estimating electric power generation and heating potential at those locations using the GeoRePORT Resource Size Assessment Tool (RSAT). This project will facilitate future deployment of geothermal heating and cooling, combined heat and power, and geothermal direct use by providing data, tools, and a workflow applicable to low-temperature geothermal resources. Increased deployment of geothermal heating and cooling and geothermal direct use will help achieve national and local decarbonization goals.

Table of Contents

List of Figures

List of Tables

Introduction

The Geothermal Heating and Cooling Geospatial Datasets and Analysis project was conducted by the National Renewable Energy Laboratory (NREL) as part of a broader effort to demonstrate the multifaceted value of integrating geothermal power and geothermal heating and cooling technologies into national decarbonization plans and community energy plans.

Geothermal resource types likely to have temperatures >150°C are better defined, characterized, and classified than lower-temperature resource types. This is likely because geothermal resources >150°C have the potential to economically generate electric power, whereas the use case for geothermal resources <150°C is primarily heating and cooling (there are exceptions where geothermal resources <150°C can be used for smaller-scale electricity generation). Recent interest in geothermal heating and cooling applications—driven by decarbonization goals and the increased cost and geopolitics of natural gas reliance—has highlighted the need to improve the understanding of the types of geothermal resources that can be used for heating and cooling.

Geothermal heating and cooling applications include **direct use**, where warm or hot water from the geothermal resource is piped through heat exchangers or directly into commercial or residential buildings to meet heating and hot water demands, or to provide heating for industrial processes (DOE GTO 2023). Geothermal direct use can also be used for cooling or refrigeration through the use of **absorption chilling**. This mature technology relies on enthalpy changes in absorption/desorption processes to make cold air or ice from hot water. Geothermal resources 90°–150°C are well suited to drive an absorption cycle (Erickson and Holdmann 2005; Liu et al. 2015; Robins et al. 2021). Where no direct-use resource is available, **geothermal heat pumps** can be used to provide heating and cooling to individual buildings or a network or district of buildings. Direct use and geothermal heat pumps can also be used in tandem depending on specific resource and demand conditions (Beckers 2021). Because there are specific resource requirements for direct use but not for geothermal heat pumps, this paper focuses on improving the classification and typologies for geothermal resource types likely to supply heating and cooling through direct use.

Geothermal systems have been classified in a variety of ways. In 2008, the U.S. Geological Survey (USGS) assessed the electric power generation potential of conventional geothermal resources in the United States, distinguishing between moderate-temperature (90°–150°C [194°–302°F]) and high-temperature (greater than 150°C) geothermal systems. Most publications (including Rybach 1981; Nicholson 1993; Moeck 2014) make a distinction between "convective" and "conductive/static" types. The thermal regime of static or conductive type systems, which typically occur in low permeability environments such as deep aquifers or sedimentary basins, is only caused by conduction.

A geothermal play type (GPT) can further be defined based on its tectonic and geological setting and can be classified by common characteristics shared by a play group (Moeck 2014). High-enthalpy convective type systems have three standard classifications: “magmatic,” which is related to anomalous heat flow produced by young intrusive rocks (<1 million years old; Cathles et al. 1997), “plutonic” rocks (Moeck et al. 2014), or “deep circulation,” originating from deep meteoric water circulation along subvertical fault/fracture zones in hotter areas. Convective type

hot springs systems also happen in regions of higher natural radioactivity, such as Pocos de Caldas Brazil and Paralana, Australia (see Hamza et al. 2005; Beitollahi et al. 2005; Brugger et al. 2005; Baranwal et al. 2006). However, only a small number of investigations have identified and described active geothermal convection systems that are driven by radiogenic heat sources. This is primarily because energy extraction from the low-enthalpy fluids connected to radiogenic heat sources has only recently proved economical. It's also likely that naturally occurring active radiogenic hydrothermal systems are not prevalent. In high-heat-producing (HHP) granites, fossil hydrothermal activity has been noted (e.g., Durrance 1985), and it's probable that this activity was cyclical and very fleeting (Kolker 2008).

Like other GPTs, low-temperature geothermal plays can be classified by their tectonic and geological settings. Some low-temperature play types such as sedimentary basin types are mainly dominated by conductive heat transfer (Moeck 2014). Due to the lack of rapid convective fluid flow mechanisms and associated short-term fluid dynamics, conduction-dominated plays serve as the home for low-enthalpy resources (Moeck 2014). Conduction-dominated plays, also known as petrothermal plays, may be classified as hydrothermal and non-hydrothermal and are found on passive continental edges and intracontinental tectonically quiescent regions (Moeck 2014).

The economic feasibility of conduction-dominated play types is linked to the local geothermal gradient. Temperature gradients that exceed the normal continental average can be found in regions of high heat flow (e.g., due to elevated concentration of radioactive elements in the crust) or where overlying lithologies are thermally insulating (Beardsmore and Cull 2001). Therefore, conductively heated geothermal reservoirs with temperatures that might be economical for power generation are located at greater depths than convectively geothermal systems (Hervey et al. 2014).

Figure 1 shows the classification of three geological settings described by Moeck (2014): (1) intracratonic basin type, (2) orogenic belt type (e.g., foreland and thrust belt basins), and (3) basement/crystalline rock type. These play types are more distinguished by the reservoir's porosity-permeability ratio and the availability or lack of geothermal fluids in the reservoir (Moeck 2014). In this study, we borrow some principles from these classifications.

Intracratonic Basin Type	Orogenic Belt Type	Basement Type
Paris Basin	Unterhaching (Germany)	Habanero (Australia)
Intracratonic/Rift Basins Passive margin basins	Fold-and-thrust belts Foreland basins	Intrusion in flat terrain Heat-producing element rock
Sedimentary aquifers Permeability/porosity with depth	Sedimentary aquifers Permeability/porosity with depth Fault and fracture zones	Hot intrusive rock (granite) Low porosity/low permeability Faults and fracture zones
Hydrothermal	Hydrothermal	Petrothermal

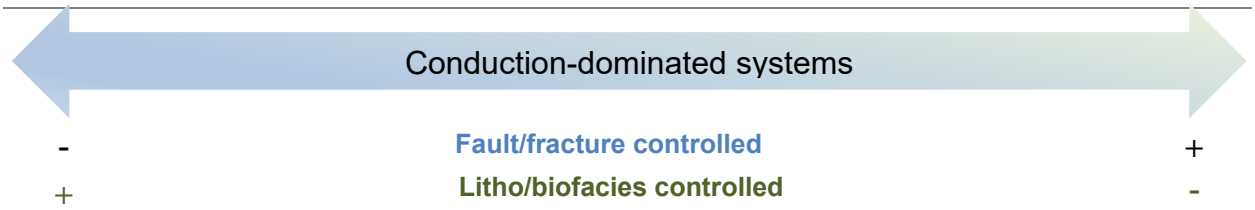

Figure 1. Conduction-dominated GPTs

From Moeck (2014)

Low-temperature geothermal resources have not been studied as extensively as higher-temperature geothermal resources, but there is recent interest in improving understanding of these types of resources because of the potential for geothermal technologies to help decarbonize heating and cooling systems. In addition, EGS, advanced geothermal systems (AGS) and other emerging technologies for exploiting petrothermal resources have opened up the possibility of utilizing deep sedimentary basin systems for heat and power, where porous media provide permeability, and high temperatures can be reached at great depths (Doughty et al. 2018). Through the application of EGS and AGS technologies, non-commercial reservoir conditions might be improved in the future for power generation (e.g., Denver Basin), but also other geothermal direct-use technologies such as geothermal heat pumps could be used immediately to heat and cool residential and districts.

Therefore, this study aims to suggest a better characterization of low-temperature GPTs (i.e., sedimentary basins, orogenic belts, and radiogenic) and, based on a literature review of these GPTs, identify relevant data and build off the PFA methodologies approach to de-risking geothermal exploration. These methodologies can be used to develop favorability maps for geothermal resources <150°C, but it is important to note that **PFA favorability maps cannot and should not be used for targeting geothermal wells**. Rather, they should be used to identify prospective areas that warrant more detailed investigations (Pauling et al. 2023; in preparation).

1 Sedimentary Basin Geothermal Play Types

A sedimentary basin geothermal play type (SBGPT) is controlled by both its historical formation and evolution, and its current tectonic and geological setting. A SBGTP includes important factors such as heat source or heat flow, circulating fluid (natural or injected) or heat transport mechanism, reservoir porosity/permeability and storage (natural or induced), and reservoir seal. These features are different from hydrocarbon play systems, which are defined by their source rock, reservoir properties, and trap (Doughty et al. 2018).

Most conduction-dominated hydrothermal plays in sedimentary basin settings are in deep aquifers heated by a near normal thermal gradient (Moeck 2014). Low and high porosity/permeability domains are controlled by the lithology, faulting, diagenesis patterns, and the stress field (Wolfgramm et al. 2009; Hartmann and Beaumont 2000), which are strongly influenced by evolution, subsidence rates, and current tectonic settings. Previous studies of sedimentary geothermal resources targeted formations with high porosity/high permeability (~100 mD) that allow significant convection (Augustine 2014) or high porosity/low permeability at a high temperature gradient, which generally occur at high depth (>3 km; Moeck 2014). SBGPTs with low permeability could contain petrothermal resources, which could be exploited by enhancing the permeability using a variety of reservoir stimulation techniques (Zimmermann et al. 2007). The storage capacity of the host rock's porosity may have a significant impact on the success of the EGS in hot sedimentary aquifers (Rybach and Muffler 1981). The geometry of the basin is a product of the basin classification and evolution that affects the temperature of the fluid in the porous of different lithologies (Moeck 2014).

1.1 SBGPT Background

Recently, there is interest in harnessing geothermal energy from sedimentary basins for electricity production (Porro et al. 2012) and/or direct use for heating and cooling. A sedimentary basin consists of a stratigraphic sequence that, when associated with oil and gas production, provides the opportunity to use existing information and technologies from the petroleum industry to develop geothermal resources (Johnston et al. 2020). For instance, well logs, temperature gradients, and reservoir properties such as formation thickness are widely known from hydrocarbon exploration. According to Allis et al. (2013) heat flow >80 mW/m^2, temperatures >175°C, depths less than 4 km, and permeability greater than 100 mD (Augustine 2014) are conditions that must be met by the sedimentary basin reservoir for geothermal energy production to be feasible (levelized cost of energy <10 cents/kWh).

Most sedimentary basins do not typically have anomalously high temperatures, hence deep drilling is required to access high to moderate enthalpy resources (Porro et al. 2012). These geothermal systems are usually referred to as deep sedimentary basins. Porro et al. (2012) assessed the geothermal energy resource of 15 major sedimentary basins in the United States (see Figure 2) that they had narrowed down to those with temperatures greater than 100°C based on factors such as temperature, volume, depth, and reservoir properties including rock type and permeability. Anderson (2013), based on the Porro et al. (2012) study, incorporated a porosity and permeability evaluation and screening basins with >125°C and <4 km depth in the marginal range for binary power systems. That work identified seven basins with power generation potential: Williston, Denver, Great Basin, Fort Worth, Sacramento, Gulf Coast, and Imperial Valley.

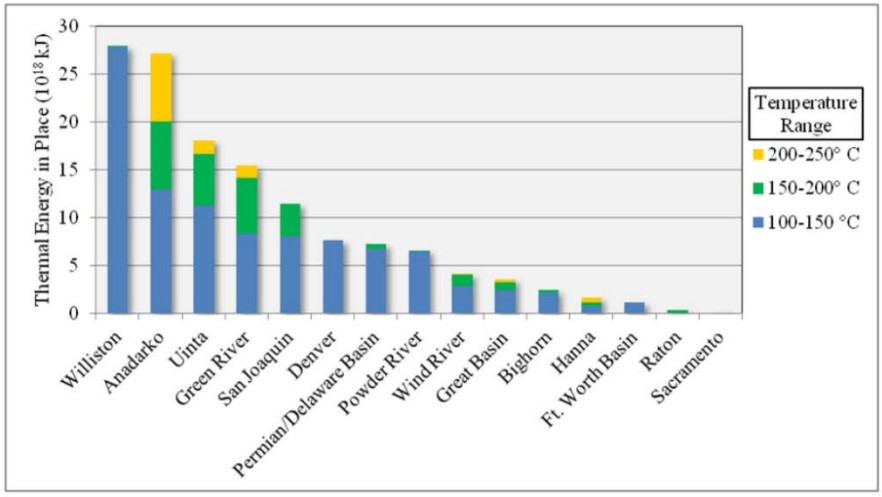

Figure 2. Total beneficial heat in place for 15 selected sedimentary basins

From Porro et al. (2012)

Few studies exist on the geothermal potential and characterization of sedimentary basins in the United States. Most of these studies have been focused on no more than 15 sedimentary basins with power generation potential of high to moderate temperatures. The low-temperature potential of all sedimentary basins in the United States has not been studied yet—this is why our study aims to identify relevant data and methodologies for assessment of low-temperature sedimentary basins (<150°C) for direct use such as heating and cooling applications.

A total of 144 sedimentary basins in the United States including Alaska and Hawaii (see Figures 4, 9, 13, and 14) were identified as part of a study to support the Geologic Carbon Dioxide Sequestration National Assessment Project by Brennan (2014) and Catalog of Sedimentary Basin by Coleman and Cahan (2012). For this study, we only excluded the sedimentary basins in Hawaii located offshore.

1.2 SBGPT Classification and Geothermal Key Controls

A systematic approach to locating geothermal resources in SBGPTs could follow the PFA framework, originally developed by the petroleum industry, that identifies key components of a sedimentary basin, associates those with geological controls, and then identifies relevant data sets. The PFA technique defines local areas that have high potential for hosting geothermal plays and eliminates large areas that have a higher potential for failure in order to reduce risk during the resource locating process. PFA for hydrothermal geothermal systems exploration involves identifying four or more critical components:

1. Heat (H)
2. Accessible fluids (F)
3. Permeability/porosity (P)
4. Caprock or seal (S)

Some of the key controls in SBGPTs (Table 1) include heat flow (anomalous or normal) or heat source (e.g., magmatic, or radiogenic), fluid chemistry and dynamics (if hydrothermal), basin

geometry, faults and fractures, stress state, permeability/porosity, and stratigraphic sequence (Moeck 2014).

The genesis and evolution of basins are important factors to understand geothermal key controls such as the geometry, structure, fluid chemistry, and stratigraphic sequence of the sedimentary basins; meanwhile, aspects such as the heat flow, stress state, active faults, and fluid dynamics are controlled by the present geological and tectonic setting where the basin is currently located (see Figure 3).

Table 1. Geothermal Key Controls of Sedimentary Basins Influenced by the Formation and Evolution History and/or the Present Time Geological and Tectonic Settings

Geological and Tectonic Settings			
Geothermal Key Controls	***Formation and Evolution***	***Present Time***	***Related PFA "Critical Component"***
Heat Flow		x	H
Lithology/ Stratigraphy	x		H, F, P, S
Fluid Chemistry	x		F, S
Fluid Dynamics		x	F, S
Basin Geometry	x	x	P
Faults and Fractures	x	x	P
Stress State		x	P
Permeability/ Porosity	x	x	P

*H= Heat/Heat Flow, F= Accessible Fluid, P= Permeability/Porosity, S= Caprock/Seal—sometimes

To classify SBGPTs, we used the classification suggested by Coleman and Cahan (2012) based on a simple geological setting scheme (see Table 2): (1) intracratonic, meaning basins formed within the boundaries of a craton; (2) pericratonic, meaning basins formed near or accreted to the margins of the craton, (3) intercratonic, meaning basins formed between cratons and extending onto oceanic crust; and (4) oceanic, meaning basins formed independent of the cratons mostly on oceanic crust. Each of these classifications has general implications for the formation of geothermal resources.

This classification can be applied to the formation and evolution history of the basins, as well as the present time of the United States (Figure 3). In addition, we include the classification based

on geothermal plays by Moeck (2014): convection and/or conduction dominated, magmatic or non-magmatic, and hydrothermal or non-hydrothermal (petrothermal), respectively.

In the United States, most of the basins currently located in the cratonic part of the continent (blue part of the bar graphs in Figure 2) show low temperature gradients (Figure 3) and are thus expected to be conduction-dominated regardless of the classification of the basin.

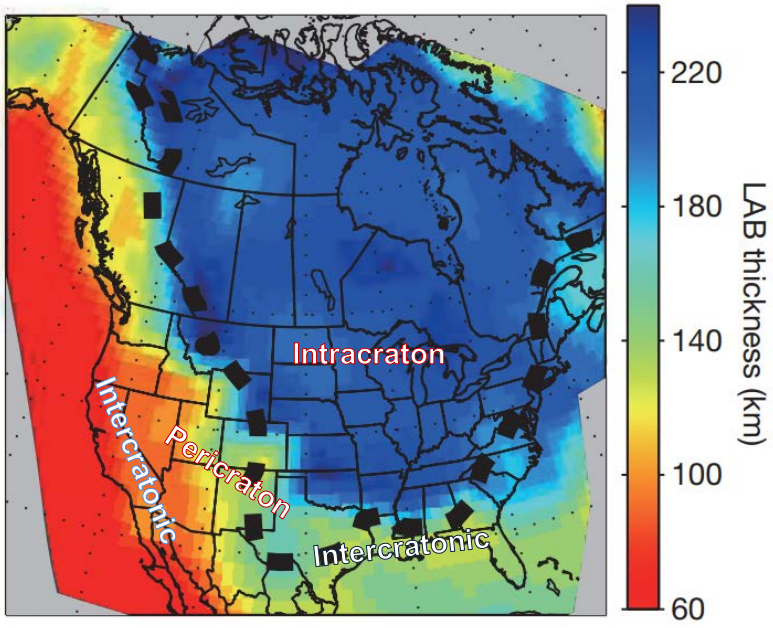

Figure 3. Present lithospheric-asthenospheric boundary thickness of North America (the thick black dashed line indicates the borders of the craton)

Note: LAB stands for lithospheric-asthenospheric boundary

From Yuan and Romanowicz (2010)

Table 2. Classification of Sedimentary Basins in the United States Based on Geological Settings at the Time of Formation and Evolution of the Basin

Basin type classifications by Coleman and Cahan (2012); GPT classifications by Moeck (2014)

Settings	Basin Type	Definition	Play Type	Examples	Model*
Intracratonic	Rift Basins	Rifts formed within continental basins, resulting in a normal-faulting bounded basin	Convective and/or Conduction	Rio Grande Rift	Figure 5
	Transtensional Basins	Basins with a substantial amount of strike-slip but net extensional	Convective and/or Conduction	Great Basin in the Basin and Range Province	Figure 6
	Aulacogens	Rift basins formed as the failed arm of a triple junction	Conduction	Anadarko Basin	Figure 7
	Sag Basins	Basins formed in continental masses as result of asthenospheric downwelling or isostatic equilibrium	Conduction	Michigan and Williston Basins	Figure 8
Pericratonic	Rift Basins (proto-oceanic rifting)	Basins formed along margins of continents leading the opening of an oceanic basin	Convective and/or Conduction	Nuwuk-Dinkum-Kaktovik Basin, Alaska	Figure 10
	Passive Margin Basins (including Deltaic Basins)	Basins formed over continental and transitional oceanic crust	Conduction	Gulf of Mexico and West Atlantic Basins	Figure 11
	Foreland Basins and Thrust Belts	Basins formed adjacent to orogenic thrust belts and fault-bounded uplifts	Conduction	Appalachian and Mesozoic Rocky Mountain Basins	Figure 12 and 16
	Borderland Basins	Basins formed along the margins of a continent as a result of transtensional and transpressional faulting associated with oblique collision of tectonic plates	Convective and/or Conduction	California borderland, Santa Maria, and Los Angeles Basins	Figure 9

Settings	Basin Type	Definition	Play Type	Examples	Model*
	Transtensional/ Transpressional Basins	Basins formed at the margins of continents, typically along plate boundaries	Convective and/or Conduction	Great Smoky Mountains Rift Basin	Figure 6
Intercratonic	Passive Margin Basin (extending onto oceanic crust)	Basins developed between cratonic masses and extended onto transitional and oceanic crust	Conduction	Canda Basin in the U.S.	Figure 11
	Accreted Back-Arc Basin	Basins formed because of trench roll-back beneath the landward side of a volcanic chain in a subduction zone	Conduction	Bristol Bay Basin in Alaska	Figure 14
	Accreted Fore-Arc Basins	Basins formed in oceanic crust between the subduction zone and an associated volcanic arc because of growth of an accretionary prism.	Conduction	Great Valley of California and Cook Inlet Basin of Alaska	Figure 14
Oceanic	Back-Arc Basin	Basins formed on oceanic crust because of trench roll-back beneath the landward side of a volcanic chain (on the other side from the subduction zone)	Convective and/or Conductive	Aleutian Basin in Alaska	Figure 15
	Fore-Arc Basin	Basins formed on oceanic crust between the subduction zone and an associated volcanic arc because of development and growth of an accretionary prism	Convective and/or Conductive	Western Washington-Oregon Basin	Figure 15

1.2.1 Sedimentary Basin—Intracratonic

Intracratonic basins are located on relatively thick continental lithosphere, away from plate boundaries, but in some cases connected by a rift or failed rift zone. Slow subsidence of the continental lithosphere occurs in these cratonic basins because they are commonly filled with shallow water and terrestrial sedimentary rocks (Allen and Armitage 2011).

The intracratonic basins classification by Coleman and Cahan (2012) encompass four types of basins: (1) continental rifts, (2) continental transtensional basins, (3) aulacogens, and (4) sag basins. The first three types of intracratonic basins are elongated and contain very thick sedimentary deposits. The aulacogen basins consist of reactivated fossil rifts at high angles to orogenic belts (Ingersoll 2011). Sag basins, in contrast, are typically circular to oval and in general have different stages of basin subsidence (Coleman and Cahan 2012). Figure 4 shows all intracratonic basins in the conterminous United States and Alaska at the time of formation and evolution.

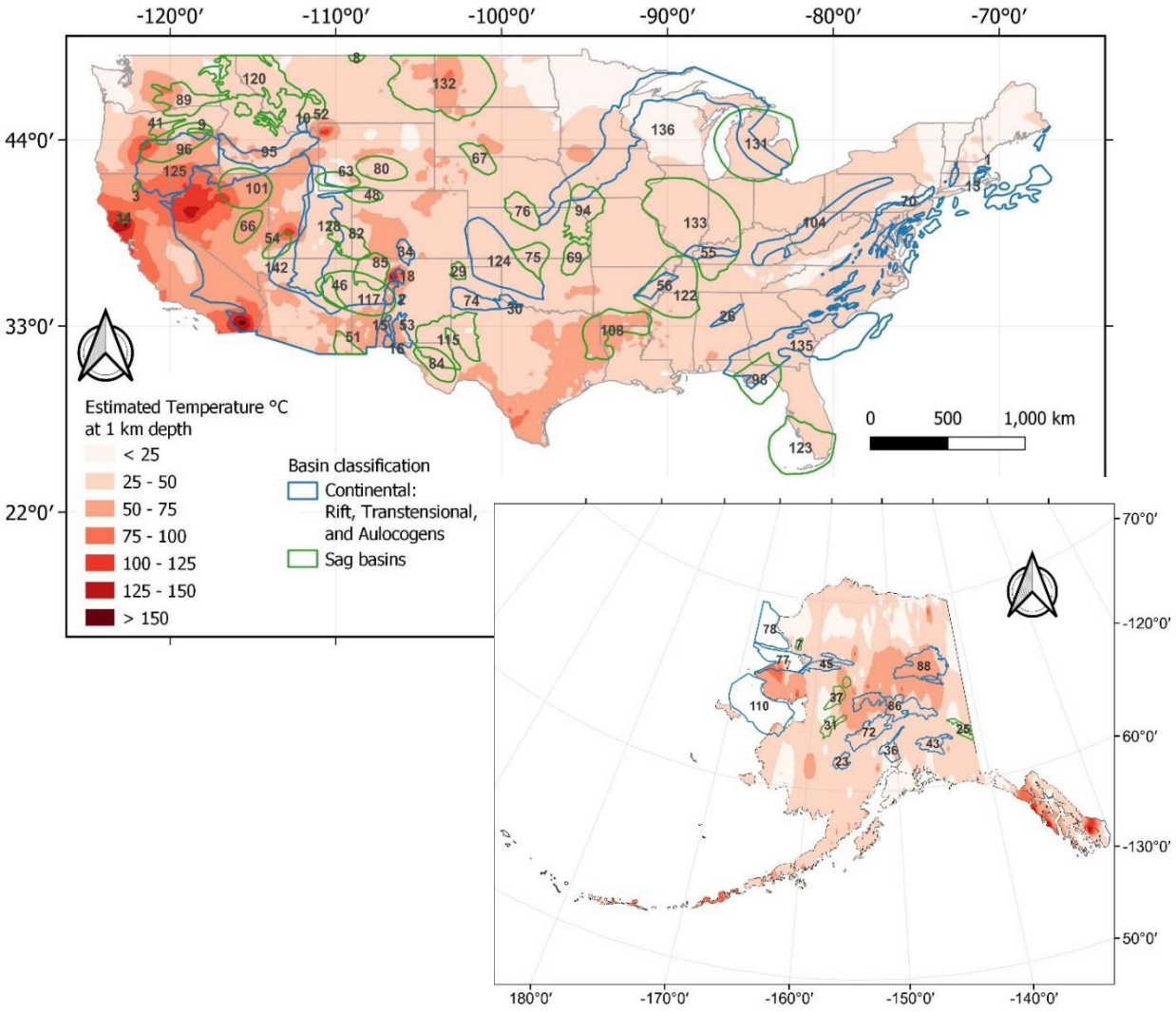

Figure 4. Intracratonic basins in the conterminous United States and Alaska overlapping the estimated temperature at 1 km

The surface map of intracratonic basins in the conterminous United States and Alaska is from Coleman and Cahan (2012); estimated temperature map of the conterminous U.S. is from Mullane et al. (2016) modified after Blackwell et al. (2011); estimated temperature map of Alaska is from Davalos-Elizondo et al. (2023) modified after Batir et al. (2016). Cenozoic: 2. Estancia Basin; 3. Montgomery Creek Basin; 7. Noatak Basin; 9. Blue Mountains Basin; 10. Ruby Basin; 14. Round Valley Basin; 15. Jornada Basin; 16. Mesilla Basin; 18. Espanola Basin; 23. Holitna Basin; 25. Northway Lowlands; 28. Albuquerque Basin; 31. Innoko Basin; 34. San Luis Basin; 36. Susitna Basin; 37. Galena Basin; 41. Clarno Basin; 45. Kobuk-Selawik Basin; 48. Brown's Park Basin; 52. Bozeman Basin; 53. Tularosa Basin; 54. Claron Basin; 63. Bridger Basin; 66. Sheep Pass Basin; 72. Minchumina Basin; 77. Kotzebue Basin; 78. Hope Basin; 80. White River–Split Rock Basin; 84. Tascotal Basin; 86. Nenana Basin; 88. Yukon Flats Basin; 89. Columbia River Plateau Basins; 95. Snake River Downwarp; 96. Clarno–John Day Basin; 101. Copper–Bull Run–Elko–Indian Wells Basin; 110. Norton Basin; 117. Baca Basin; 125. Southeast Oregon–Northern California Basins; 142. Basin And Range Basins. Mesozoic: 43. Copper River Basin; 67. Kennedy Basin; 70, 135. Newark Group Basins; 85. San Juan Basin; 98. Apalachicola Embayment; 122. Mississippi Embayment; 123. South Florida Basin. Paleozoic: 8. Hogeland Basin; 13. Narragansett Basin; 26. Birmingham Graben; 29. Dalhart Basin; 30. Hollis-Hardeman Basin; 46. Holbrook Basin; 51. Pedregosa Basin; 55. Rough Creek Graben; 56. Reelfoot Rift; 69. Cherokee Basin; 74. Palo Duro Basin; 75. Sedgwick Basin; 76. Salina Basin; 82. Paradox Basin; 94. Forest City Basin; 104. Rome Trough; 115. Permian Basin; 124. Anadarko Basin; 131. Michigan Basin; 132. Williston Basin; 133. Illinois Basin; 168. Post-Ouachita Successor Basin. Neoproterozoic: 1. Boston Basin; 120. Belt Basin; 128. Chuar Group Area Basin; 136. Midcontinent Rift.

1.2.1.1 Continental Rift Conceptual Model

Continental break-up and the formation of new oceanic lithosphere occur when tensional stresses are generated away from plate boundaries, and when pressure and stress gradients caused by asthenospheric upwellings and convection, continental collision, dike intrusions, and/or tractions at the base of the lithosphere are enough to inherently weaken and thin the strong and thick continental lithosphere to a few tens of kilometers (e.g., Ebinger and Scholz 2011). A small percentage of continental rifts experience stretching and strain localization to the point of rupture, as shown by the scars left by failed rifts worldwide (Ebinger and Scholz 2011).

A tectonic conceptual model of a continental rift SBGPT (Figure 5) applies to those basins that are currently under an extensional regime and located on thick intracratonic or pericratonic continental lithosphere, such as basins in the East African Rift System. In the United States, the only current basin classified as a failed continental rift is Rio Grande basin in New Mexico (Figure 4; Albuquerque Basin).

Continental rift conceptual models can be developed based on the lithospheric stretching models proposed for the evolution of continental rifts (e.g., McKenzie 1978). These conceptual models have been classified as "active" and "passive" in relation to mantle upwellings in rift initiation and the different stages of development (Ebinger and Scholz 2011). Active rifts are dominated by regional uplift due to mantle buoyancy with magmatism or non-magmatism (e.g., Sengör and Burke 1978). The continental rifts with high magmatic activity are in general convection-dominated and host high- to medium-enthalpy geothermal systems (e.g., Kenya). Passive rifting models, on the other hand, are driven by plate tectonic forces away from the continent where the basin is developed (Ebinger and Scholz 2011), and associated basins are thus mainly conduction dominated. These basins can have normal or anomalous regional heat flow (see passive margin Section 1.2.2.2).

In continental rifts, there are kinematically connected basins that run the length of the rift system, significant fault-bounded sedimentary basins, and frequent periods of faulting, either with or without magmatism (e.g., Rosendahl 1987). In the beginning, isolated border fault segments interact kinematically and mechanically to create accommodation zones, transfer fault zones, relay ramps, and oblique-slip normal faults, which are known to be ideal environments for the creation of geothermal fluid pathways and storage (see, for example, Faulds and Hinz 2015). In this context, is important to notice that geothermal systems in continental rifts are generally fault controlled or fault-leakage controlled. Fault leakage refers to fluids moving through a fault into a permeable stratigraphic layer (Moeck 2014).

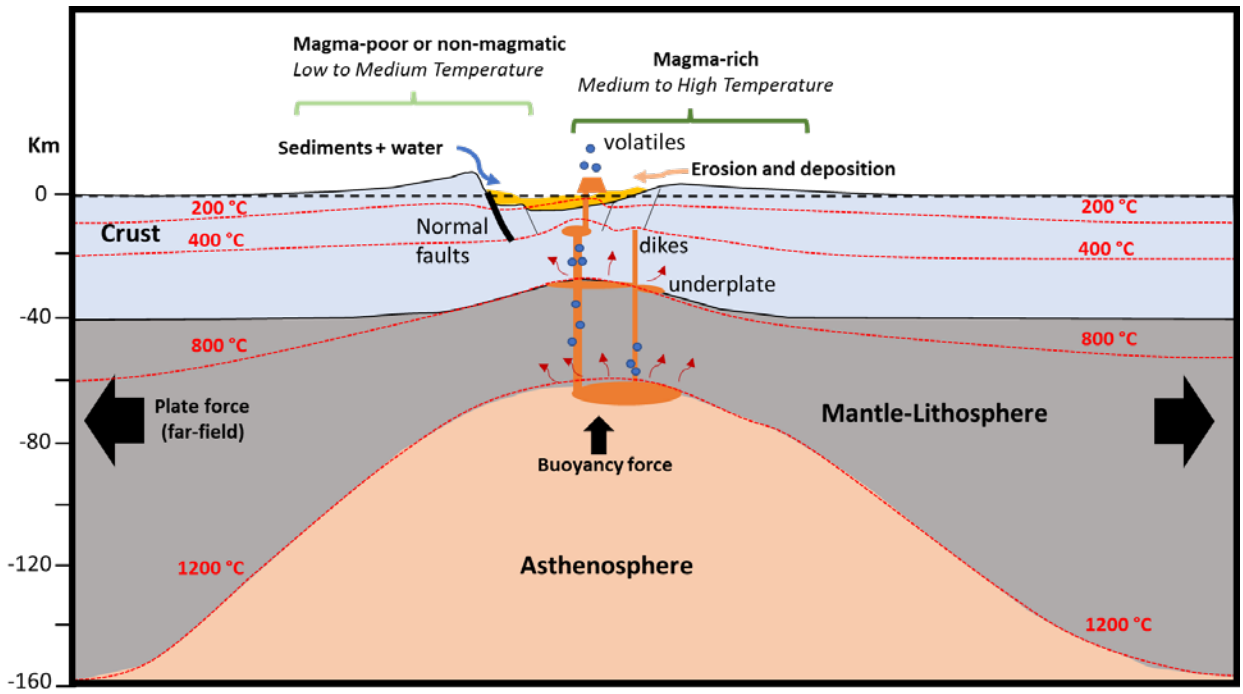

Figure 5. Continental rift basin geothermal conceptual model with schematic isotherm distribution (red lines)

All report figures by NREL, unless otherwise noted.

1.2.1.2 Transtensional Basin Conceptual Model

Transtensional intracontinental basins form in response to brittle deformation of the crust that results in association with strike-slip and normal faults due to strain partitioning (Jayko and Bursik 2011). These basins are not only characterized by this extensional and oblique component but also display block tilting and rotation around vertical and horizontal axes (Basile and Brun 1999). Transfer across fault systems creates asymmetric half-grabens, which are typical in stepover or relay systems, as well as relay ramps, releasing bends, pull apart basins, and tilting blocks. Sinistral, dextral, or oblique strike-slip faults can partially tolerate rotation; the slight variations in strain transmission result in bends and flower-like formations (Jayko and Bursik 2011). All these favorable structures have been reported to create pathways and storage of geothermal fluids (e.g., Great Basin; Faulds and Hinz 2015).

In Western Great Basins, the Walker Lane is a good example of transtensional intracontinental basin. It consists of right-lateral strike-slip faults and west-northwest extension where abundant geothermal systems cluster in northeast-trending belts in the northern Great Basin (Faulds et al. 2004). Most of these geothermal systems (~32%) are found in favorable settings such as step-overs or relay ramps and pull-apart basins and displacement transfer zones (3%). These last ones are more abundant in the transtensional western part of the Great Basin. However, high temperature geothermal resources are restricted to these regions of extensional to transtensional strain (Faulds and Hinz 2015). Faulds and Hinz (2015) also reported that more than 75% of the geothermal resources are blind in this region.

A transtensional conceptual model of intracontinental play types (Figure 6) is modeled off those geothermal systems in the Walker Lane region. Types of geothermal resources include structurally controlled geothermal resources, deep sedimentary basin hydrothermal and petrothermal resources (i.e., the EGS demonstration site FORGE in Utah), and hybrid (e.g., deep sedimentary basin and structurally controlled). The heat source could be related to anomalous heat flow and geothermal fluids are mostly fault controlled within low-medium temperatures. While high temperature systems could be related with recent magmatism and transtensional pull-apart basins.

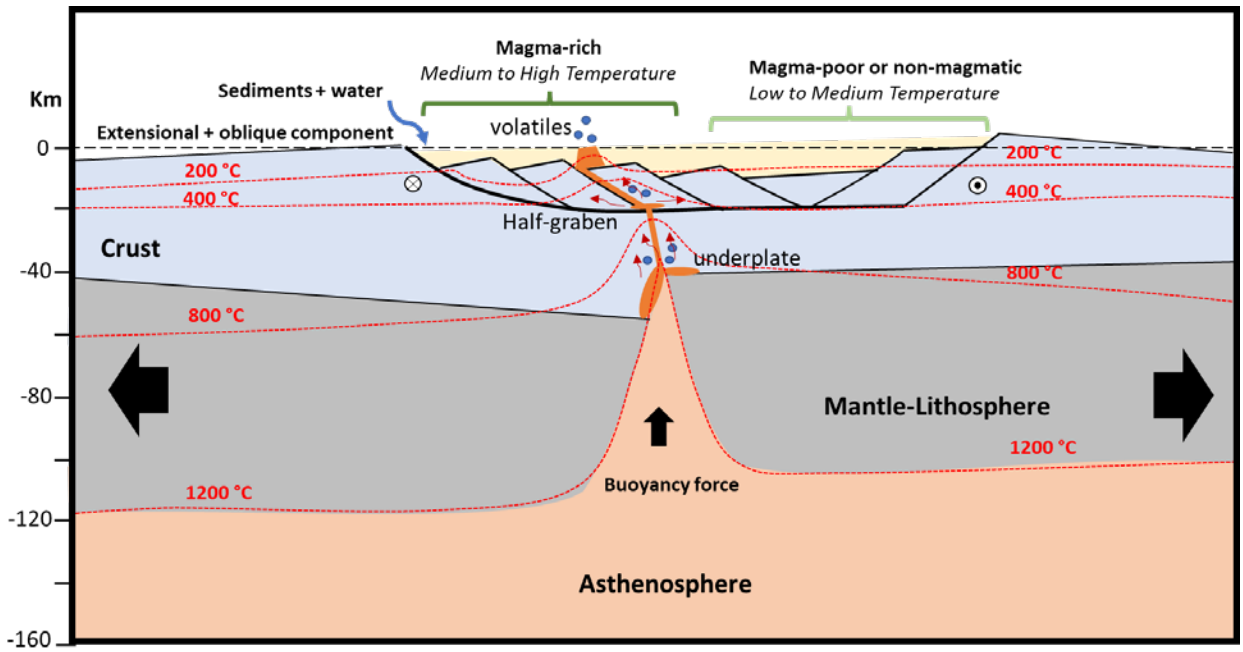

Figure 6. Transtensional basin geothermal conceptual model with schematic isotherm distribution (red lines)

1.2.1.3 Aulacogen Basin Conceptual Model

Three rifts normally occur at an angle of approximately 120° during continental rifting (Burke and Dewey 1973). In general, one of the arms fails before continental separation occurs and the other two arms satisfactory proceed to seafloor spreading (Ingersoll 2011). These fossil rifts are precursors to form aulacogen basins. Hoffman (1974) outlined five stages for formation of these types of basins: (1) rift stage, (2) transitional stage, (3) downwarping stage, (4) reactivation stage, and (5) post-orogenic stage (Figure 7). When fossil rifts evolve to capture drainage from continental interiors, they construct continental basins that could be reactivated, and then orogenic deformation proceeds to form aulacogens (Dickinson 1974; Ingersoll 1988), such as Anadarko basin in Oklahoma.

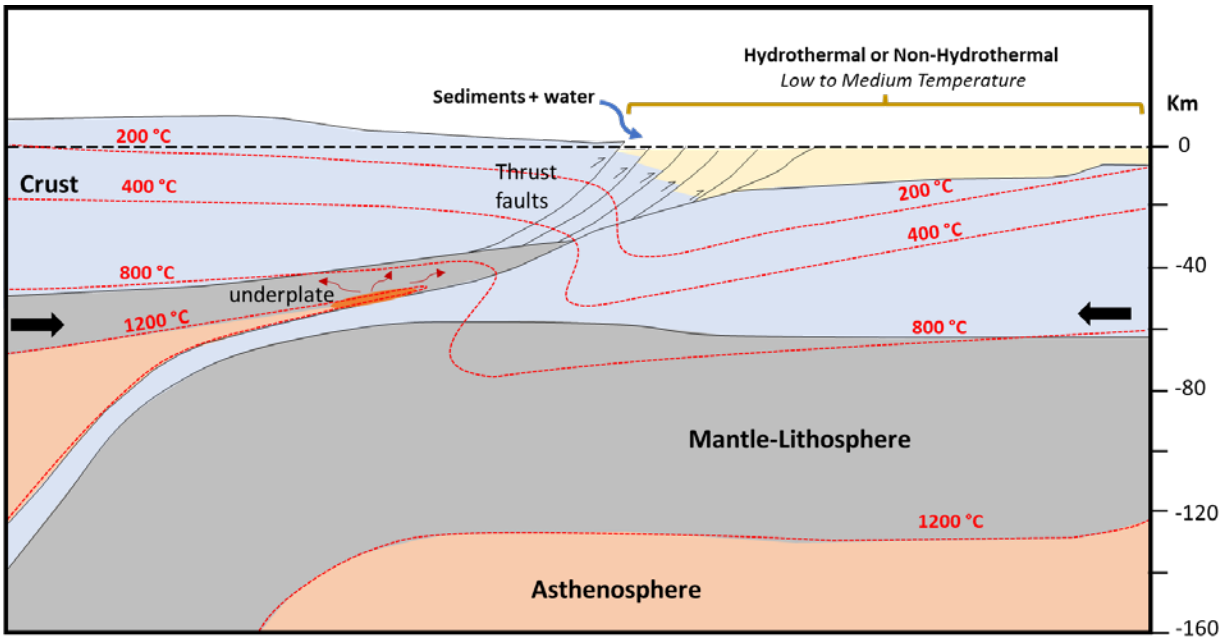

Figure 7. Aulacogen basin geothermal conceptual model with schematic isotherm distribution (red lines)

1.2.1.4 Sag Basin Conceptual Model

Intracratonic sag basins are found in the center of stable continental blocks. In general, they are not confined by major faults, but strike-slip faulting has been reported to occur occasionally within these basins (Middleton 1989). Some good examples of sag basins in the United States are the Michigan, Williston, and Illinois basins (Figure 4). Allen and Allen (2013) proposed that cratonic basins such as the Michigan and Illinois basins formed during an extreme part of a failed rift-drift suite, but some cratonic basins such as Williston show no evidence of a rift structure (Oyepeju 2013).

The creation of sag basins is not completely understood and is still debated. Middleton (1989) proposed a simple model for the evolution of these types of basins. They suggested that the mechanism is driven by slightly coupled convective downwelling of the asthenosphere beneath the lithosphere. First, a descending plume forms because of a quick change in the mantle convection system. In consequence, a depression up to 600 m wide may form at the surface of the earth. Then, this depression starts to be filled with sediments, forming a sedimentary basin up to 2.5 km thick. The lithosphere undergoes a period of thermal cooling if the convective downwelling mantle persists. The basin will experience uplift and erosion if the downwelling convective plume is eliminated, which may result in the removal of a significant portion of sediments and the reduction of the basin thickness (Middleton 1989).

Another mechanism, proposed by Fowler and Nisbet (1985) and Haxby et al. (1976), is that a phase change from lower density gabbro to higher density eclogite (Figure 8) is responsible for the formation of depressions on cratons. Fowler and Nisbet (1985) in particular proposed this mechanism as the origin of the Williston Basin. The subsidence record of this basins is linear rather than exponential, supporting this hypothesis known as delamination.

A low temperature gradient is assumed in this type of basin at the time of its formation when the driving force for delamination is negative buoyancy of the continental lower crust. However, the removal of mantle lithosphere induces regions of contraction and thickening, as well as extension and thinning of the crust. Mature delamination generates a crustal uplift as the sinking, dense lithosphere is replaced by the mobilized hot asthenosphere, which can cause an increase of gradient temperature (Meissner and Mooney 1998).

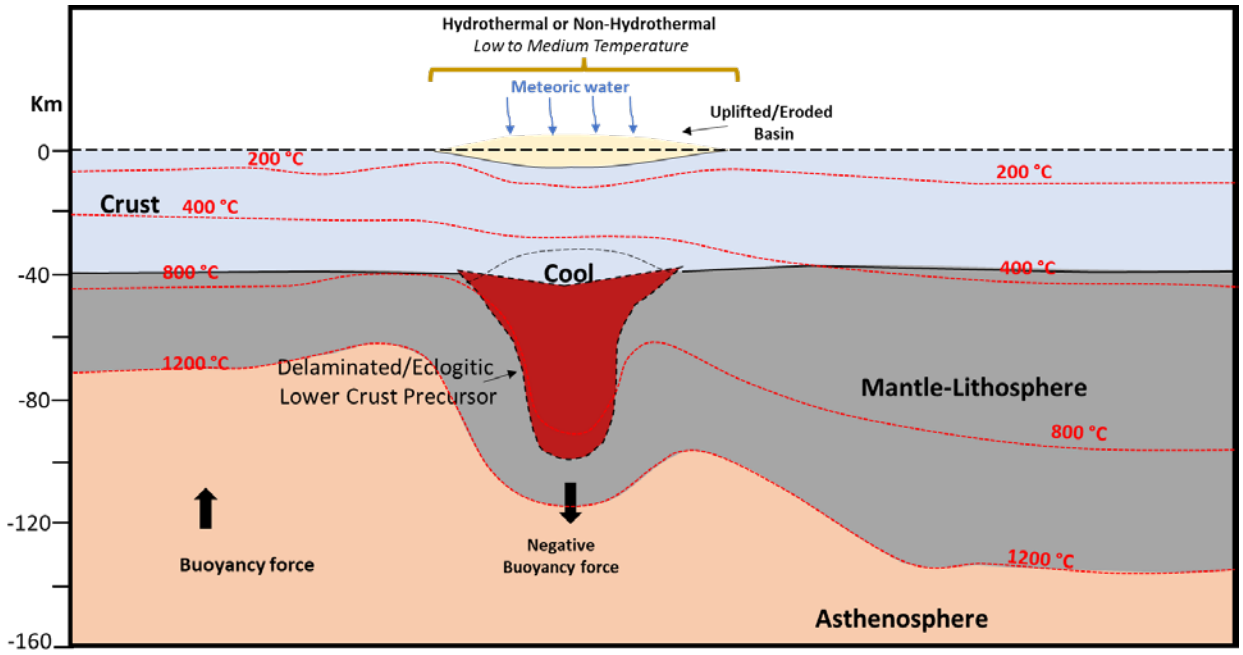

Figure 8. Sag basin geothermal conceptual model with schematic isotherm distribution (red lines)

1.2.2 Sedimentary Basin—Pericratonic

Pericratonic rift basins develop on reworked and juvenile crystalline basement accreted to a craton. The lithosphere underlying these basins on the margins of the craton appears to have been weakened, and it is susceptible to rifting (Figure 5; Saintot et al. 2006).

The pericratonic basins classification by Coleman and Cahan (2012) included five types of basins: (1) rift basins (proto-oceanic); (2) passive margin basins, including deltaic; (3) foreland basin and thrust belts basins; (4) borderland basins; and (5) transtensional/transpressional basins (see Section 1.2.1.1; Figure 6). Figure 9 shows all the pericratonic basins in the conterminous United States and Alaska at the time of formation and evolution of the basin.

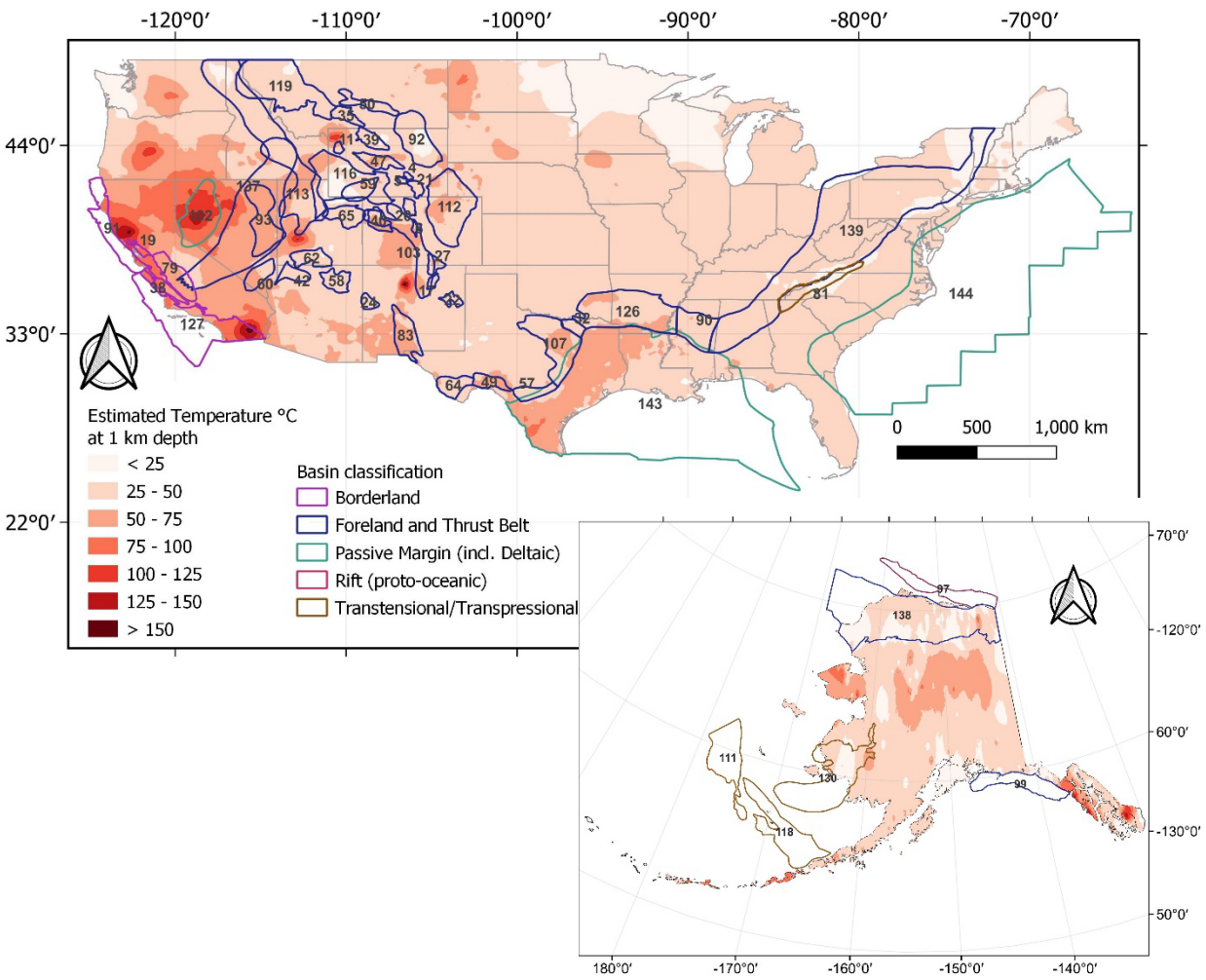

Figure 9. The surface of pericratonic basins in the conterminous United States and Alaska overlapping the estimated temperature at 1 km

Pericratonic basin map by Coleman and Cahan (2012); estimated temperature map of the conterminous U.S. from Mullane et al. (2016), modified after Blackwell et al. (2011); estimated temperature map of Alaska from Davalos-Elizondo et al. (2023), modified after Batir et al. (2016). Cenozoic: 4. Shirley Basin; 5. Hanna Basin; 11. Jackson Hole Basin; 19. Sonoma-Livermore Basin; 38. Central Coastal Basin; 79. San Joaquin Basin; 91. Northern California Borderland Basins; 99. Middleton-Yakataga Basin; 111. Navarin Basin; 118. Amak–St. George–Pribilof–Walrus Basin; 127. Southern California Borderland Basins. Mesozoic: 6. Middle Park Basin; 20. North Park Basin; 21. Laramie Basin; 24. Zuni Basin; 27. Raton Basin; 35. Crazy Mountains Basin; 40. Piceance Basin; 47. Wind River Basin; 50. Judith–Wheatland–Bull Mountains Basins; 58. Black Mesa Basin; 62. Kaiparowits Basin; 65. Uinta Basin; 92. Powder River Basin; 97. Nuwuk–Dinkum–Kaktovik Basin; 112. Denver Basin; 116. Idaho-Wyoming Thrust Belt–Greater Green River Basin; 119. North Montana Thrust Belt; 130. Bethel Basin; 138. Colville Basin And Foldbelt; 143. Gulf Of Mexico Basin; 144. West Atlantic Basin. Paleozoic: 17. Las Vegas Basin; 22. Tucumcari Basin; 32. Sherman Basin; 49. Val Verde Basin; 57. Kerr Basin; 59. Sweetwater Trough; 60. Bird Spring Basin; 64. Marathon-Marfa Basins; 83. Orogrande Basin; 90. Mississippi Ouachita Thrust Belt–Black Warrior Basin; 93. Ely Basin; 102. West Nevada Permian-Triassic Basin; 103. Central Colorado–Taos Trough; 107. Fort Worth Basin; 113. Oquirrh Basin; 126. Arkoma Basin–Ouachita Thrust Belt; 137. Antler Foreland Basin; 139. Appalachian Basin. Neoproterozoic: 81. Great Smoky Mountains Rift Basin.

1.2.2.1 Proto-Oceanic Rift Basin Conceptual Model

The continental rift stage, or proto-oceanic rift, is characterized by the production of oceanic crust, which separates two passive continental margins as a result of lithospheric extension,

thinning and magmatic activity (Figure 10). Basaltic flow on top of a layer of serpentinized mantle forms a proto-oceanic crust triggered by a little melt from the mantle (Klingelhoefer et al. 2014). More intense mantle upwelling may occur as the spreading continues, supplying more melting and resulting in the creation of a thin igneous oceanic crust (Klingelhoefer et al. 2014).

This type of basin indicates a transitional stage between continental rift and passive margin basins (Section 1.2.2.2, Figure 11). A current example of proto-oceanic rift is the Red Sea. Sediments are supplied from the adjacent highlands of the uplifted fault blocks.

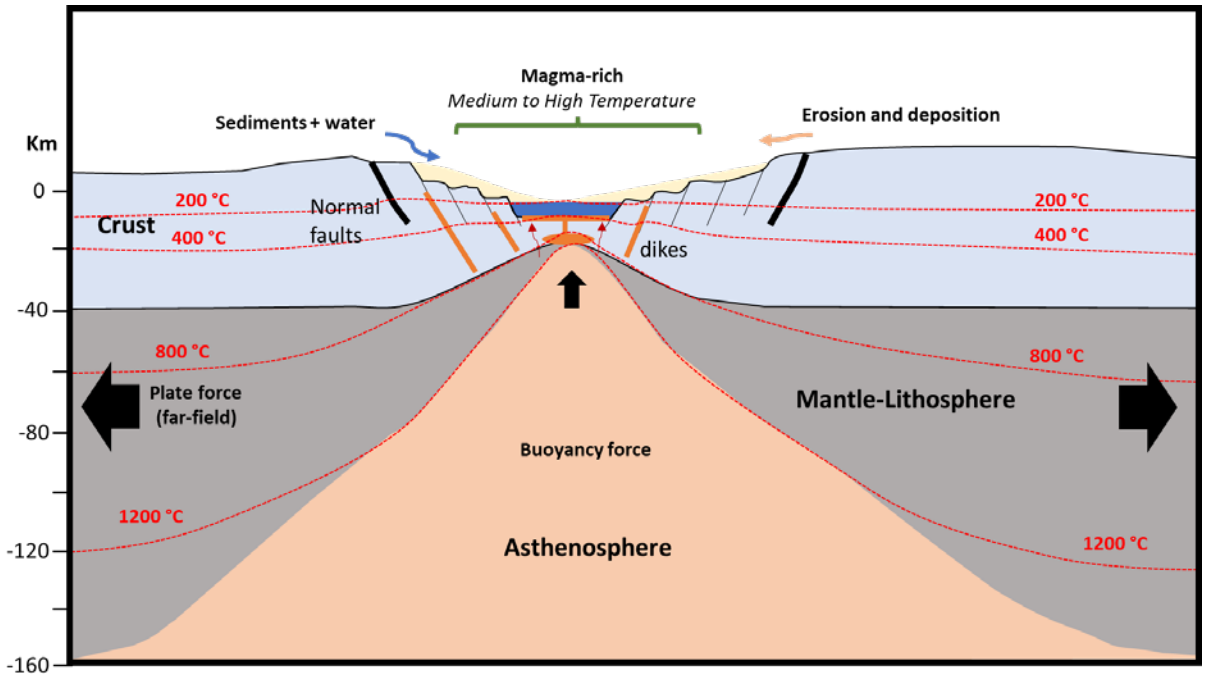

Figure 10. Proto-oceanic basin geothermal conceptual model with schematic isotherm distribution (red lines)

1.2.2.2 Passive Margin Basin Conceptual Model

Passive margin basins evolve during continental break-up, opening of oceanic basins (e.g., the Atlantic Ocean) and then close-up of the ocean. Passive margin basins can be subclassified as modern or ancient margins, depending on the stage of evolution. In general, modern passive margins contain sediments accumulated only from the rift and drift stages, such as a continental and oceanic lithosphere across an igneous contact (Bradley 2008). Cenozoic passive margin basins are found in the eastern part of the United States and are associated with the extension of the Atlantic Ocean (Figure 11), such as the Gulf of Mexico Basin and the West Atlantic Basin. Most of Earth's first-order tectonic structures are passive edges, about 105,000 km. They range in age from 5 million to 180 million years, with an approximate mean age of 104 million years.

Passive margins are seismically inactive, and in mature examples, heat flows are close to normal (Allen and Allen 2013). Indeed, many of these passive margin basins are in the post-rift phase, where the high heat flow associated with rifting has a minimal effect. The amount of burial is the primary factor affecting the temperature regime of the source rock interval in the hydrocarbon context that can also have an important impact in the geothermal gradient (Figure 11).

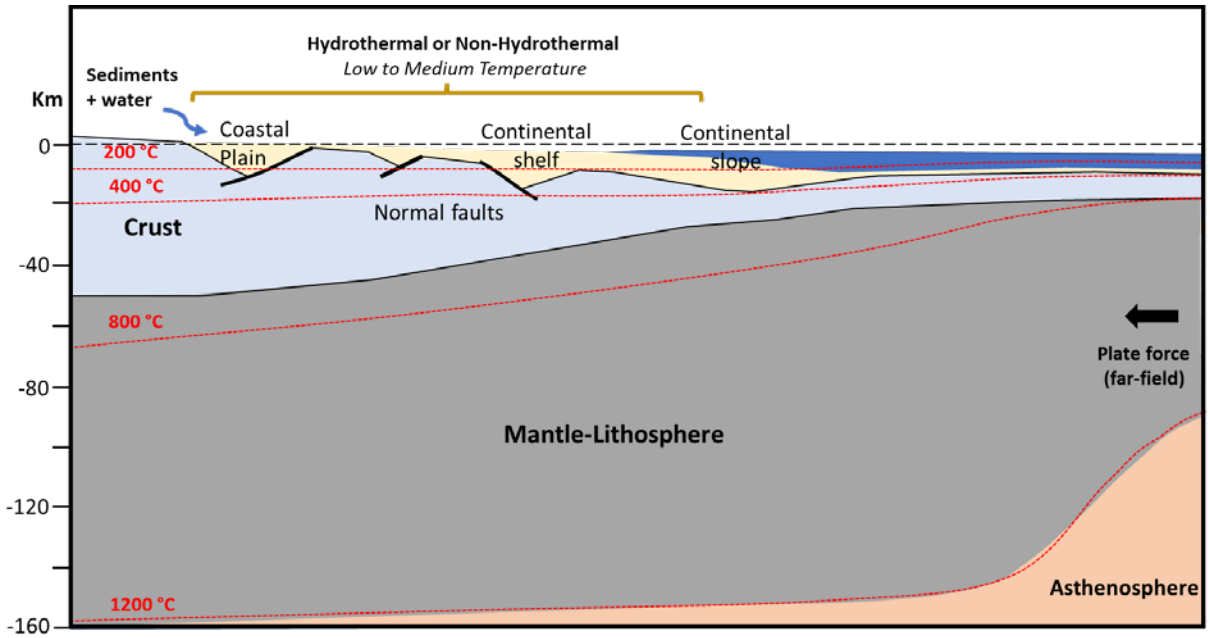

Figure 11. Passive margin basin geothermal conceptual model with schematic isotherm distribution (red lines)

1.2.2.3 Foreland Basins and Thrust Belts Conceptual Models

A foreland basin is defined as a basin located between an orogenic belt (see Section 2) and a craton (Allen et al. 1986). The term foreland basin refers to thick sedimentary succession formed in the undeformed areas of an orogen resulting from a convergent tectonic margin (Dickinson 1984). Foreland basins are asymmetric, with maximum depths next to the orogen and wedge-shape (Figure 12) along its passive margin (Allen et al. 1986). They comprise some of the Earth's greatest sedimentary accumulations (DeCelles et al. 2011).

Significant crustal subsidence occurs in foreland basins due to the weight of the thickened crust and the loading sediments deposited from the erosion of the mountain belt (Hervey et al. 2014). The non-thickened lithosphere is bent downward because of this process, creating localized zones of extension and normal faulting within a compressional plate tectonic margin (Moeck 2014).

There is scientific consensus on the theory that foreland basins form by a flexural isostatic subsidence mechanism (Garcia-Castellano and Cloetingh 2011). Different foreland basin types have been recognized to form in convergent plate tectonic settings: retroarc, collisional, and retreating collisional. The following factors are recognized to be important drivers for flexural subsidence in foreland basins: horizontal compression, slab pull, sometimes slab retreat, lateral asthenospheric push due to the opening of the back-arc, and delamination of the retreating mantle lithosphere (Garcia-Castellano and Cloetingh 2011). It has also been suggested that lateral variations in plate rigidity are key factors controlling geometry and drainage history of foreland basins.

Section 2, Orogenic Belt Geothermal Play Type, describes this type of geothermal play in more detail.

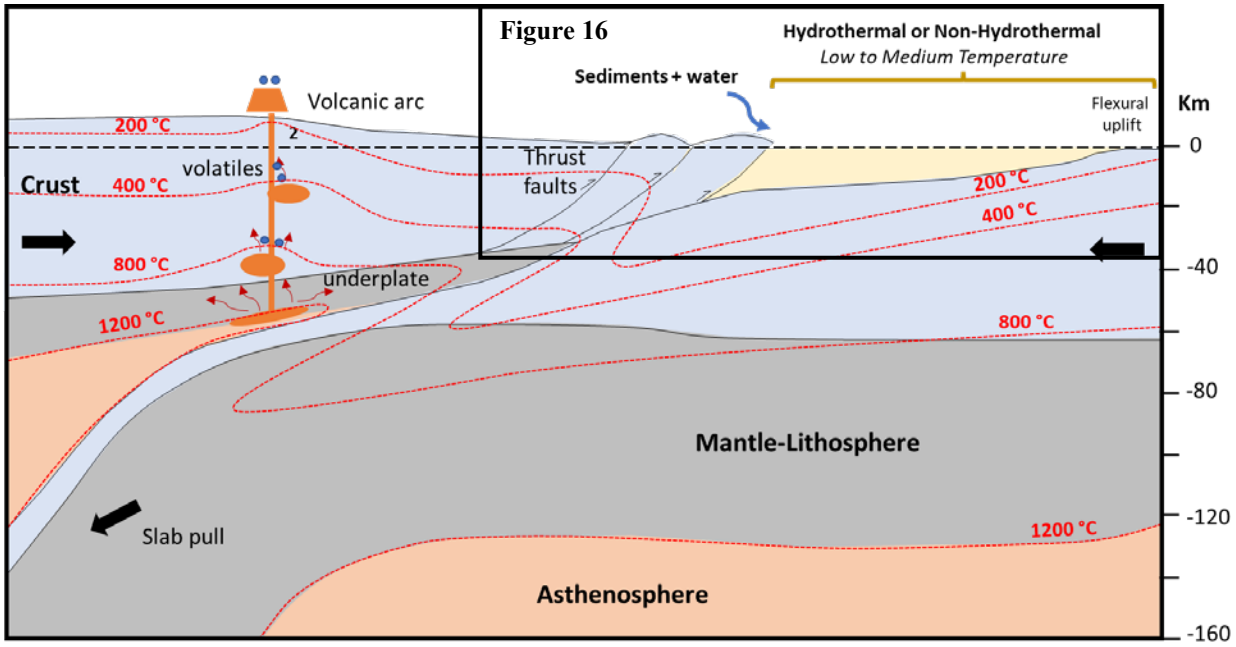

Figure 12. Foreland basin geothermal conceptual model with schematic isotherm distribution (red lines)

1.2.2.4 Borderland Basin Conceptual Models

The perfect example of a borderland is the southern California and Los Angeles basins (Figure 9). This is an area that experiences large-scale oblique crustal extension and translation associated with the initiation and development of the Pacific-North American transform plate boundary (Schindler 2010). The Southern California Continental Borderland consists of block-faulted continental crust that includes part of the San Andreas transform-fault plate boundary (Hein et al. 2007).

This borderland basin has a complex basin and range topography that is characterized by a regional structural transition from strike-slip and transpressional oblique-slip faults to reverse and thrust faults (Schindler 2010). The borderland consists of a series of shallow ridges separating deep sedimentary basins (Schindler 2010). Basins are relatively filled with pelagic, hemipelagic, and turbidite sediments, and they are characterized by high degree of thermal maturation of organic matter (Cenozoic sedimentary rocks) and the presence of hydrocarbon (Hein et al. 2007).

Due to thinning of the continental crust and Neogene volcanism, the California borderland basin has high heat flow and geothermal gradients (Hein et al. 2007). High heat flow and tectonic stresses promote circulation of fluids along a variety of faults (normal, thrust, strike-slip, detachment) that bound and cut the basins and ranges (Hein et al. 2007). Lee and Henyey (1975) reported geothermal gradients from short cores from 90° to 200°C/km. This high heat flow has driven hydrothermal circulation, and crustal thinning may have been brought on by spreading associated with pull-apart basins (Legg 1991). Geothermal systems are also present in these borderland basins such as the Geysers (which is the largest geothermal field worldwide), Salton Sea, Imperial Valley, and Coso geothermal fields.

1.2.3 Sedimentary Basin—Intercratonic

The intercratonic basins classification by Coleman and Cahan (2012) includes three types of basins: (1) passive margin extending onto oceanic crust (see Section 1.2.2.2; Figure 11), (2) accreted back-arc basin (see Section 1.2.4.1; Figure 15), and (3) accreted fore-arc basin (see Section 1.2.4.2; Figure 15). Figure 13 show all the intercratonic basins in conterminous U.S. and Alaska.

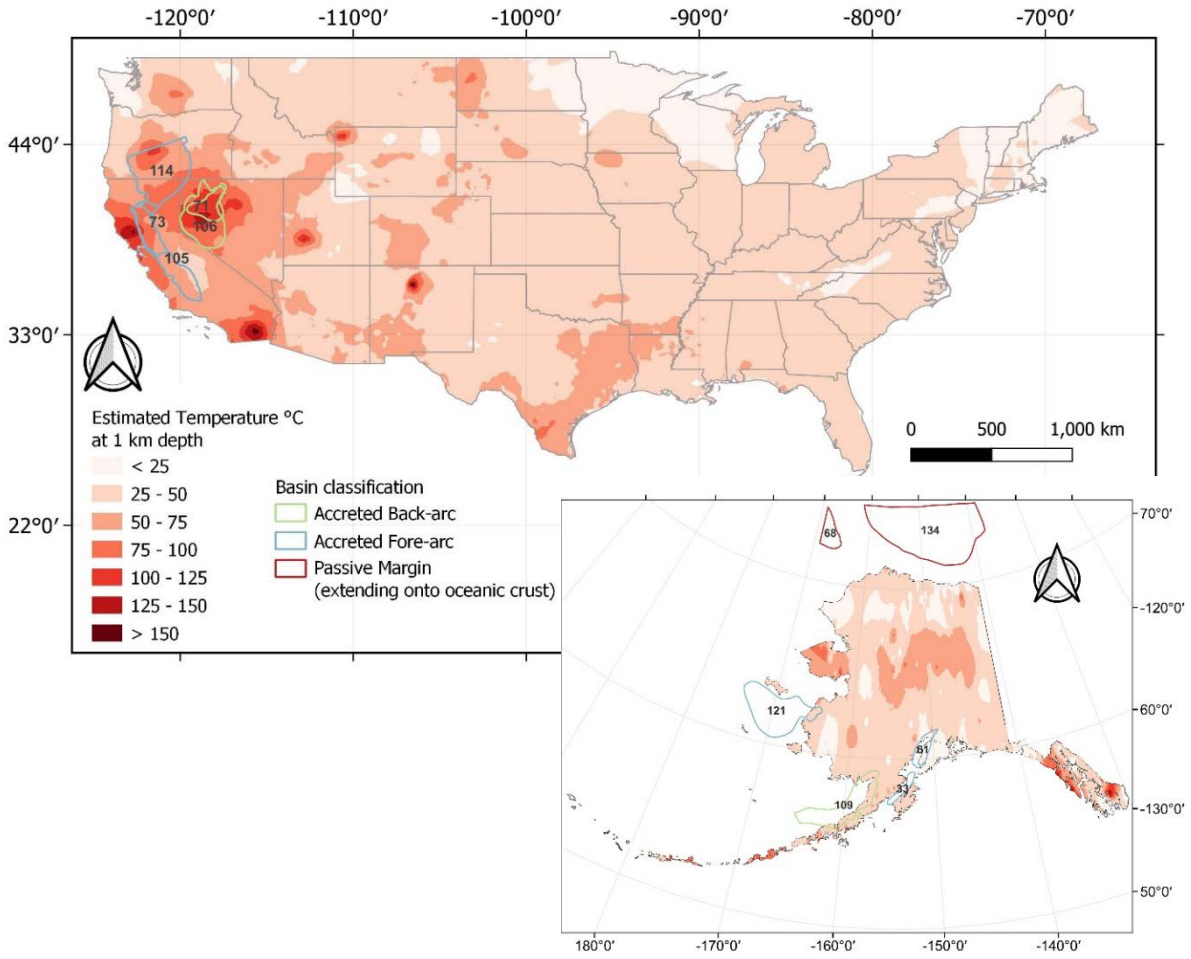

Figure 13. The surface of intercratonic basins in the conterminous United States and Alaska overlapping the estimated temperature at 1 km

Map of intercratonic basins in the conterminous United States and Alaska by Coleman and Cahan (2012); estimated temperature map of the conterminous U.S. from Mullane et al. (2016), modified after Blackwell et al. (2011); estimated temperature map of Alaska from Davalos-Elizondo et al. (2023), modified after Batir et al. (2016). Cenozoic: 68. North Chukchi Basin; 121. St. Matthew- Hall Basin; 134. Canada Basin; 164. Bristol Bay Basin. Mesozoic: 33. Shelikov Basin; 61. Cook Inlet Basin; 73. Sacramento Basin; 105. Great Valley Basin; 114. Hornbrook-Ochoco Basin. Paleozoic: 41. Auld Lang Syne Basin; 106. Havallah Basin.

1.2.4 Sedimentary Basin—Oceanic

Oceanic basins are covered by water below sea level. The oceanic basin classification by Coleman and Cahan (2012) includes two types of basins: (1) back-arc basin, and (2) fore-arc basin. Figure 14 shows all the oceanic basins in the conterminous United States and Alaska.

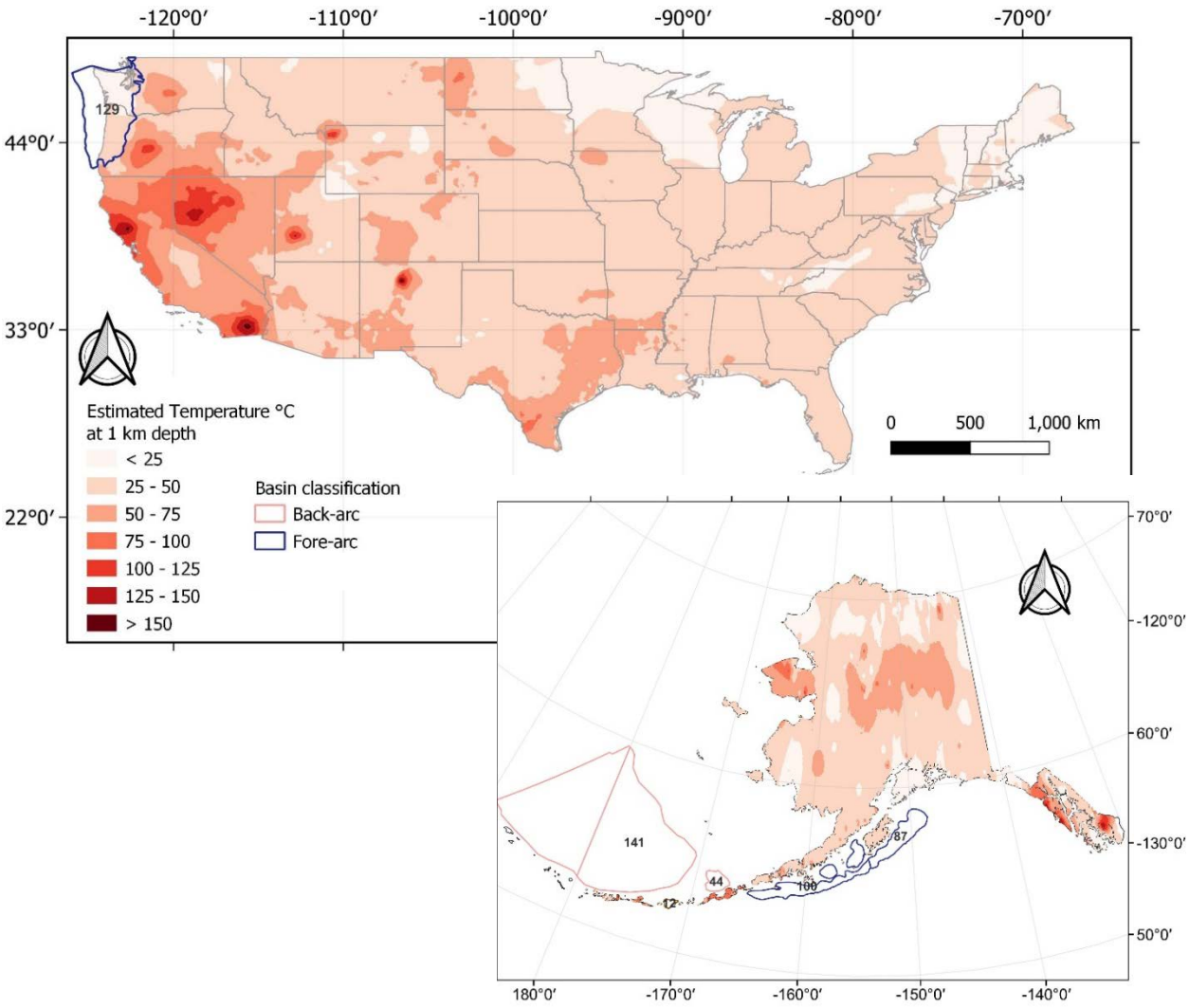

Figure 14. The surface of oceanic basins in the conterminous United States and Alaska overlapping the estimated temperature at 1 km

Map of oceanic basins in the conterminous United States and Alaska by Coleman and Cahan (2012); estimated temperature map of the conterminous U.S. from Mullane et al. (2016), modified after Blackwell et al. (2011); estimated temperature map of Alaska from Davalos-Elizondo et al. (2023), modified after Batir et al. (2016). Cenozoic: 12. Amukta Basin; 44. Umnak Plateau Basin; 87. Stevenson-Albatross Basin; 100. Sanak-Shumagin-Tugidak Basin; 129. Western Washington–Oregon Basins; 141. Aleutian Basin.

1.2.4.1 Back-Arc Basin Conceptual Model

A back-arc basin is found in convergent plate boundaries. However, back-arc basins are defined as regions of extension at convergent plate margins where rifting and seafloor spreading develops on the overriding plate (Sdrolias and Muller 2006). They are the result of tensional forces caused by the rollback of the subducted plate (Figure 15). Back-arc basins are typically elongated and narrow and found in subduction zones where the subducted plate is very old and dense to cause a rollback. Once back-arc extension is established, rollback of the subduction hinge appears to be the primary force responsible for the continued creation of accommodation space (Sdrolias and Muller 2006). Sdrolias and Muller (2006) indicated that the driving mechanism for back-arc extension is a combination of surface kinematics, properties of the

downgoing slab, the effect of lateral mantle flow on the slab, and mantle wedge dynamics. Ancient back-arc basins are typically subducted or accreted (intercratonic basins, see Section 1.2.3), and their sediments are either lost or preserved only as a fragment in mélange sequences (Draut and Clift 2011).

1.2.4.2 Fore-Arc Basin Conceptual Model

Fore-arc basins form in convergent margins and in front of the volcanic arc (Fuller et al. 2006). The area between the trench and the volcanic arc is the fore-arc basin (Figure 15). Accommodation space in fore-arc basins is controlled by the geometry of the volcanic arc (Draut and Clift 2011). Foreland basins can form as a natural consequence of intra-plate coupling at subduction zones (Fuller et al. 2006). Fore-arc basins do not need active subsidence to form, but a slight uplift is necessary to allow sediments to erode and deposit between the uplifted region and the volcanic arc (Draut and Clift 2011). The geometry of fore-arc basins varies greatly depending on the mechanical characteristics of the basin lithosphere (Draut and Clift 2011). Sediments in the fore-arc before collision include mass-flow deposits from volcanic centers, volcaniclastic turbidites, ophiolitic debris, and pelagic sediments (Draut and Clift 2011). Fore-arc basins can be preserved during collision and even continue subsidy and sedimentation throughout the collision (intercratonic basins, see Section 1.2.3).

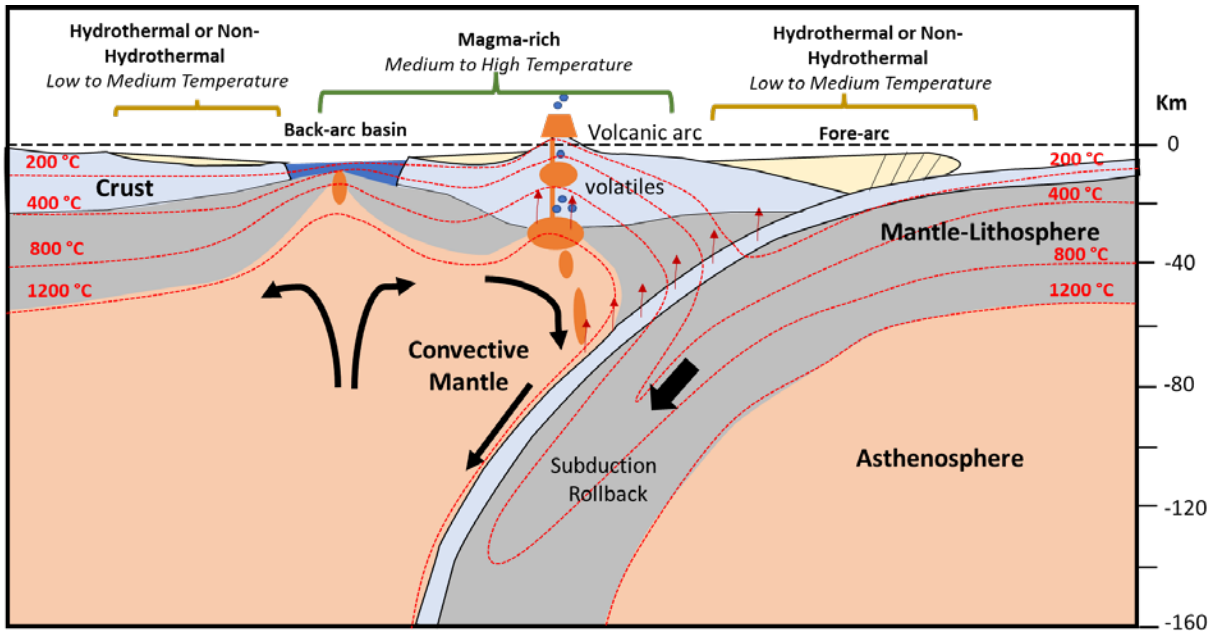

Figure 15. Back-arc and fore-arc basin geothermal conceptual model with schematic isotherm distribution (red lines)

2 Orogenic Belt Geothermal Play Types

Orogenic belt geothermal play types (OBGPTs) are rarely linked to hydrothermal systems; rather, they are the result of deep circulation systems associated with major deep faults in the crust (Moeck 2014). Conductive thermal gradient in OBGPTs can be lower beneath high mountains to about 15°–20°C/km and increase beneath a foreland basin to about 30°–50°C/km (Craw et al. 2005, Grasby and Hutcheon 2001, Hervey et al. 2014). In general, higher geothermal gradient temperatures are associated with the wedge-shaped areas of the foreland basin (see Section 1.2.2.3) where deeper potential aquifers rocks lie beside the orogen (Figure 16; Hervey et al. 2014).

The bulk-rock permeability of the host rock plays a major role in the creation of geothermal plays in mountain ranges. Particularly in locations of high topography, the permeability allows the meteoric water to infiltrate deeper. Active faults act as fluid flow pathways to reach discharge spring areas (Moeck 2014). The discharge of most of the water recharged in the mountains occurs on valley floors (Figure 16), which are roughly at the same height as the typical foreland basin elevation (Moeck 2014). The mountain belts and the related foreland basins are hydraulically isolated by the frontal fault of the foothills (Moeck 2014). The foreland basin is not adequately supplied with water for deeper circulation due to the short penetration depth of flowing meteoric water in mountain belts (Figure 16; Toth 2009).

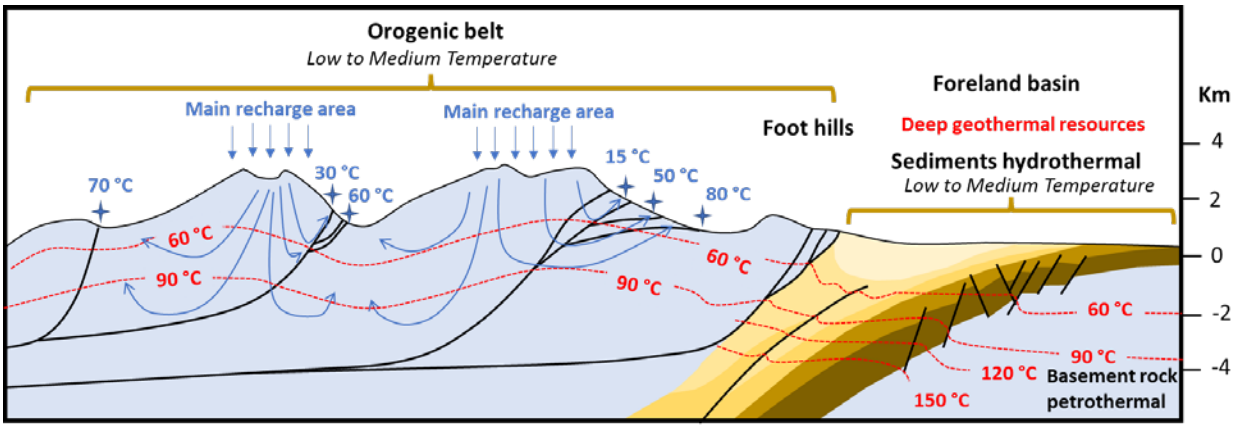

Figure 16. OBGPTs and related foreland basin

Schematic isotherm distribution shown with red lines; fault geometry and basin geometry shown with black lines; water flow (shown with blue lines) results from heat advection and topography controlled hydraulic head; discharge temperatures shown with blue stars.

Modified from Moeck (2014)

2.1 OBGPT Background

Recent studies of OBGPT have suggested that deep temperatures in geothermal reservoirs within an orogenic mountain belt have been undervalued (e.g., Diamond et al. 2018). Diamond et al. (2018) studied the penetration depth of meteoric water in the Grimsel Pass geothermal system in the Swiss Alps and suggested that higher enthalpy may be available around the upflow zones that was previously thought.

Other examples of OBGPTs are the Alpine-Himalayan orogenic belt, where Turkey has 90% low or medium enthalpy geothermal resources (Bilgin 2018). The most famous high-temperature geothermal zone is the Mediterranean-Himalayan orogenic belt, which is distributed in Yunnan, Tibet, and western Sichuan in China (Liao and Zhao 1999). However, in recent years other geothermal belt systems have started to be explored, such as the Sanjiang Orogenic Belt in the southeast Tibetan Plateau (Yi et al. 2021). This OBGPT is characterized by high and low enthalpies. The high-reservoir temperatures of geothermal waters controlled by regional faults heated after deep circulation have been estimated from silica-enthalpy mixing models from 175°–200°C to 200°–225°C (Yi et al. 2021). In contrast, low reservoir temperatures of geothermal waters controlled by the folded complex that were heated after shallow circulation have been estimated around 100°–125°C (Yi et al. 2021). Seismic data reported by Wang et al. (2003) shows that the crust of eastern Tibet has been thickened to 60–65 km, but a low-velocity anomaly zone at a depth of about 20 km has been interpreted as partial melting of the crust by Yang et al. (2020).

Some examples of geothermal reservoirs within foreland basins related to orogenic belts are the Molasse Basin of the Alps in Germany with over 40 MWe of geothermal power installed in the last decade (Bertani 2016), and the Western Canadian Sedimentary Basin associated with the Rocky Mountains with reservoir depths ranging from about 2,500 m to over 5,000 m, and temperatures ranging from 60° to 150°C (e.g., Banks and Harris 2018; Moeck 2014).

2.1.1 Examples of OBGPTs in the United States

In the United States, the Appalachian and the Rocky Mountain OBGPTs (see Figure 9; foreland basins and thrust belts) are poorly understood. The Western United States of the Cordilleran orogenic belt and foreland basin system (Figure 17) presented several geothermal potential areas that need more detailed studies and characterization. For example, in Colorado 127 thermal waters and hot water wells are emerging in the southern Rocky Mountains of southwestern Colorado, but little exploration has occurred at individual sites. There is currently no electric generation associated with OBGPT in the Appalachian and Rocky Mountains; however, there are some small direct-use developments.

Adjacent to the Rocky Mountain orogenic belt are the Denver and Raton Basins, which are located east of the foothills of the Rockies in the foreland basin and related to the orogeny. These basins have identified geothermal potential with temperatures in the range of 160°–210°C at 3–4 km depth for some regions, with an average heat flow of 90 mW/m^2 (Crowell et al. 2012).

A recent PFA study of hidden geothermal resources in the Appalachian foreland basin was conducted by Cornell University. This methodology may be applied to other foreland basins as a foundation of low-temperature (<150°C), because that study was focused on direct-use applications rather than on electricity production (Jordan et al. 2016). However, OBGPTs located in mountain ranges remain poorly understood and there are few studies focused on these types of geothermal systems in the United States.

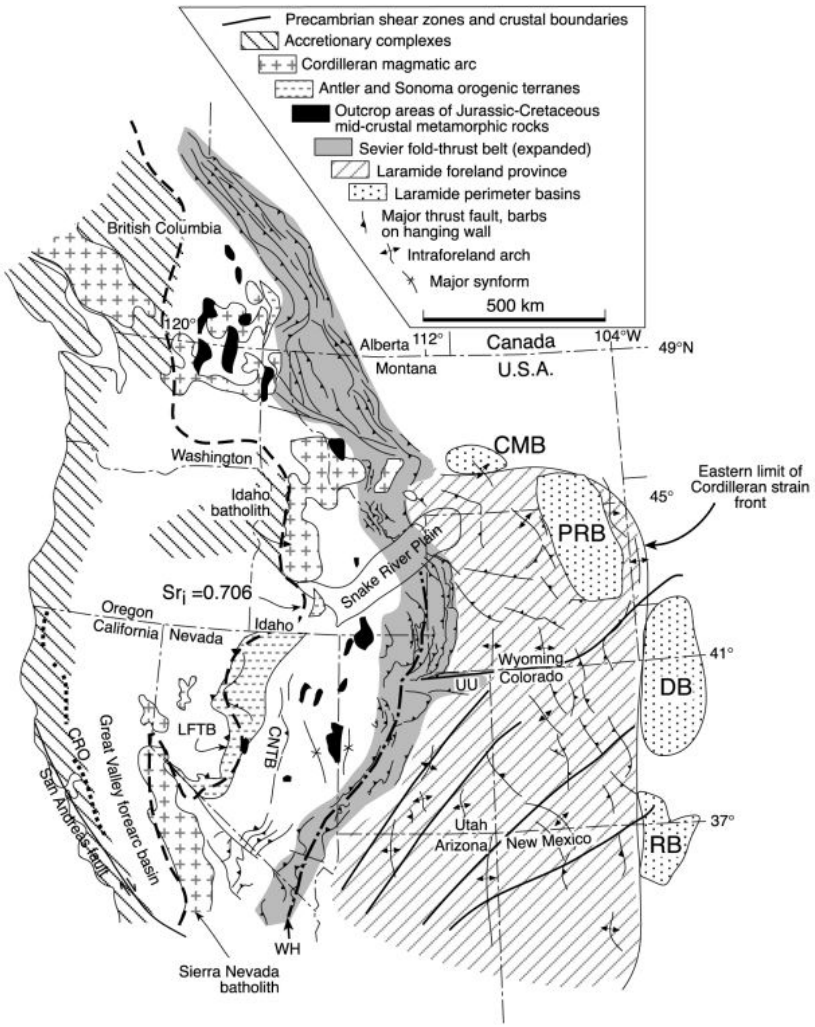

Figure 17. Tectonic map of the western United States, showing the major components of the Cordilleran orogenic belt

CMB: Crazy Mountains Basin; PRB: Powder River Basin; DB: Denver Basin; RB: Raton Basin

From DeCelles (2004)

2.2 OBGPT Classification and Geothermal Key Controls

OBGPTs can be divided into two different reservoir classifications: (1) a geothermal reservoir within an orogenic mountain belt (Figure 16); and (2) sedimentary reservoirs within foreland basins adjacent to orogenic mountain belts, as described in Section 1.2.2.3, see Figure 12. This section focuses on the first classification.

OBGPT consists mainly of a conductive thermal domain temporarily disrupted when cold groundwater infiltrates and reduces the temperature of the rock mass in high topography (Hervey et al. 2014). The discharge takes place in valley floors or shallow valley slopes (Figure 16) due to the relative shallow infiltration of recharge waters into the small width mountain belt valleys (Toth 2009; Hervey et al. 2014). The fluid must have enough time to get from the recharge location to the spring (Moeck 2014). Depending on the effective porosity of the rock, the transit

period for meteoric water in mountainous locations can range from a few decades to more than 5,000 years (Nimz et al. 1999).

The key geothermal controls of OBGPTs are high permeability rock formations (structurally or fracture-controlled), and circulating groundwater from advective heat transport (e.g., Moeck 2014). The infiltration water's transit duration, fluid circulation depth, rock permeability, major thrust fault geometry, lateral ramps, the tectonic setting, and the local stress field are factors that affect the temperature of hot springs and the geothermal system in general (see Table 3).

Table 3. Geothermal Key Controls of Orogenic Belts Influenced by the Formation and Evolution History and/or the Present Time Geological and Tectonic Settings

Geological and Tectonic Settings			
Geothermal Key Controls	***Formation and Evolution***	***Present Time***	***Related PFA: Critical Component****
Heat Flow		**x**	**H**
Fluid Chemistry	**x**		**F, S**
Fluid Dynamics		**x**	**F**
Faults and Fractures	**x**	**x**	**P**
Stress state		**x**	**P**

*H= Heat/Heat Flow, F= Accessible Fluid, P= Permeability/Porosity, S= Caprock/Seal—sometimes

3 Radiogenic Geothermal Play Types

A radiogenic geothermal play type (RGPT) is controlled by the presence of high-heat-producing (HHP) rocks, such as intrusive bodies containing anomalous concentrations of radioelements such as uranium-238 (^{238}U), thorium-232 (^{232}Th), and potassium-40 (^{40}K). Intrusive rocks such as granitoids (e.g., granite, granodiorites, tonalites) have the greatest amount and distribution of radiogenic elements in crustal rocks that influence on surface high heat flow and the geothermal regime of the upper crust (McLaren et al. 2006; McLaren and Powell 2014; Zhou et al. 2020). The radiogenic elements tend to concentrate toward the more evolved stages of a magma, therefore an increase in the heat production rate can be related to SiO_2 content (Artemieva 2011; Pleitavino et al. 2021).

High-grade metamorphism, metasomatism, partial melting, and fluid and melt migration are some of the processes that can transport ^{238}U, ^{232}Th, and ^{40}K to the middle and upper crustal levels (Taylor and McLennan 1986). Age-related reductions in heat output brought on by radioactive decay occur differently for various rock types (Artemieva et al. 2017). The most radioactive granites are A-type (anorogenic), and many of them intruded in the Middle Proterozoic, suggesting that large plate reorganizations triggered a sudden shift in the geodynamic conditions for granitic magma formation (Artemieva et al. 2017).

In these play types, radioactive decay of ^{238}U, ^{232}Th, and ^{40}K within HHP rocks cause a localized heat anomaly responsible for elevated geothermal gradients, driving low-temperature convective geothermal systems to form where structural controls such as open faults and fractures allow permeability. Geothermal fluids associated with intrusive RGPTs are thus often enriched in B, Li, and F, due to circulation within plutonic rocks enriched in these elements (e.g., early Tertiary granites of Interior Alaska; Thompson and Newberry 2000).

RGPTs are poorly understood—their existence is often attributed simply to deep circulation of meteoric water along faults and fractures. While structures such as faults and fractures commonly control the upwelling of RGPTs, “deep circulation” GPTs as exemplified by geothermal systems in the Basin and Range area are quite different with respect to heat source, tectonic setting, geologic features, and fluid chemical characteristics. Kolker (2008) proposed an alternative model for geothermal resources in central Alaska: radiogenic heating from HHP plutons. Anomaly high U, Th, and K contents in plutons and the helium isotope signatures of CAHSB fluids, which point to a solely crustal origin (with no mantle input), support this concept. Calculations of heat generation confirmed the viability of this concept; however the hydrothermal convection systems seem to be somewhat small-scale and temporally constrained. Convecting fluids require permeability channels, which small-scale faults and fractures offer.

All convective hydrothermal systems, whether they are magmatic, deep circulation, or radiogenic, require permeability pathways of sparsely spaced fractures and/or faults in order for groundwater to effectively convect through or around the heat source. This can be confusing when separating RGPTs from "deep circulation" play types. Therefore, considering that the term "deep" is vague, all convective geothermal systems are fundamentally profoundly circulating groundwaters. The heat source for the usual deep circulation geothermal systems, however, is connected to an anomalous thermal gradient, which is associated with active, broad-scale (>100 km long surface expression) normal faults in extensional settings. In turn, a deep mafic intrusion

may produce an atypical temperature gradient, giving rise to confusion with the "magmatic" type (Kolker 2008).

RGPTs are likely to be low- or medium-temperature (<150°C) based on geothermometry, hydrothermal alteration mineralogy, heat transfer models, and other evidence (Miller et al. 1975; Kolker 2008; Zhang et al. 2022). RGPT can be convection-dominated or conduction-dominated, which likely depends on the stress state of the host rocks. Since temperatures are low, specific stress conditions are required to cause hydrothermal convection. In some HHP environments, multiple distinct episodes of hydrothermal activity are observed, for example in Cornwall, England (Kolker 2008). This can cause additional challenges in interpreting geologic and geophysical data sets due to difficulty distinguishing between present-day hydrothermal circulation episodes and older-extinct hydrothermal circulation episodes.

Better understanding of the geologic mechanisms driving RGPTs could advance deployment of geothermal heat-and-power microgrids in states like Alaska, Idaho, and Montana, and possibly others like Colorado, Arizona, New Mexico, and Utah. This could support the goal of providing baseline heating and electrical load in rural and remote communities from a sustainable source that is independent of external power, increasing the resiliency of power supply and decreasing cost over a project lifetime (Zody and Gisladottir et al. 2023).

3.1 RGPT Background

Several authors have argued that RGPTs are quite distinct from “deep circulation” GPTs, as exemplified by geothermal systems in Basin and Range (Cathles et al. 1997; Kolker 2008); for one thing, they tend to be lower-temperature resources. Chemical geothermometers applied to hot springs near radiogenic plutons suggest subsurface temperatures in the range of 80° to 150°C (Miller et al. 1976). Based on three different pieces of information, the geothermal reservoir fluids connected to the one generating geothermal system (Chena Hot Springs, Alaska) appear to be 120°C or lower: (1) hydrothermal alteration mineral assemblages in well rocks (heulandite, smectite, cryptocrystalline SiO_2 and sulfides); (2) SiO_2 and Na-K chemical geothermometry; and (3) homogenization temperatures measured in fluid inclusions in quartz from well cuttings (Kolker 2008). However, there are rare high-temperature RGPT resources, such as the granitoid of western Sichuan, Tibetan Plateau (Zhang et al. 2022).

Felsic igneous rocks are the main major source of the radioactive elements U, Th, and K. Felsic igneous rocks typically have a U content of 4 ppm and a Th concentration of 18 ppm. Average U content in felsic igneous rocks is 4 ppm, whereas average Th concentration is 18 ppm. For instance, the typical U content for sedimentary rocks ranges from 1.3 to 3.2 ppm, whereas it is just 0.8 ppm for mafic igneous rocks (Eakins et al. 1977). The long half-life radioactive isotopes 40K, 235U, 238U, and 232Th decay to produce radioactive heat in granitic rocks. U is very soluble and mobile under oxidizing circumstances, although Th is not. In Mesozoic and Cenozoic plutonic rocks in the western United States, U contents have been found to be unusually high (Marjaniemi and Basler 1972).

HHP and significant post-magmatic hydrothermal convection were demonstrated to result from abnormally high radioactive element concentrations in southwest England granites (Fehn 1985). According to Durrance (1985), HHP granites undergo a several million-year cycle that includes heating from radioactive decay with little conductive heat loss, inflation as a result of the

heating, fracturing as a result of the inflation, convective groundwater circulation, and finally deflation and cooling as a result of effective convective cooling. For granites from Cornwall, England, radiometric dating has shown at least four such cycles (Stone and Exley 1985). Furthermore, the creation of heat in granites can lead to thermal expansion-induced fracture (Durrance 1985), which creates the vertical permeability necessary for convecting fluid circulation (Kolker 2008).

In countries like Brazil, China, Taiwan, India, Canada, Greenland, United States, Canada, Iran, Uganda, and Kenya, there are several radioactive (HHP) plutonic bodies. Granite, alkali granite, syenite, pegmatite, and (or) related rock types are frequently found in the plutons. There are low-temperature thermal zones in many of these sites as well, although few studies have linked radioactive granitic structures to active hydrothermal circulation (Kolker 2008). According to Brugger et al. (2005), a zone of abnormally high heat flow caused by highly concentrated radioactive elements in a neighboring plutonic body is what is responsible for the heat driving of the Paralana hot springs system in South Australia (Kolker 2008).

A method for calculating heat generation capacity (A) of the decay of the radiogenic isotopes (^{232}Th, ^{235}U, ^{238}U, ^{40}K) from plutonic rocks is given by Rybach (1981):

$$A\ (\mu W/m^3) = 10^{-5}\rho\ (9.52cU + 2.56cTh + 3.48cK), \quad (1)$$

where c is the concentration of the radioactive elements U and Th in ppm and K in %, and ρ is the rock density.

Another type of RGPT is the HHP granitoids that are buried in the proximity of an insulating sedimentary cover, where information about the stratigraphy, thickness, and thermal conductivity are important factors to consider (Lacasse et al. 2022).

3.1.1 Alaska Example of RGPT

Kolker (2008) studied this type of geothermal occurrence in central Alaska as part of a Ph.D. thesis supported by the National Science Foundation and related to a DOE-funded Geothermal Resource Evaluation and Definitions program (GRED III) study. The goal of the GRED III project was to ascertain if one such resource—at Chena Hot Springs, more than 50 miles from Fairbanks—had the ability to provide enough electricity sustainably to make the expense of a transmission line to Fairbanks worthwhile. As a part of the GRED III project, geological explorations, thermal gradient drilling, fluid geochemistry, aerial and ground-based geophysics, hydrology, reservoir engineering, and remote sensing studies were all carried out. The interaction between the shallow geothermal system and the deeper geothermal reservoir was also investigated using a series of shallow temperature gradient holes that were bored to depths of up to 300 m. Most of the following information is paraphrased from the Kolker (2008) Ph.D. thesis, published by the University of Alaska, Fairbanks.

A broad zone of geothermal activity extends from Alaska's Seward Peninsula to Canada's Yukon Territory. The Central Alaskan Hot Springs Belt (CAHSB) is the new name for this group of hot springs. Within the CAHSB, there are more than 30 hot springs regions. Hot springs are comparable in composition (alkali-chloride type fluids; Miller et al. 1976) and temperature (between 30° and 88°C) while spanning multiple distinct geologic provinces.

The local geology of most hot springs sites in Alaska is poorly constrained—this applies to the CASHB as well as other hot springs in southeast and southwest Alaska (Figure 18; Motyka et al. 1983: Alaska Division of Geological and Geophysical Surveys). Studies of geothermal potential in Alaska are significantly hampered by the scant subsurface data that are currently accessible. When attempts are made to interpolate these data, the scarcity of data raises the threshold of uncertainty because the temperature and other properties of hot springs in the CASHB are relatively localized.

The active volcanism and tectonic setting in Alaska, however, point to the possibility of geothermal resources (Kolker 2008). Alaska has more than 108 hot springs that are currently known in the state (Motyka et al. 1983). Between 1970 and 1985, the majority of Alaska's geothermal exploration activity was carried out with DOE funding. All known surface expressions of geothermal systems in Alaska were cataloged and sampled during this time by the Division of Geological and Geophysical Surveys. The geothermal resources of Alaska 1:2,500,000 scale map (Motyka et al. 1983) provides a summary of this effort.

Preliminary exploration studies were carried out in the Aleutian arc, western Alaska, and southeast Alaska. Three locations—Makushin, Mt. Adagdak, and Pilgrim Hot Springs—have undergone geothermal drilling. These early exploratory activities did not include the CAHSB. The first geothermal power plant in Alaska was erected in 2006 at Chena Hot Springs (Figure 18), which is located in the eastern CAHSB and 60 miles northeast of Fairbanks. It is the world's lowest-temperature geothermal resource that has ever been used to produce electricity. This created numerous opportunities for using Alaska's low-temperature resources, which had previously been ruled out as possible locations for power generation (Davalos-Elizondo et al. 2023).

The only geothermal power facility in Alaska is still Chena Hot Springs. It utilizes a 73°C low-temperature geothermal resource to generate 730 kW (Chena Power Company; Boyd et al. 2015), in addition to many cascaded direct uses such greenhouse heating, absorption chilling, district heating, and others (Batir et al. 2016, Boyd et al. 2015). Chena Hot Springs uses 4°C cooling water from a stream, allowing for a temperature differential across the power system that results in a tolerable cycle efficiency (Lund 2006).

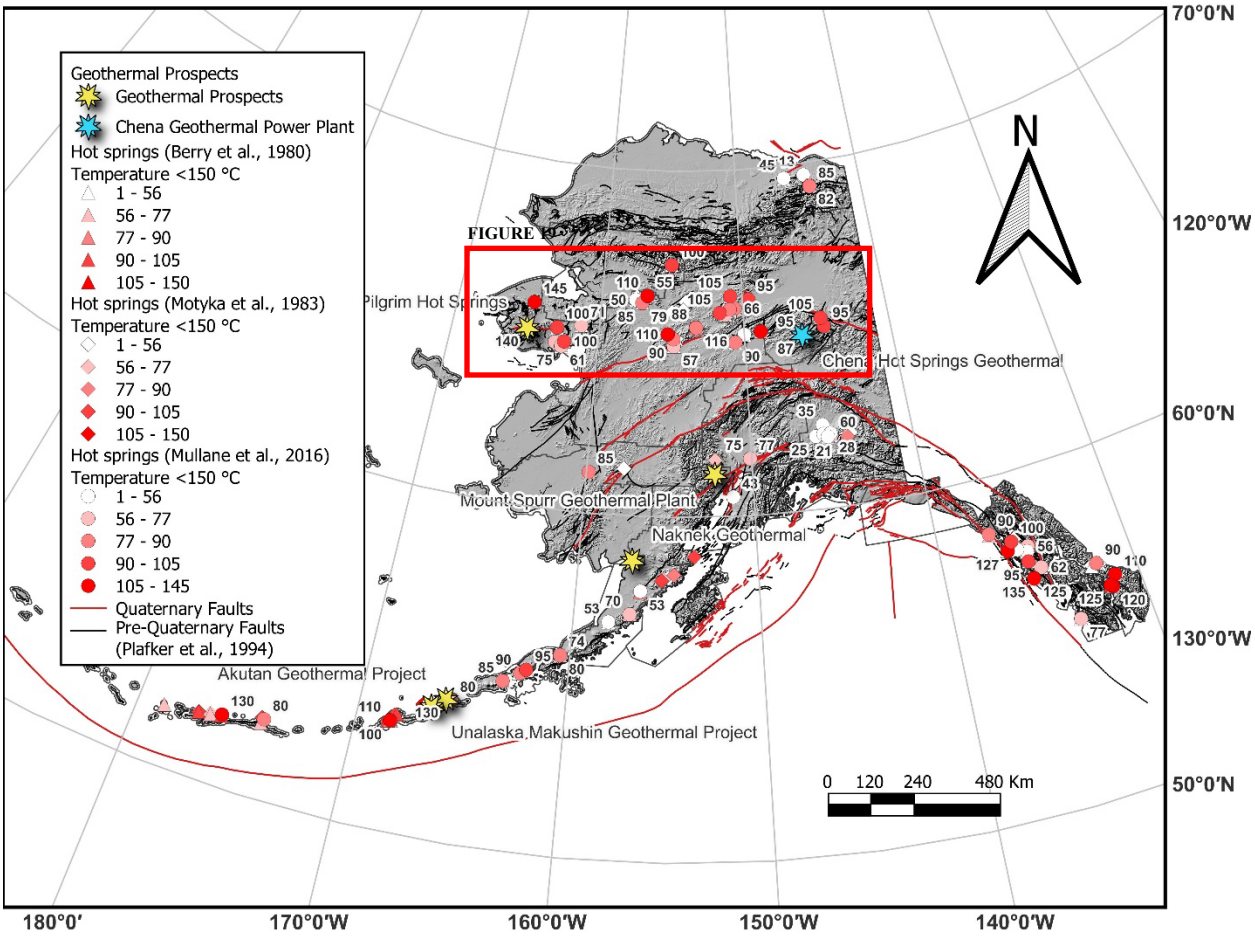

Figure 18. Geothermal resources in Alaska

Red rectangles delineate hot springs that are part of the CAHSB.

Map from Davalos-Elizondo et al. (2023)

According to Miller et al. (1975), hot springs in interior Alaska are typically remote from any Quaternary volcanic centers and do not show any signs of magmatic input. There are few exceptions in Alaska's extreme western region, where an active rift zone may be contributing to high crustal heat flow and the potential existence of shallow magma, even if the interior hot springs do not appear to be related to recent volcanism (Turner and Swanson 1981).

In or close to granitoid plutons that date from the Mesozoic to the early Tertiary, almost all of the hot springs in central Alaska are found. According to research by Miller and Bunker in 1976 and Thompson and Newberry in 2000, many of the bodies had abnormally high quantities of the radioactive isotopes U and Th. Many hot springs in the CAHSB have a linear surface expression, which suggests structural control, and thermal upwelling frequently occurs at pluton-country rock contacts. A few large faults, nevertheless, have been found close to a couple of the hot springs (Figure 19).

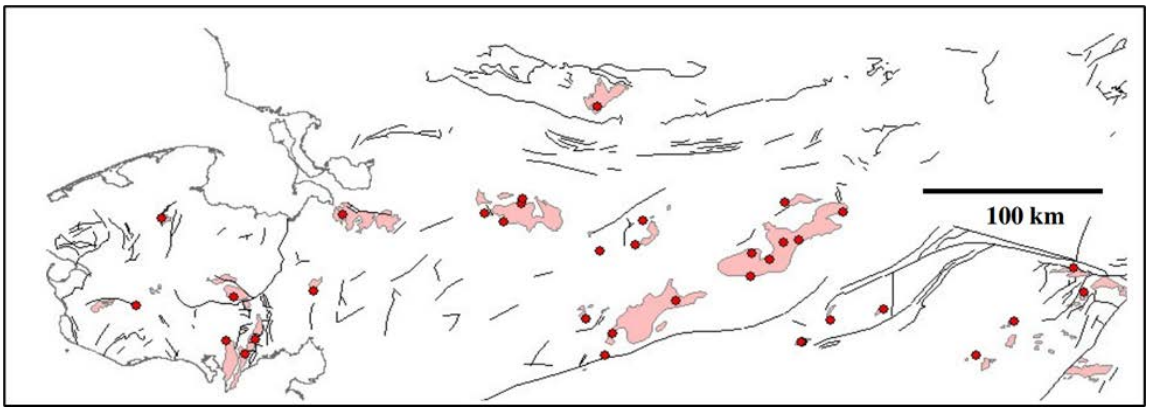

Figure 19. Central Alaskan Hot Springs Belt (CAHSB)

Pink shapes = plutons; red shapes = hot springs; black lines = mapped faults

Note: few of the faults shown are known to be active.

From Kolker (2008)

Based on airborne radiometric data, U concentrations in certain regions of the intrusive bodies are approximately five times higher and Th two to three times higher as in other regions (Kolker 2008; Figure 20). In Alaska, this highly evolved phase of intrusive activity with enrichment in U, Th, Rb, F, B, and Li appears to be of mid-plate origins and have occurred primarily in the Paleogene period (~60 Ma).

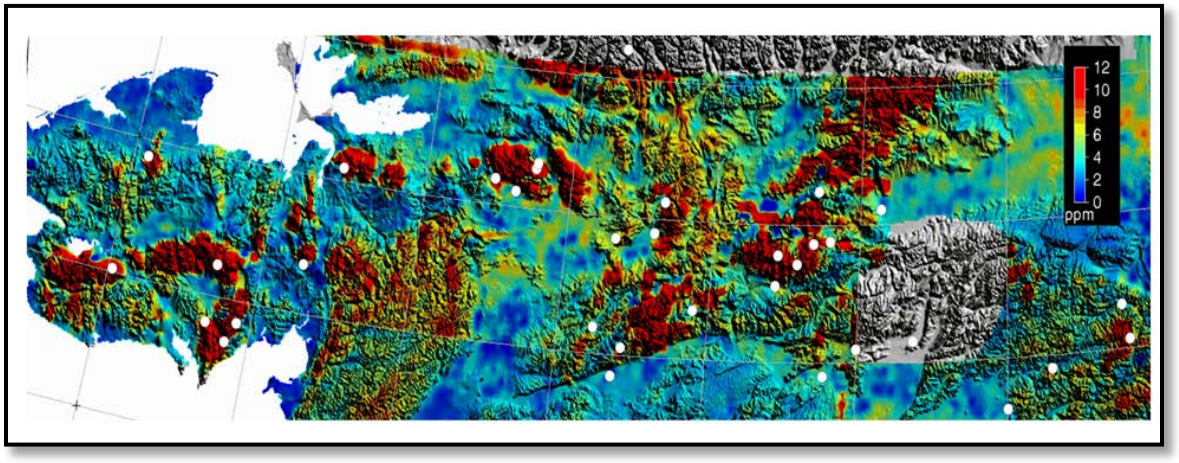

Figure 20. Hot springs in the CAHSB (white circles) and surface equivalent Th concentrations draped over a shaded Alaskan digital elevation map

Colors represent equivalent Th in parts per million (ppm) averaged over the upper meter of the land surface, from merged airborne gamma-ray surveys with 6 mile spacing. Areas with no data shown in grey.

Surface equivalent Th concentrations from Saltis (1999); figure from Kolker (2008).

The airborne radiometric data are consistent with X-ray fluorescence (XRF)-determined values for U and Th in the main portions and the east margin of the Chena pluton. Figure 21 displays XRF data from four rock types at Chena Hot Springs, showing that Paleogene granites have radioelement concentrations 4–10 times higher than surrounding rocks (Kolker 2008).

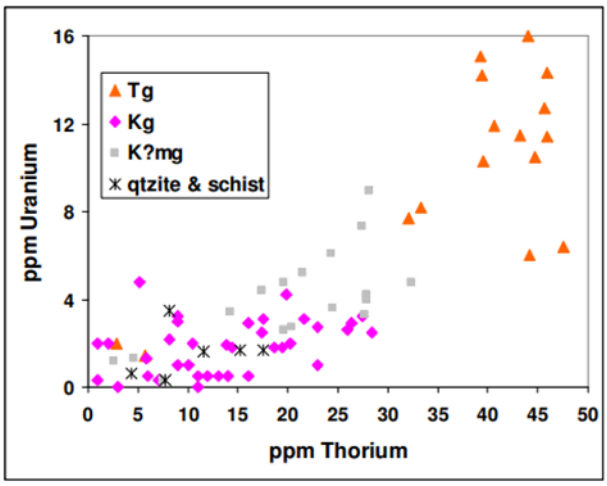

Figure 21. Uranium and thorium concentrations in rocks from Chena pluton, an HHP granite in Alaska

Tg = granitic rocks of likely early Paleogene period; Kg = granitic rocks of Cretaceous age or older; K?mg = metamorphosed granitic rocks of likely cretaceous age or older; qtzite & schist = Paleozoic quartzites and schists.

While there are intrusive bodies of various sorts and ages along the CAHSB, only granite and syenite plutons from the late Cretaceous and Paleogene have geothermal activity. Anomalous quantities of U and Th are regularly found in rock samples from late Cretaceous and Paleogene age plutons (Kolker 2008). Numerous separate alteration events can be seen in multiply brecciated and multiply re-annealed rocks, which may indicate faulting in numerous episodes or fast expansion associated with repeated boiling of geothermal fluids (Kolker 2008).

3.1.2 Other Examples of RGPT

According to Brugger et al. (2005), subsurface plutonic masses are likely to have generated radiogenic heating that produced the Paralana hot springs in South Australia. According to Brugger et al. (2005), 507 tons of the Paralana gneiss or 4,300 tons of British Empire granite (average 16 ppm U, 11 ppm Th) are needed to elevate the temperature of 1 kilogram of water by 65°C over the course of a year.

Brazil has numerous conduction-dominated RGPTs—a recent study conducted by Lacasse et al. (2022) integrated a geothermal assessment of EGS resources. They identified geothermal prospects in the Tocantins and Borborema provinces. Results by the National Observatory showed a surface heat flow of over 60 mW/m^2 and an excess temperature above 100°C at depths between 3 and 6 km.

Another recent study in the Gonghe Basin in the northeastern Tibetan Plateau studied the implications of HHP in hot dry rock geothermal resources. They estimated production values of 1.21–2.02 $\mu W\ m^{-3}$ for the sedimentary cover and 1.17–5.81 $\mu W\ m^{-3}$ for the basal granitic rocks (Zhang et al. 2020). Hot dry rock with temperatures exceeding 180°C are reported in this region.

The Cornwall geothermal power plant in the United Kingdom is in a RGPT, and the main heat source is the HHP Cornubian granite (Farndale and Law 2022). A production well has been drilled to 5,275 m MD and deviating from 3,390 m, it is the deepest onshore well in the United

Kingdom and has successfully encountered temperatures of 180°C (Farndale and Law 2022). It has been expected to generate 2–3 Mwe during 2023 (Farndale and Law 2022).

3.2 RGPT Classification and Geothermal Key Controls

An unofficial classification for RGPT exists; however, we propose a classification based on studied geothermal systems in particular locations (see Figure 22): (1) non-buried or exhumed HHP plutons (e.g., Chena, Alaska; Sierra de Cordoba, Argentina; Western Sichuan, China; Cornwall, UK); (2) buried HHP plutons in sedimentary basins (e.g., Western Canada Sedimentary Basin; Gonghe Basin, China; Cooper Basin, Australia); and (3) sediments with high concentrations of radioactive elements eroded from near HHP plutons (e.g., Karoo Basins, Africa).

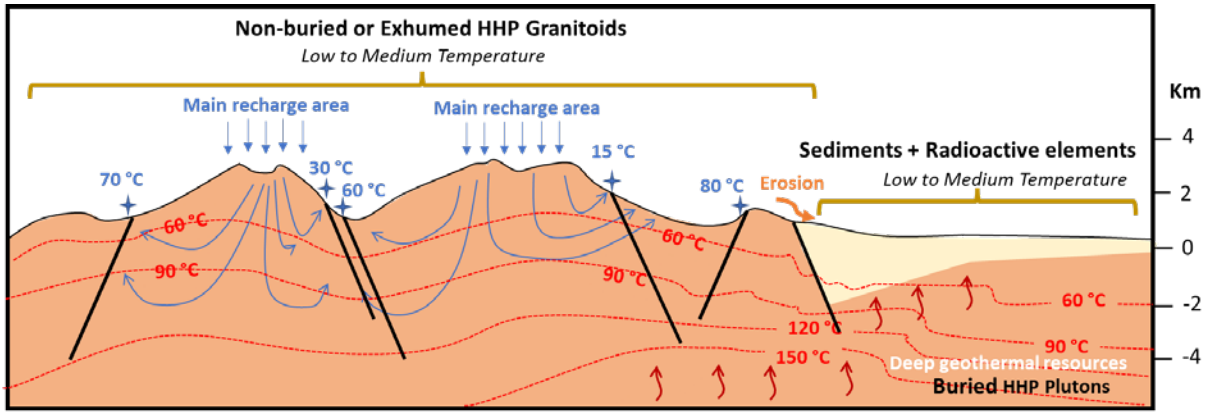

Figure 22. RGPTs and related sedimentary basin

Figure shows schematic isotherms distribution (red lines), fault geometry and basin geometry (black lines), and water flow (blue lines).

A systematic approach to locating geothermal resources from radiogenic heating from HHP rocks currently does not exist. We propose an approach following PFA framework that identifies key components of a RGPT system, associates those with geological controls, and then identifies relevant data sets.

Some of the critical components in radiogenic geothermal plays (Table 4) include magma type (pluton lithology) and radioelement concentration, size of pluton, fluid chemistry, the degree and type of hydrothermal alteration, and the presence/orientation of faults and fractures, the tectonic setting, and the local stress state. This impacts the three major hydrothermal controls as identified by geothermal PFA methodology (Pauling et al. 2023; in preparation): heat, fluid, and permeability (H, F, P, and sometimes S; see Table 4).

Table 4. Geothermal Key Controls of HHP Rocks Influenced by the Intrusive Event and/or the Present Time Geological and Tectonic Setting

	Geological Controls		
Geothermal Key Controls	***Intrusive event***	***Present Time***	***Related PFA: Critical Component***
Magma Type (Pluton Composition)	x		H, F
Radioelement Concentration	x		H
Pluton Volume	x	x	H
Fluid Chemistry		x	F, S
Hydrothermal Alteration		x	F, P, S
Faults and Fractures	x	x	P
Stress State		x	P
Tectonic Setting	x	x	P
Degree of Sedimentary Overburden		x	H, S

*H= Heat/Heat Flow, F= Accessible Fluid, P= Permeability/Porosity, S= Caprock/Seal—sometimes

4 Data and Methods for Assessment of Low-Temperature Geothermal Play Types

PFA methodologies have been adopted in the geothermal industry from the oil and gas industry. Recently, GTO funded development of geothermal PFA for de-risking of geothermal exploration. A total of 11 projects were awarded in different areas across the United States in diverse geologic and tectonic settings (Pauling et al. 2023; in preparation). However, from the 11 projects only one was focused on a study area with low-temperature geothermal resources—the Appalachian Basin. The rest were focused on high- to medium-temperature resources.

This study proposes a classification scheme for low-temperature GPTs (i.e., sedimentary basins, orogenic belts, and radiogenic systems) and, based on literature review of these GPTs, identifies relevant data to build a PFA approach to de-risking geothermal exploration of these type of resources.

The forthcoming *Geothermal Play Fairway Analysis Best Practices* report (Pauling et al. 2023; in preparation) identified a general geothermal PFA process: (1) selection of study area, (2) compilation of existing data and identification of data gaps, (3) definition of common risk segments and appropriate conceptual model framework(s), (4) measures of data confidence/uncertainty, (5) transformation and weighting of data to support combination into common risk segments, (6) combination of confidence and common risk segments, and (7) combination of confidence-scaled common risk segments into composite risk segment maps of geothermal favorability. The report also emphasizes the importance of adapting geothermal PFA to other geothermal resource types and explores refinement for more play types.

The following Sections 4.1, 4.2, and 4.3 are mainly focused on the compilation of regional existing data and identification of data gaps and definition of common risk segments or criteria and appropriate conceptual model frameworks. Section 4.4 summarizes the PFA process steps 4, 5, 6, and 7 listed in the paragraph above. Based on a literature review (e.g., Jordan et al. 2016; Palmer-Wilson et al. 2018; Williams and DeAngelo 2008; Moeck 2014; Lacasse et al. 2022)—and considering that potential areas for geothermal power and direct use is a geospatial multi-criteria decision problem (Greene et al. 2011)—we suggest three essential criteria/risks for the evaluation of low-temperature resources in SBGPTs, OBGPTs, and RGPTs: (**1) geologic, (2) risk, and (3) economic criteria** (Figure 23).

Even though the geologic component remains the most important criteria of the PFA, mainly in the first stages of exploration (Pauling et al. 2023; in preparation), it is critical to include risk and economic concerns to fully represent the likelihood and economic feasibility of developing low-temperature geothermal resources (Wang et al. 2021). However, the input layers and criteria should be selected depending on data availability, scale of the study area, and the nature of the GPT.

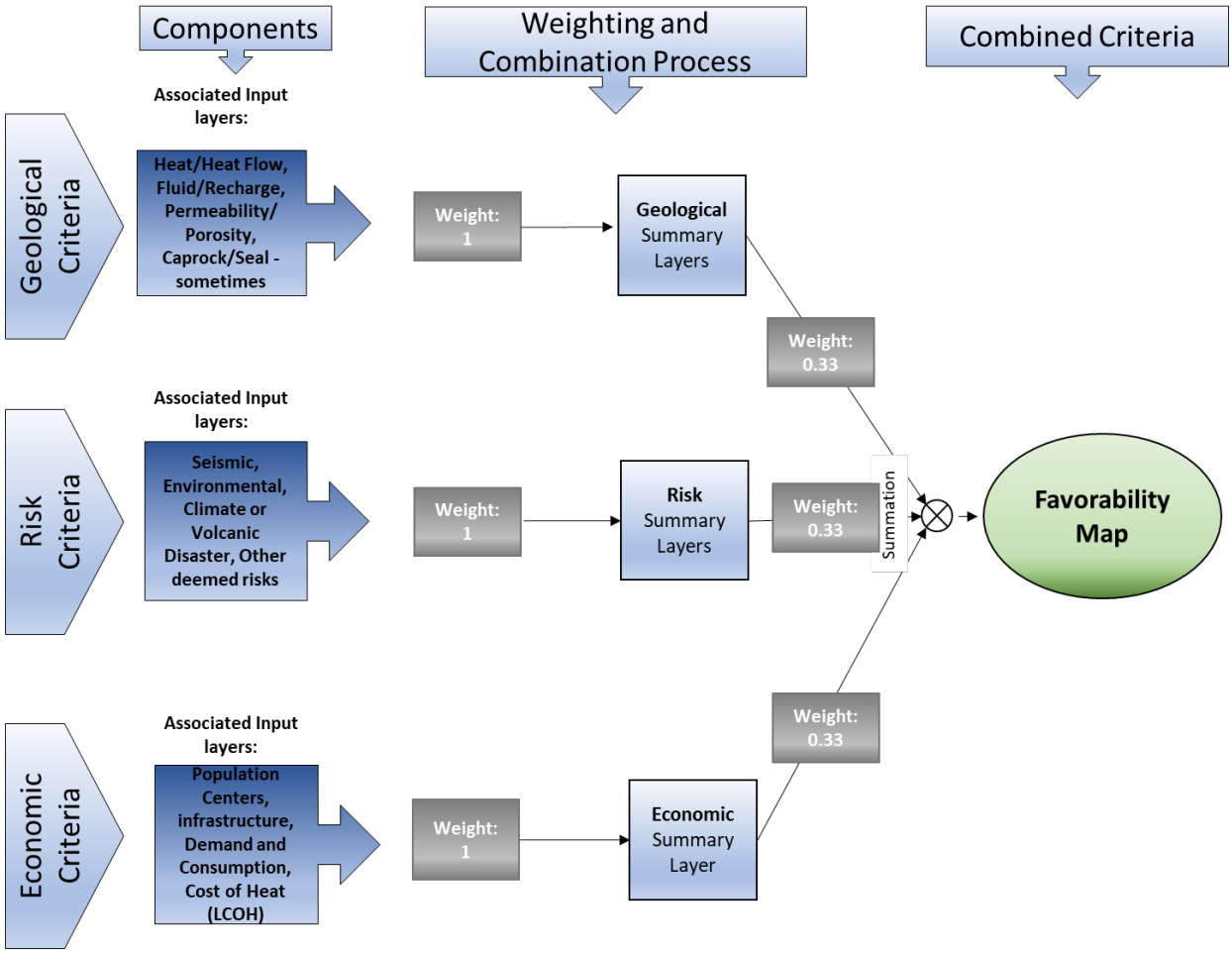

Figure 23. Flowchart of mapping geothermal favorability

Geological, risk, and economic criteria are represented by input layers which can consist of several data sets. Weighting and combination process and summation produces summary layers. Summary layer weighting and summation produces the favorability map.

4.1 Relevant Data and PFA Methods for SBGPTs

This section is focused on describing relevant data and PFA methods for geothermal resource assessment in sedimentary basins, with a focus on low-temperature GPTs. The relevant input data and methodologies are mainly based on the following studies in SBGPTs:

(1) "The Low Temperature Geothermal Play Fairway Analysis for the Appalachian Basin project" conducted by Jordan et al. (2018) at Cornell University and funded by DOE is probably one of the few of its kind that expanded and introduced novel approaches that can be applied in other sedimentary basins for low-temperature (50°–150°C) direct-use heat.

(2) "Sedimentary basin geothermal favorability mapping and power generation assessment" by Palmer-Wilson et al. (2018). The authors applied a PFA approach using available data from oil and gas production to identify favorable location for geothermal energy and

estimate electric power generation potential. This study gives an example of a PFA methodology workflow in the Western Canadian Sedimentary Basin, see Figure 24.

(3) "Mapping geothermal potential in the Western United States" by Williams and DeAngelo (2008). They conducted an updated assessment of geothermal resources to estimate the spatial distribution and quantify undiscovered geothermal resources. They used weights of evidence and logistic regression models to create favorability maps.

(4) "When less is more: How increasing the complexity of machine learning strategies for geothermal energy assessments may not lead towards better estimates" by Mordensky et al. (2023). This paper extends beyond Williams and DeAngelo (2008) by applying a complex machine learning approach to reduce bias and improve predictive ability to create favorability maps in the western United States.

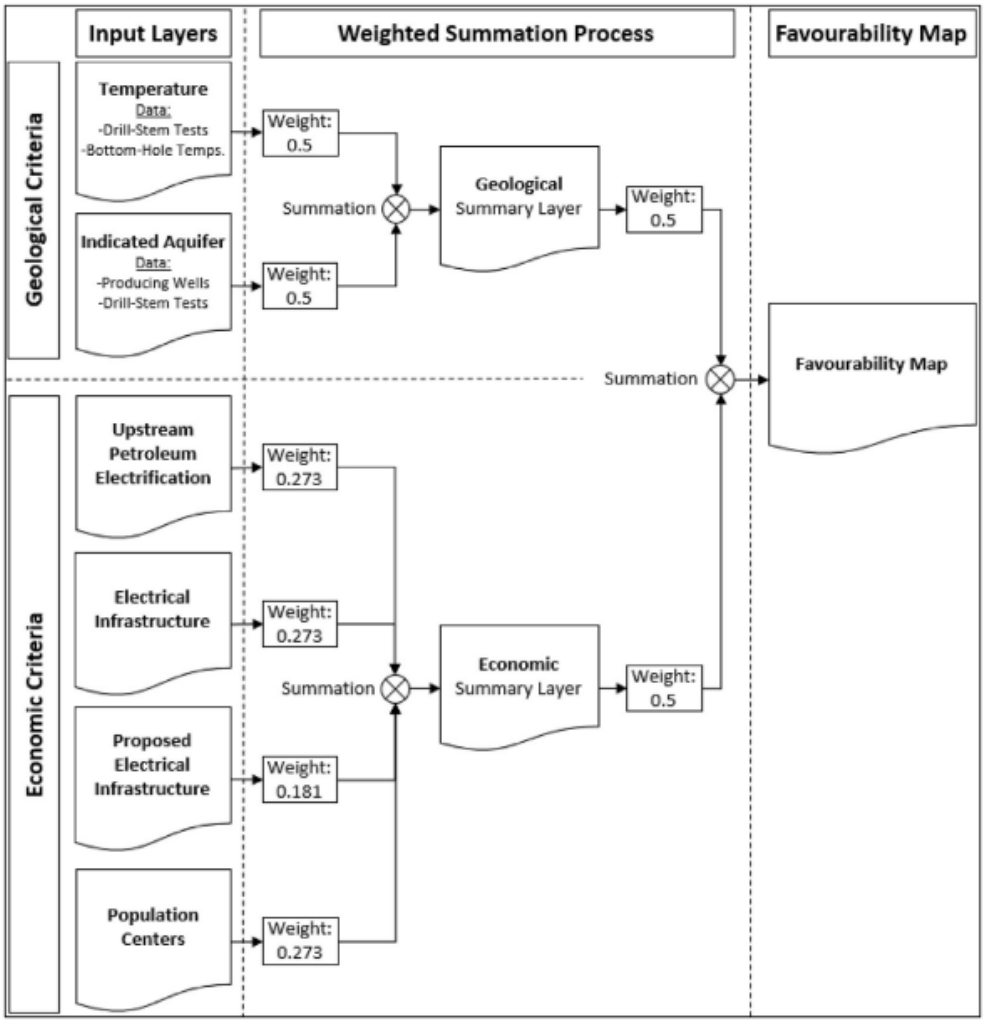

Figure 24. Example of flowchart of mapping geothermal favorability in the Western Canadian Sedimentary Basin

From Palmer-Wilson et al. (2018)

4.1.1 Associated Input Data

Selecting potential areas for geothermal power and direct use is a geospatial multi-criteria decision problem (Greene et al. 2011). Based on the studies listed above (e.g., Jordan et al. 2016; Palmer-Wilson et al. 2018; Williams and DeAngelo 2008), we suggest three essential criteria for the evaluation of low-temperature resources in sedimentary basins: geologic, risk, and economic criteria (Figure 23). However, the input layers and criteria should be selected depending on data availability of the study area and the nature of the SBGPT.

4.1.1.1 Geological Criteria

The purpose of geological data sets is to evaluate the thermal regime and the distribution of potential natural reservoirs and properties, relevant to sedimentary geothermal viability. Geologic data can be divided into temperature resource quality and reservoir quality.

Heat (H) Input Data:

1. **Oil and gas bottom-hole temperature measurements** (BHT) are abundant in sedimentary basins. BHTs should be corrected with equilibrium temperature logs appropriate for each basin (e.g., Harrison correction) to account for the cooling effect of drilling mud.

   Conterminous U.S. and Alaska BHT data (<150°C) can be accessed via:

   a. The American Association of Petroleum Geologists data set of the entire U.S. provides **BHT recorded** from log headers, and includes other information such as well logs, temperature measurements, etc. This data set originated for the EGS Site Planning and Analysis project (Augustine 2013). The data set can be downloaded from the Geothermal Data Repository (GDR) https://gdr.openei.org/submissions/252.

   b. The Southern Methodist University (SMU) data set consists of **corrected BHT data** from oil and gas wells in the United States, including Alaska and Hawaii. Additionally, this data set includes valuable information such as temperature gradient from the surface to the BHT depth (°C/km), thermal conductivity, and heat flow values (mW/m^2). The BHT data sets can be downloaded from http://geothermal.smu.edu/static/DownloadFilesButtonPage.htm.

2. **Thermal conductivity** is based on a stratigraphic model for each basin. The thermal conductivity baseline data sets of the conterminous United States and Alaska could be compiled for onshore sedimentary basins and include thermal conductivity values derived from lithological models from Correlation of Stratigraphic Units of North America (COSUNA). Thermal conductivity values derived from stratigraphic models have an expected error of 10%, while thermal conductivity measurements of rock samples have errors below 5% (Gallardo and Blackwell 1999). This data set can be downloaded from http://geothermal.smu.edu/static/DownloadFilesButtonPage.htm

3. **Heat flow data sets** if available in the region. The most recent heat flow map for Alaska and the conterminous United States was updated by Batir et al. (2016) and Blackwell,

Negraru, and Richards (2006), respectively. The data set is available at the SMU repository at http://geothermal.smu.edu/static/DownloadFilesButtonPage.htm

Accessible Fluid (F) Input Data:

1. Isolated hydrothermal systems of low temperature (<150°C) in the conterminous United States and Alaska can be identified from three different data sets:

   a. Berry et al. (1980) conducted an early compilation of **thermal springs** lists for the United States by the National Oceanic and Atmospheric Administration (NOAA). The report is available at https://www.ngdc.noaa.gov/hazard/data/publications/Kgrd-12.pdf.

   b. Mullane et al. (2016) compiled data sets from three USGS primary sources: Muffler (1979), Reed et al. (1982), and Williams et al. (2008). This database is available on the GDR: https://gdr.openei.org/submissions/842.

   c. Motyka et al. (1983) compiled and interpreted **hot springs** data sets for Alaska (108 hot springs and 3 wells) to inform the first Geothermal Resources of Alaska map by the Department of Natural Resources Geological and Geophysical Survey. The geothermal resource shapefile of the hot springs in Alaska is available to download at https://dggs.alaska.gov/pubs/pubs?reqtype=citation&ID=671.

2. Water production data from oil and gas wells can be used as a proxy for permeability, which is a key factor in resource assessment of natural geothermal reservoirs. Water production data provides information about the natural reservoir quality of rocks (i.e., their ability to maintain sufficient fluid flow rates between injection and production wells to mine heat from reservoir rocks).

   The baseline database of water production from oil and gas wells in the conterminous United States and Alaska identified by this study are:

   (a) USGS database of aggregated oil and natural gas drilling and **production history** of the United States. The USGS data set provides an overview of the production history of all U.S. wells from 1817 to 2020. The USGS database was built from data compiled by IHS Markit, a commercial database. The production data is aggregated in 2- to 10-square-mile-increments that sum the total production of oil, gas, and water volumes. This data has been released by USGS and it is available at: https://www.sciencebase.gov/catalog/item/632b67a5d34e900e86c509ce.

   (b) Alaska Oil and Gas Conservation Commission (AOGCC) **produced water** data. The AOGCC is a public data set that provides daily updates of oil and gas well history, production, and injection. The data sets consist of water volume production pre-2000 and post-2000 per well. It is available at: https://www.commerce.alaska.gov/web/aogcc/Data.aspx.

Caprock and Seal (S) Input Data:

1. Basin lithology: stratigraphic column and reservoir properties could be obtained from published literature from a specific basin. When that is not available, seismic reflection, oil and gas well logs, and other geophysical methods can be used to determine basin stratigraphy.

    a. The USGS released a **generalized lithology** for the conterminous United States. The data contain generalized lithology classes (rock types) as reassigned from the USGS state geologic map compilation for the conterminous United States (Schweitzer 2011). Lithology was classified into 12 categories. The data are available at: https://www.sciencebase.gov/catalog/item/598b471de4b09fa1cb0eacfd

Permeability/Porosity (P) Input Data:

1. Available **porosity and permeability** data can be identified from USGS Open-File Report (Nelson and Kibler 2003). This report records data from 70 data sets that include a total of 49 basins globally. The information can be obtained by searching the USGS Core Research Center catalog: http://my.usgs.gov/crcwc/.

2. Quaternary fault slip-dilation tendency analysis identifies local permeability, mostly in fault-controlled geothermal systems. The data sets used for this analysis are the same for identifying risk criteria in Section 4.1.1.2. Because active faults may serve as pathways for geothermal fluids and at the same time, they are potentially susceptible to induced seismicity during geothermal operations.

4.1.1.2 Risk Criteria

The purpose of the risk data sets is to review seismicity as a risk factor and identify regions with high probability for inducing seismic activity during preparation of a reservoir, or during geothermal heat production and utilization.

1. The USGS maintains the most complete database of global and national **earthquakes**: https://earthquake.usgs.gov/earthquakes/search/. Another earthquake catalog for Alaska is available at the Alaska Earthquake Center website: https://earthquake.alaska.edu/earthquakes.

2. Information about current **stress fields** (orientation and magnitudes) is key in understanding the susceptibility of faults to slip and/or dilation. The orientation and relative magnitudes of tectonic stresses in the conterminous United States, Alaska, and Hawaii can be derived from the World Stress Map Project (WSM; Heidbach et al. 2016). The WSM is a global compilation of crustal stress field magnitudes and directions maintained since 2009 at the Helmholtz Centre Potsdam German Research Centre for Geosciences. The WSM is an open-access public database: https://www.world-stress-map.org/download.

3. **Quaternary Faults:** The USGS Quaternary fold and faults database (Machette et al. 2003) can be evaluated to determine relationships between active deformation in the

upper crust and location of geothermal systems, as well as seismic risk during exploitation and utilization of geothermal resources. The data of Quaternary Faults can be download from: https://www.usgs.gov/programs/earthquake-hazards/faults.

4.1.1.3 Economic Criteria

Economic input data relevant to sedimentary geothermal viability include potential locations for commercial power sales or offtakes of heat for direct use (e.g., regions with electrical infrastructure and population centers). The utilization viability input layers identify regions with the capacity to utilize low-grade geothermal heat and estimated levelized cost of heat (LCOH) for a set of communities.

1) **Roads and electrical infrastructure:** The roads data set can be downloaded as a shapefile from the Topologically Integrated Geographic Encoding and Referencing (TIGER) data set: https://tigerweb.geo.census.gov/tigerwebmain/TIGERweb_nation_based_files.html.

2) Building **heat demand** and **energy consumption:** Thermal demand in the residential, commercial, and manufacturing sectors was updated by Oh and Beckers (2023) using the Energy Information Administration's (EIA) end-use energy consumption and expenditure survey data. The energy consumption data can be obtained as well from EIA power consumption data, available at: https://www.eia.gov/outlooks/aeo/tables_ref.php and http://www.eia.gov/consumption/manufacturing/.

3) **Levelized cost of heat:** The cost estimates include pipes, pumps, and heat exchangers, and the annual demand expectations rely on place-specific climate conditions. **LCOH** can be calculated using the open-source GEOPHIRES tool (Beckers et al. 2014) which simulates techno-economic scenarios for geothermal direct use. The software can be found at: https://github.com/NREL/GEOPHIRES-v2.

4) **Population centers** data sets can be obtained from the U.S. Census Bureau population data that include state, county, and place. A place is used to identify specific cities, towns, villages, universities, or any census-designated places. These data are available at: http://factfinder.census.gov.

4.2 Relevant Data and PFA Methods for OBGPTs

This section is focused on describing relevant data and PFA methods for geothermal resource assessment in orogenic belts, with a focus on low-temperature GPTs. The relevant input data and methodologies are mainly based on the following studies in OBGPTs:

1. "Catalog of geothermal play types based on geological controls" by Moeck (2014). This study focused on characterizing and identifying different GPTs based on the geological controls and tectonic setting. The study gave a good understanding of OBGPTs and their geological controls.

2. "Geothermal energy development roadmap of Taiwan by play fairway analysis" by Wang et al. (2021). This study aimed to assess geothermal resources using a PFA approach in

Tawain Island, which is characterized as an OBGPT/foreland basin correlated with the Central Mountain Range area. An associated PFA-based workflow was developed for these OBGPT resources (Figure 25).

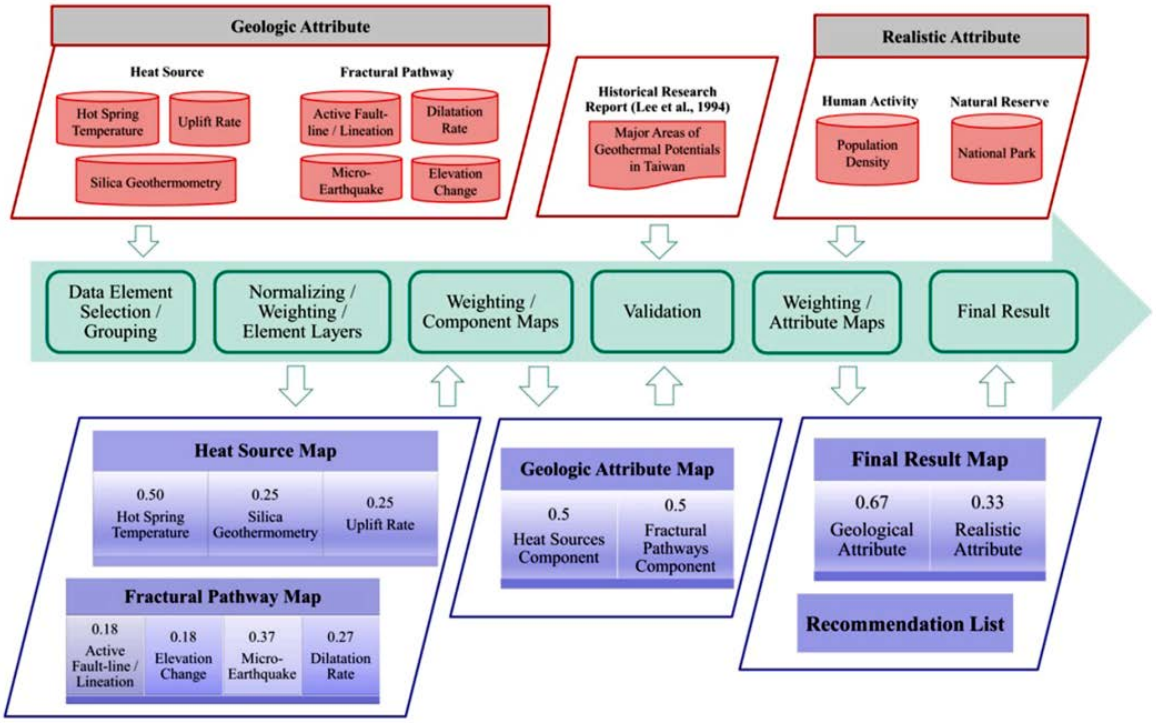

Figure 25. Example of flowchart of PFA geothermal favorability map of Taiwan

From Wang et al. (2021)

4.2.1 Associated Input Data

As mentioned previously, selecting geothermal potential areas for geothermal power and direct uses is a geospatial multi-criteria decision problem (Greene et al. 2011). Based on the geothermal resources' studies provided above (Moeck 2014; Wang et al. 2021), we suggest three essential criteria for the evaluation of low-temperature resources for OBGPT: geologic, risk, and economic criteria (Figure 23). However, the input layers and criteria should be selected depending on data availability of the study area and the nature of the OBGPT.

4.2.1.1 Geological Criteria

Heat (H) Input Data:

1. Determination of the geothermal potential of each region is highly dependent on the heat discharge values related to the Earth's heat flow. Heat flow maps are extremely useful to identify areas of high geothermal resources potential in a particular region or country (Blackwell et al. 2007).

a. **Heat flow** data sets if available in the region. The most recent heat flow map for the conterminous United States and Alaska was updated by Blackwell, Negraru, and Richards (2006) and Batir et al. (2016), respectively. The data set is available at the SMU repository at http://geothermal.smu.edu/static/DownloadFilesButtonPage.htm

2. Uplift rate data could be used for active orogenic belts, which can be calculated through GPS record (e.g., Blume and Sheehan 2003) and implicitly reflect the altered temperature gradients from the flat line by diagenesis (Pollack and Chapman 1977).

    a. The **GPS data** provided by the Nevada Geodetic Laboratory at the University of Nevada, Reno. The selected data set is provided as north, east, and up components for more than 15,700 GPS sites in the IGS08 reference framework, with its origin in the center of mass of the total Earth system. This data set can be found at: http://geodesy.unr.edu/.

    b. A **new global GPS** data set for testing and improving modeled glacial isostatic adjustments uplift rates was generated from 4,000 GPS vertical velocities as observational estimates of global glacial isostatic adjustments. The Global Mass GPS data set is available at: https://doi.pangaea.de/10.1594/PANGAEA.889923.

Accessible Fluid (F)

1. Hot springs and geothermometers of low-temperature (<150°C) resources in the conterminous United States and Alaska can be identified from different data sets with geothermometer estimations:

    a. Mullane et al. (2016) compiled data sets from three USGS primary sources: Muffler (1979), Reed et al. (1982), and Williams et al. (2008). This database is available on the GDR: https://gdr.openei.org/submissions/842. Reed et al. (1982) identified 42 delineated areas related to conduction-dominated systems.

Permeability/Porosity (P):

The Quaternary fault map, dilation-tendency analysis map, micro-earthquake locations, elevation patterns, and lineation from LiDAR images are elements that represent implications of the permeability of fracture pathways component (Wang et al. 2021), and at the same time they are potentially susceptible to induced seismicity during geothermal operations.

1. Active faults along earthquake activities indicate the occurrence of abrupt rock movements and fracturing (e.g., Faults and Hinz 2015; Siler et al. 2016).

    a. **Quaternary Faults:** The USGS Quaternary fold and faults database (Machette et al. 2003) can be evaluated to determine relationships between active deformation in the upper crust and location of geothermal systems, as well as seismic risk during

exploitation and utilization of geothermal resources. It is available at: https://www.usgs.gov/programs/earthquake-hazards/faults.

2. Local stress field magnitudes and orientations along with active faults geometry could be used to estimate slip and dilation tendency in active structures (e.g., Faults and Hinz 2015; Siler et al. 2016)

    a. Information about current **stress fields** (orientation and magnitudes) is key in understanding the susceptibility of faults to slip and/or dilation. The orientation and relative magnitudes of tectonic stresses in the conterminous United States, Alaska, and Hawaii can be derived from the World Stress Map Project (WSM; Heidbach et al. 2016). The WSM is a global compilation of crustal stress field magnitudes and directions maintained since 2009 at the Helmholtz Centre Potsdam German Research Centre for Geosciences. The WSM is an open-access public database: https://www.world-stress-map.org/download.

3. Micro-earthquakes at shallow depths may be associated with geothermal activity and/or fractures stress release (Foulger 1982; Simiyu 2009)

    a. The USGS maintains the most complete database of global and national **earthquakes**: https://earthquake.usgs.gov/earthquakes/search/. Another earthquake catalog for Alaska is available at the Alaska Earthquake Center website: https://earthquake.alaska.edu/earthquakes.

4. Higher dilation rate calculated from GPS data shows higher odds for increasing permeability for subsurface pathways where tensional strain is occurring (Dixon 1991; Hsu et al. 2009).

4.2.1.2 Risk Criteria

Environmental and seismic risk are important factors to consider. For example, a few areas are labeled as national parks in orogenic belts; preserved land protected by public regulations prohibits any industrial development. Other types of environmental risk are landslide risk due to the active uplift rates in active orogenic belts.

1. The purpose of the risk data sets is to review seismicity as a risk factor and identify regions with high probability for inducing seismic activity during preparation of a reservoir (e.g., EGS), or during geothermal heat production and utilization.

    a. Quaternary fault slip-dilation tendency analysis identifies local seismicity risk. The data sets used for this analysis are the same for identifying permeability/fractural pathways in Section 4.2.1.1. Because active faults may serve as pathways for geothermal fluids and at the same time, they are potentially susceptible to induced seismicity during geothermal operations.

2. Environmental risk in OBGPT accounts for exclusion layers such as national parks or landslide risk areas.

a. **National parks boundaries** data to use for display and general GIS analysis can be found in the National Park Service Data Store: https://irma.nps.gov/DataStore/Reference/Profile/2224545?lnv=True.

b. The USGS interactive map with **landslide data** includes contribution from many local, state, and federal agencies and provides links to the original digital inventory files: https://usgs.maps.arcgis.com/apps/webappviewer/index.html?id=ae120962f459434b8c904b456c82669d.

4.2.1.3 Economic Criteria

Geothermal energy development must consider the socio-economic aspects in high-population regions with higher electricity demand (Lautze et al. 2017). The utilization viability input layers identify regions with the capacity to utilize low-grade geothermal heat and estimated LCOH for a set of communities.

1. **Population centers**: Data sets can be obtained from the U.S. Census Bureau population data that includes state, county, and place. A place is used to identify specific cities, towns, villages, universities or any census-designated places. This data is available from: https://data.census.gov/.

2. **Roads and electrical infrastructure**: The roads data set can be downloaded as a shapefile from the Topologically Integrated Geographic Encoding and Referencing (TIGER) data set: https://tigerweb.geo.census.gov/tigerwebmain/TIGERweb_nation_based_files.html

3. Building **heat demand** and **energy consumption**: Thermal demand in the residential, commercial, and manufacturing sectors was updated by Oh and Beckers (2023) using the Energy Information Administration's (EIA) end-use energy consumption and expenditure survey data. The energy consumption data can be obtained as well from EIA power consumption data, available from: https://www.eia.gov/outlooks/aeo/tables_ref.php and http://www.eia.gov/consumption/manufacturing/.

4. **Levelized cost of heat**: The cost estimates include pipes, pumps, and heat exchanger, and the annual demand expectations rely on place-specific climate conditions. **LCOH** can be calculated using the open-source GEOPHIRES tool (Beckers et al. 2014), which simulates techno-economic scenarios for geothermal direct use. The software can be found at: https://github.com/NREL/GEOPHIRES-v2.

4.3 Relevant Data and PFA Methods for RGPTs

This section is focused on describing methodologies and relevant data for geothermal resource assessment for radiogenic geothermal plays. The relevant input data and methodologies are mainly based on the following studies:

1. "Geologic setting of the Central Alaska hot springs belt: Implications for geothermal resource capacity and sustainable energy production" by Kolker (2008). This study focused on the CAHSB region in Alaska that has low-temperature geothermal potential.

This study proposed a radiogenic heat source model, wherein the anomalously radioactive plutons are associated with nearby hot springs and provide a heat source for the geothermal activity in that region.

2. "Integrated assessment and prospectivity mapping of geothermal resources for EGS in Brazil" by Lacasse et al. (2022). This study focused on the development of methods for EGS favorability in Brazil where radioactive heat production from granitoids are the main source of heat transfer. Geothermal resources that might be associated with these areas can occur in hot sedimentary aquifers and hot dry rocks that are hosted in intracratonic sedimentary basins and HHP granites. This study suggested a PFA method workflow based on three factors: heat source, heat insulation, and fracture pathways, see Figure 26.

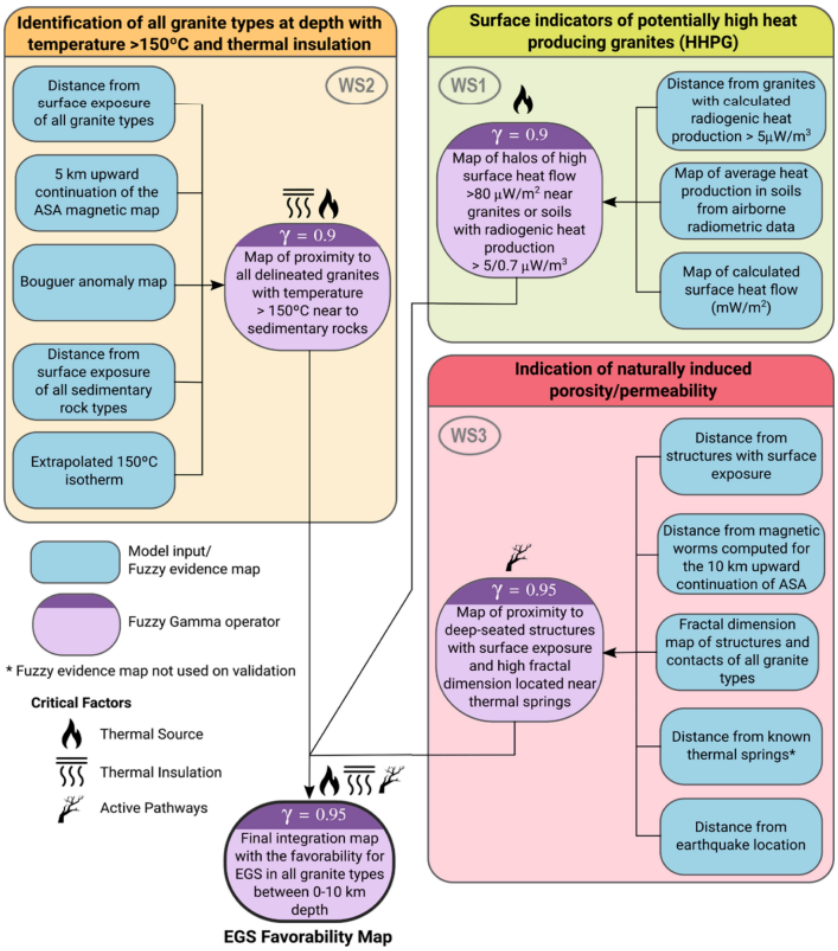

Figure 26. Example of flowchart of EGS geothermal favorability map of Brazil

From Lacasse et al. (2022)

4.3.1 Associated Input Data

The first step in developing a methodology for assessing the favorability of RGPTs is to identify relevant data sets that provide input to the critical components for a PFA. We suggest three essential criteria for the evaluation of low-temperature resources in RGPTs: geologic, risk, and

economic criteria (Figure 23), based on the studies listed above (e.g., Kolker 2008; Lacasse et al. 2022).

4.3.1.1 Geological Criteria

Table 5 summarizes the data sets that can address key unknowns related to the geological criteria components H, P, F, and sometimes S. However, the input layers and criteria should be selected depending on data availability of the study area and the nature of the GPT.

Important geological factors to consider in a PFA methodology for an RGPT area as recommended by Lacasse et al. (2022): (1) the existence of HHP granites (heat source), (2) identification of all granite types at depth with temperature >150°C and thermal insulation (caprock/seal: thermal insulation), and (3) indication of naturally induced porosity/permeability (fracture pathways).

Table 5. Critical Components of an RGPT, Key Data Sets, and Qualitative Assessment of Relative Uncertainty Around the Key Data Sets

Component	Key Unknowns	Key Data Sets	Uncertainty
Heat (H)	• Rock types at depth • Volume of plutons at depth • HHP plutons (K age) vs. "normal" (T age) • Role of magmatic heat from related intrusive event(s)	• U, Th concentration data (whole rock data and/or airborne radiometric data • Heat flow models • Fluid geothermometry • He isotopic data	High
Accessible Fluids (F)	• Presence of fluid • Degree of circulation or convection (dynamics) • Temperature and chemistry of reservoir fluids	• Hydrology data • Chemical composition of fluids (from hot springs or well samples) • Fluid geothermometry • Hydrothermal alteration data	Medium
Permeability (P)	• Key structures • Stress	• Stress data • Geophysical data (seismic, magnetotelluric, magnetic, and gravity) relevant to structure identification • Geologic maps/cross sections/models • Fault/fracture orientations relative to local stress field • Fracture data (size, aperture, orientation etc.)	High
Caprock or Seal (S)	• Quality and presence of caprock or seal • Degree of insulation from unconsolidated sediments	• Stratigraphy data from well logs or geologic models • Heat flow/basin models • Geophysical data (seismic)	Low to Medium

Heat (H) input Data:

1. **U, Th concentration data and heat flow models:** U and Th concentration data for RGPT plutons can be collected through a variety of methods, including INAA (instrumental neutron activation analysis); AA (atomic absorption); DN (delayed neutron); γS (gamma ray spectroscopy); and XRF (X-ray fluorescence). To test whether radiogenic heat sources can account for all of the heat transferred to a given RGPT system, the following parameters would need to be known:
    - Heat generated by pluton (volume * heat production of plutons)
    - Heat required by geothermal fluids (volume of water * temperature differential)

    Kolker (2008) proposed a basic heat flux model based on U, Th concentrations using equations as follows:

$$H_{gen}\ (cal/sec) = Vol_{pluton}\ (m^3) * HP_{pluton}\ (cal/sec/m^3) \quad (2)$$

$$H_{req}\ (cal/sec) = Vol_{fluid}\ (m^3) * \Delta T_{fluid}\ (m^3\ /sec) * 1cal \quad (3)$$

where H_{gen} denotes the heat generated by a pluton; H_{req} denotes heat needed by the geothermal system; ΔT_{fluid} is the change in fluid temperature, calculated as the estimated reservoir temperature minus 5°C (the assumed temperature of meteoric waters); and Vol_{fluid} is the observed spring flow.

a. **Radiogenic heat production** data in content model format is available for Idaho, Montana, Minnesota, and Oregon. This data set is an aggregation of radiogenic heat values provided in different submission files. It includes data from gamma ray spectrometry measurements conducted by University of North Dakota, and also includes any heat generation values from the heat flow determination by SMU, Cornell, and University of North Dakota. The data set is available at the SMU repository at http://geothermal.smu.edu/static/DownloadFilesButtonPage.htm.

b. **Heat production in granitic rocks**: Global analysis based on a new data compilation GRANITE2017 is constrained by compilation data from original publications where information on rock type, heat production and concentrations of radiogenic elements have been reported. The database is an electronic supplement to Artemieva et al. (2017). The data set is available at https://data.mendeley.com/datasets/yjjx5fvhvm/2.

c. **Heat flow data sets** (if available in the region): The most recent heat flow map for the conterminous United States and Alaska was updated by Blackwell, Negraru, and Richards (2006) and Batir et al. (2016), respectively. The data set is available at the SMU repository at http://geothermal.smu.edu/static/DownloadFilesButtonPage.htm.

2. **Helium isotopic data:** In order to distinguish between magmatic, "deep circulation," and radiogenic types of geothermal systems, helium isotopes may be helpful (Kolker 2008). Helium isotopes give unmistakable proof that mantle-derived volatiles exist in geothermal systems, indicating the presence of a heat source. The $^3He/^4He$ ratio in mid-ocean ridge basalts around the world is 8–9 R_A (where R is the measured sample $^3He/^4He$ ratio and R_A is the ratio in air), which is generally believed to represent the upper mantle composition (Kennedy and van Soest 2007). Geothermal fluids from regions of young volcanic/magmatic activity show a clear mantle signature in that they contain elevated ^3He concentrations (Oxburgh and O'Nions 1987). The specific helium isotopic composition of fluids that mine heat from active near-surface magmatic systems are typically similar to the composition in the mantle source (e.g., Coso, ~7 R_A, Welhan et al. 1988; Long Valley, ~2-7 R_A, Sorey et al. 1993; The Geysers, ~8-9 R_A, Kennedy and Truesdell 1996).

   Helium derived from mantle sources but with no magmatic input (for instance, in deep circulation/crustal thinning settings) is also enriched in ^3He but characterized by lower $^3He/^4He$ ratios than magmatic settings. Therefore, any value higher than 0.1 R_A is considered to have a significant mantle He component (Ballentine et al. 2002). For

example, fluids from the Dixie Valley, NV geothermal field range from 0.70 to 0.76 R_A, indicating that 7.5% of the total helium is derived from the mantle (Kennedy and van Soest 2007).

A summary of helium isotope signature from the different types of geothermal systems is given in Table 6. Helium associated with crustal fluids that have experienced no mantle influence is dominated by radiogenic ^4He produced from radioactive decay of U and Th to Pb and is characterized by a $^3He/^4He$ ratio of ~0.02 R_A.

Table 6. Compiled Data from the Literature on $^3He/^4He$ Ratio (R) in Geothermal Fluids Relative to the $^3He/^4He$ Ratio in air (R_A)

Geothermal Play Type	He Isotope Signature (R/R_A)	Geologic Origin of He
Radiogenic[a]	0.02–0.04	Shallow crust
Volcanic or Magmatic[b,d,e,f]	2–16	Mantle
Deep Circulation[b,c,e]	~0.7 average	Deep crust and/or mantle

Sources: (a) Brugger et al. 2005; (b) Kennedy and van Soest 2007; (c) Kennedy and van Soest 2007; (d) Christenson et al. 2002; (e) Ballentine et al. 2002; (f) Poreda et al. 1988.

a) The USGS released a data set of **helium concentrations** in U.S. wells by Brennan et al. (2021). This data set provides national-scale location information for known, publicly available data on helium gas concentrations, reported in mol%. The data set is available at: https://www.sciencebase.gov/catalog/item/609e8fe1d34ea221ce3f39e6.

Accessible Fluid (F)

1. **Fluid geothermometry:** Chemical geothermometry methods classically used to estimate geothermal reservoir temperatures (e.g., quartz and cation exchange geothermometers) described by Fournier (1981) and Truesdell (1984) may be chemically inappropriate for the highly chemically evolved plutons frequently associated with RGPTs (Kolker 2008). Chalcedony geothermometers are likely applicable but tend to give conservative estimates for RGPT fluids (~92°C for Chena Hot Springs reservoir, Kolker 2008; ~95°C for the Paralana hot springs reservoir, Brugger et al. 2005).

2. **Chemical composition of fluids:** Because it is the most conservative element in geothermal waters, chloride (Cl) concentrations in fluids are frequently utilized in ratios with other elements in the interpretation of water chemistry (Nicholson 1993). In deep circulation systems, Cl is assumed to originate directly from the deep reservoir, but in magmatic hydrothermal systems, Cl is thought to be introduced by crystallization of the accompanying magma. Cl/B and Cl/Li ratios in geothermal fluids were utilized by Arehart et al. (2003) to discriminate between extension-driven ("deep circulation" type) and magmatic-driven ("magmatic" type) geothermal systems in the Great Basin.

   Alaska's CAHSB fluids differ from magmatic and deep circulation hot springs in terms of fluid chemical properties. The CAHSB is similar to other radiogenic Paralana hot springs fluids in South Australia in terms of its low surface temperatures, low concentrations of total dissolved solids (on average 2,000), and other features (Kolker 2008). The Cl/B and Cl/Li ratios of CAHSB fluids don't mimic either deep circulation or magmatic systems. Li and B concentrations are many orders of magnitude lower in CAHSB fluids than in fluids from either of the other types of systems, while Cl concentrations are lower overall.

a) **Hot springs** and **geothermometers** of low-temperature (<150°C) resources in the conterminous United States and Alaska. Mullane et al. (2016) compiled data sets from three USGS primary sources: Muffler (1979), Reed et al. (1982), and Williams et al. (2008). This database is available on the GDR: https://gdr.openei.org/submissions/842. Reed et al. (1982) identified 42 delineated areas related to conduction-dominated systems.

Permeability/Porosity (P)

The Quaternary fault map, dilation-tendency analysis map, micro-earthquake locations, elevation patterns, and lineation from LiDAR images are elements that represent implications of the permeability of fracture pathways component (Wang et al. 2021) and at the same time, they are potentially susceptible to induced seismicity during geothermal operations. The permeability/porosity datasets for RGPTs are similar to OBGPTs, see Section 4.2.1.1.

Caprock/Seal (S: Thermal Insulation)

The proximity of an insulating sedimentary cover needs to be evaluated in RGPTs. The occurrence of sediments in contact with the HHP granites, lithology, thickness, and thermal conductivity are important data to consider.

1. Basin lithology: stratigraphic column and reservoir properties could be obtained from published literature from a specific basin. When that is not available, seismic reflection and other geophysical methods can be used to determine basin stratigraphy.

    a. The USGS released a **generalized lithology** for the conterminous United States. The data contain generalized lithology classes (rock types) as reassigned from the USGS state geologic map compilation for the conterminous United States (Schweitzer 2011). Lithology was classified into 12 categories. The data are available at: https://www.sciencebase.gov/catalog/item/598b471de4b09fa1cb0eacfd.

2. Thermal conductivity is based on a stratigraphic model for each basin.

    a. The **thermal conductivity** baseline data sets of the conterminous United States and Alaska could be compiled for onshore sedimentary basins and include thermal conductivity values derived from lithological models from Correlation of Stratigraphic Units of North America (COSUNA). Thermal conductivity values derived from stratigraphic models have an expected error of 10%, while thermal conductivity measurements of rock samples have errors below 5% (Gallardo and Blackwell 1999). This data set can be downloaded from http://geothermal.smu.edu/static/DownloadFilesButtonPage.htm.

4.3.1.2 Risk Criteria

Environmental and seismic risk are important factors to consider. For example, a few areas are labeled as national parks, and preserved land protected by public regulations prohibits any industrial development. The risk criteria data sets for RGPTs are similar to OBGPTs and SBGPTs, see Sections 4.1.1.2 and 4.2.1.2.

4.3.1.3 Economic Criteria

Economic input data relevant to RGPT viability include potential locations for commercial power sales or offtakes of heat for direct use (e.g., regions with electrical infrastructure and population centers). The utilization viability input layers identify regions with the capacity to utilize low-grade geothermal heat and estimated LCOH for a set of communities. The same data sets used for SBGPTs and OBGPTs can be used for RGPTs, see Sections 4.1.1.3 and 4.2.1.3.

4.4 PFA Techniques and Processes

As noted at the beginning of Section 4, the forthcoming *Geothermal Play Fairway Analysis Best Practices* (2023; in preparation) from NREL identified a general geothermal PFA process: (1) selection of study area, (2) compilation of existing data and identification of data gaps, (3) definition of common risk segments and appropriate conceptual model framework(s), (4) measures of data confidence/uncertainty, (5) transformation and weighting of data to support combination into common risk segments, (6) combination of confidence and common risk segments, and (7) combination of confidence-scaled common risk segments into composite risk segment maps of geothermal favorability. This report also emphasizes the importance of adapting geothermal PFA to other geothermal resource types and explores refinement for more play types.

A generalized flow chart showing the proposed PFA methodology in this study for assessment of low-temperature conduction or conductive-dominated GPTs is shown in Figure 27.

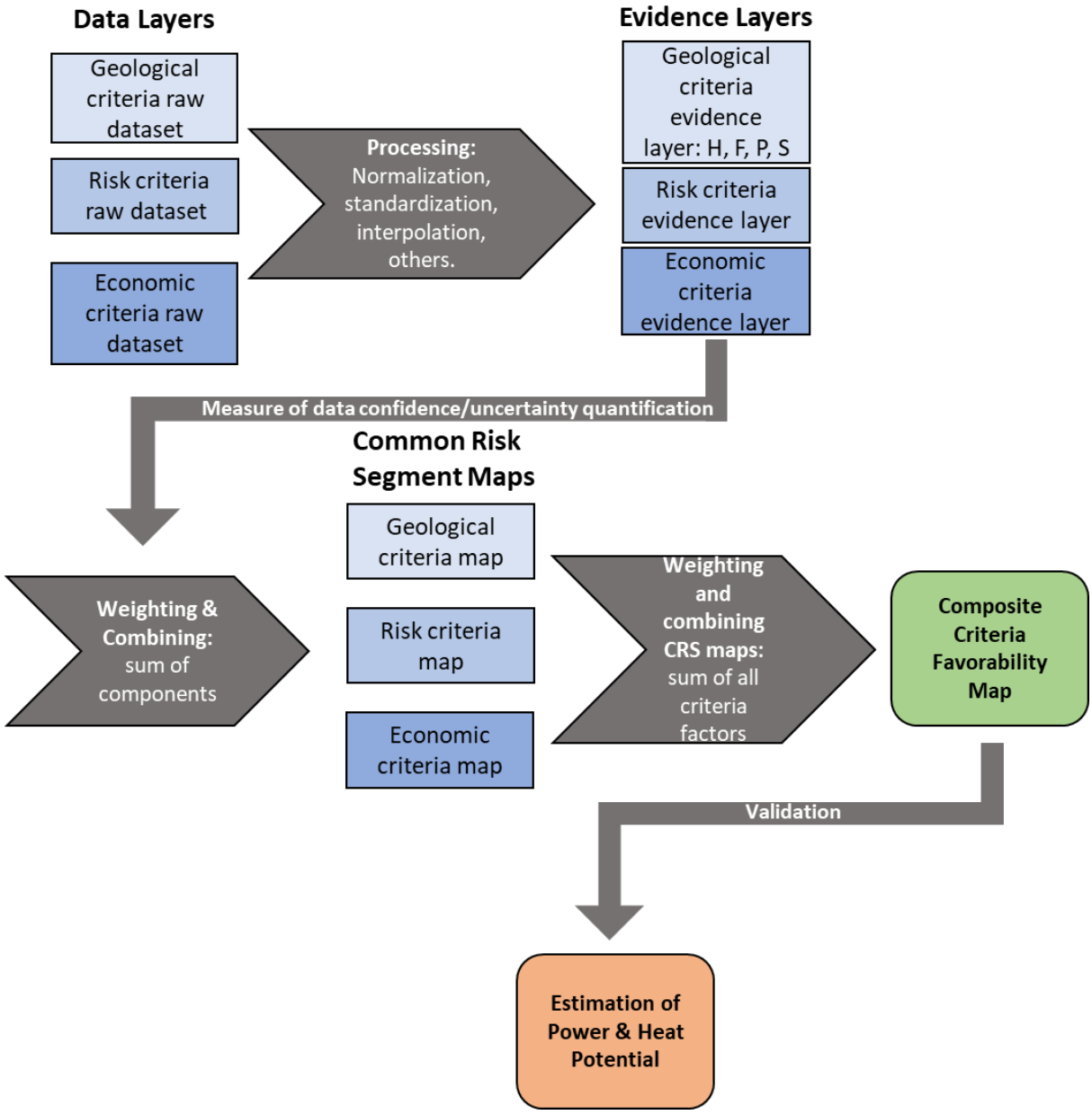

Figure 27. Flow chart outlining a generalized methodology for low-temperature assessment resources in conduction-dominated GPTs

4.4.1 Data Processing

Data processing transforms raw data into evidence layers that give information about the criteria to investigate. This process depends on the type of data (discrete or continuous) and the methods to apply (Pauling et al. 2023; in preparation). For example, discrete data tend to be interpolated to develop continuous layers, and some input data need to be standardized and normalized to a same unit-scale to apply weight summation methods or apply a machine learning algorithm

(Burkov 2019). Some data need to be transformed into more valuable information with higher impact to the PFA; for example, inverting gravitational acceleration data to density (Pauling et al. 2023; in preparation). Software such as ArcGIS can be used to apply these analytical tools for statistical calculations and map-producing routines (Wang et al. 2021).

4.4.2 Weighting Evidence Layers

Figure 24 includes an example of data criteria scores, or weighting evidence layers, based on the relevant data selected (see Section 4.1). The sum or product of the evidence layers is weighted to highlight the layers that are considered to contribute most significantly to the common risk segment of interest (i.e., heat, permeability, fluid, caprock/seal, and/or heat demand), as not all evidence layers are equally diagnostic and informative. Criteria scores can equally contribute to a single common risk factor with various data densities (Figure 24).

The weights applied to evidence layers can be based on expert opinion, data confidence, and/or statistical models. Quantitative approaches attempt to reduce biases that are introduced using expert opinions include statistical methods (g., Palmer-Wilson et al. 2018), machine learning (e.g., Mordensky et al. 2023), and/or a combination of quantitative and expert opinions (Faulds et al. 2021). Other methods such as the analytical hierarchy process, fuzzy logic, and Bayesian weights of evidence have been applied to generate weights in other geothermal assessment favorability studies (e.g., Forson et al. 2016).

For instance, Palmer-Wilson et al. (2018) used a criteria score that can be input-value dependent such as temperature input layers, distance dependent such as electrical infrastructure, or location dependent such as hot springs. They used a favorability score which is the weighted sum of individual criteria score range from 0 to 1 (see Figure 24) and measuring which criteria are satisfied by input data at a given location. To enable weighted summation, the input data need to be normalized to a same unit-less scale (Palmer-Wilson et al. 2018). The favorability score is a two-stage weighted linear combination (Malczewski 2000). Palmer-Wilson et al. (2018) used the follow equation for the first-stage summation:

$$S_j = \sum_{i=1}^{n} \left(S_{ij}\, w_i\right) \forall \mathrm{j} \in \{1,2,\ldots,\mathrm{J}\} \quad (1)$$

Second-stage summations produce favorability scores (see Figure 17). The sum of all weights (wi) in each summation stage (Sj) equals 1.

4.4.3 Measure of Data Confidence and Uncertainty Quantification

Despite the availability of a large number of data sets, the selectivity is limited by correlation and distribution issues (Witter et al. 2019). Each data needs to be analyzed and assigned its own confident layer based on the specific characteristics of how it was collected, density of data, spatial resolution, grid scale, etc. (Pauling et al. 2023; in preparation).

Data confidence is evaluated using different criteria such as kriging standard error, spatial coverage, collecting methods, availability of co-located data sets, scale of mapping, spatial resolution, etc. Different methods of analyzing the scarcity of data are applied, for example: reliability can be analyzed with Bayesian analysis, fuzzy logic, multi-criteria decision-making, and expert knowledge (Pauling et al. 2023; in preparation).

There are different methods to quantify uncertainty for different types of data in the literature; however, geological uncertainty specific to the geothermal industry is less common (Witter et al. 2019). Some examples of these uncertainty methods are listed below (Witter et al. 2019):

1. The summed distance to existing data calculations. This analysis shows the area where geologic interpretations are relatively well constrained by data, and the relative decrease in uncertainty upon compilation of new data in next stages (Siler et al. 2018).

2. Sensitivity analysis, parameter estimation, and uncertainty propagation (Wellmann et al. 2014).

3. A stochastic Monte Carlo simulation approach to generate an array of geothermal parameter values (Vogt et al. 2010). These authors utilized stochastic geostatistical methods to obtain heterogeneity of thermal conductivity data.

4. The kriging error uncertainty increases from a measured point according to a variogram (Isaaks and Srivastava 1989). This kriging is used in geospatial data interpolation such as subsurface temperature measurements in geothermal (Williams and DeAngelo 2011).

5. Machine learning methods such as algorithms, convolutional neural networks, and fry analysis can decode uncertainty for complex seismic data (e.g., Trainor-Guitton et al. 2018; Carranza 2008; Lu et al. 2018).

4.4.4 Favorability Mapping Procedure

After evidence layers, confidence layers, and weighted sums are united into a combined risk segment map (e.g., geological, risk, economic), a favorability map can be created using geographic information systems, MATLAB, Python, or other environments. Mordensky et al. (2023) and Williams and DeAngelo (2008) used machine learning approaches to estimate resource favorability.

The favorability maps allow visualization of the final score generated by the weighting and combination of all evidence layers and combined risk segment maps (see workflow shown in Figure 27). The score map displays different color scales corresponding to a common risk segment or favorability map of multiple evidence layer of a specific criteria (e.g., geological, risk, economic). For example, a geological criteria favorability map with different evidence layers such as heat flow, hot springs, faults, stress field, and earthquakes could be created to identify promising areas for that particular risk factor. Moreover, a composite common risk segment map is the weighted product of all evidence layers and risk factors. This final composite map highlights areas where all the criteria of interest are likely present (Palmer-Wilson et al. 2018).

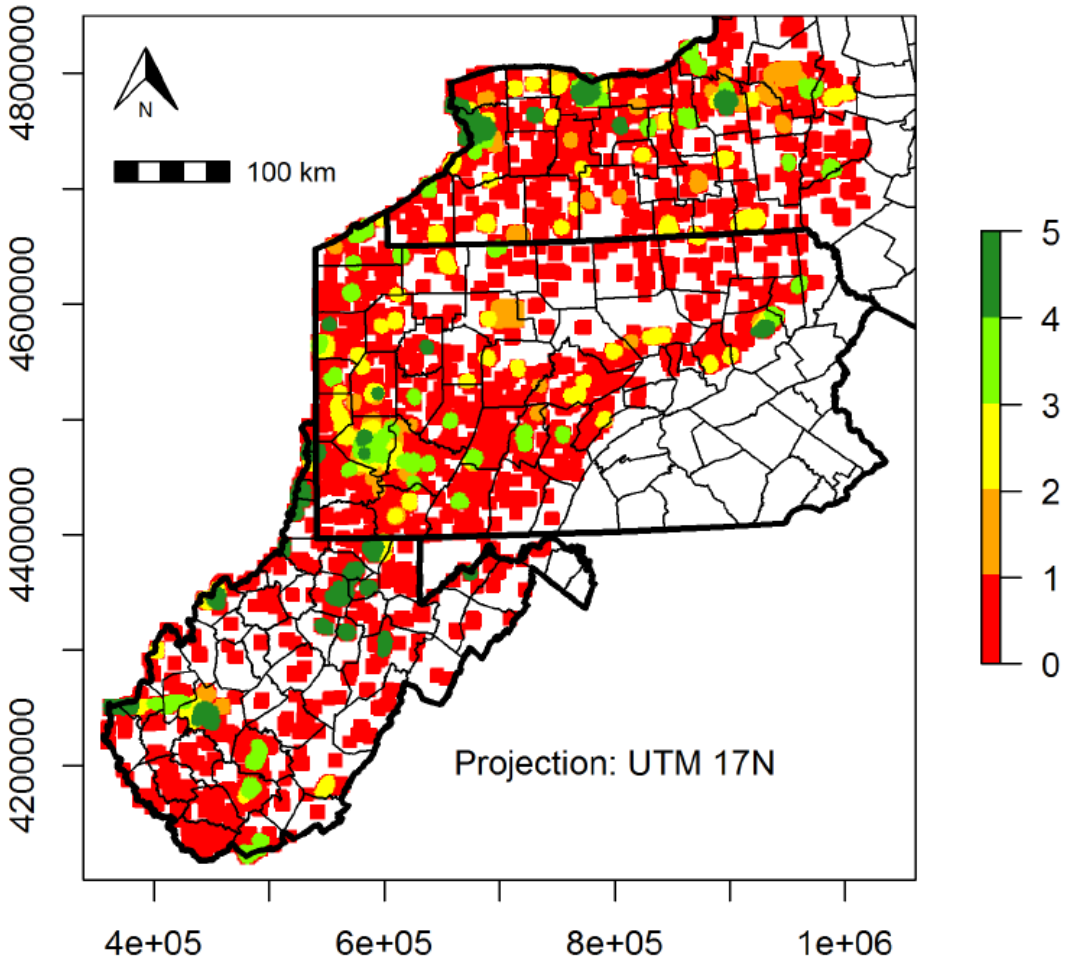

Figure 28. Example favorability map based on utilization viability criteria (5 km radius buffer)

Green is favorable (lower LCOH), and red is less favorable (higher LCOH)

From Jordan et al. (2018)

Figure 28 shows an example of common risk map of utilization viability criteria of the Appalachian basin (Jordan et al. 2016). Figure 29 shows a favorability map of the western United States where the probability of amagmatic geothermal systems were determined by a combination of faults, stress field, earthquakes, and heat flow evidence layers (Williams and DeAngelo 2008). Figure 30 shows EGS favorability maps of RGPTs in Brazil by Lacasse et al. (2022).

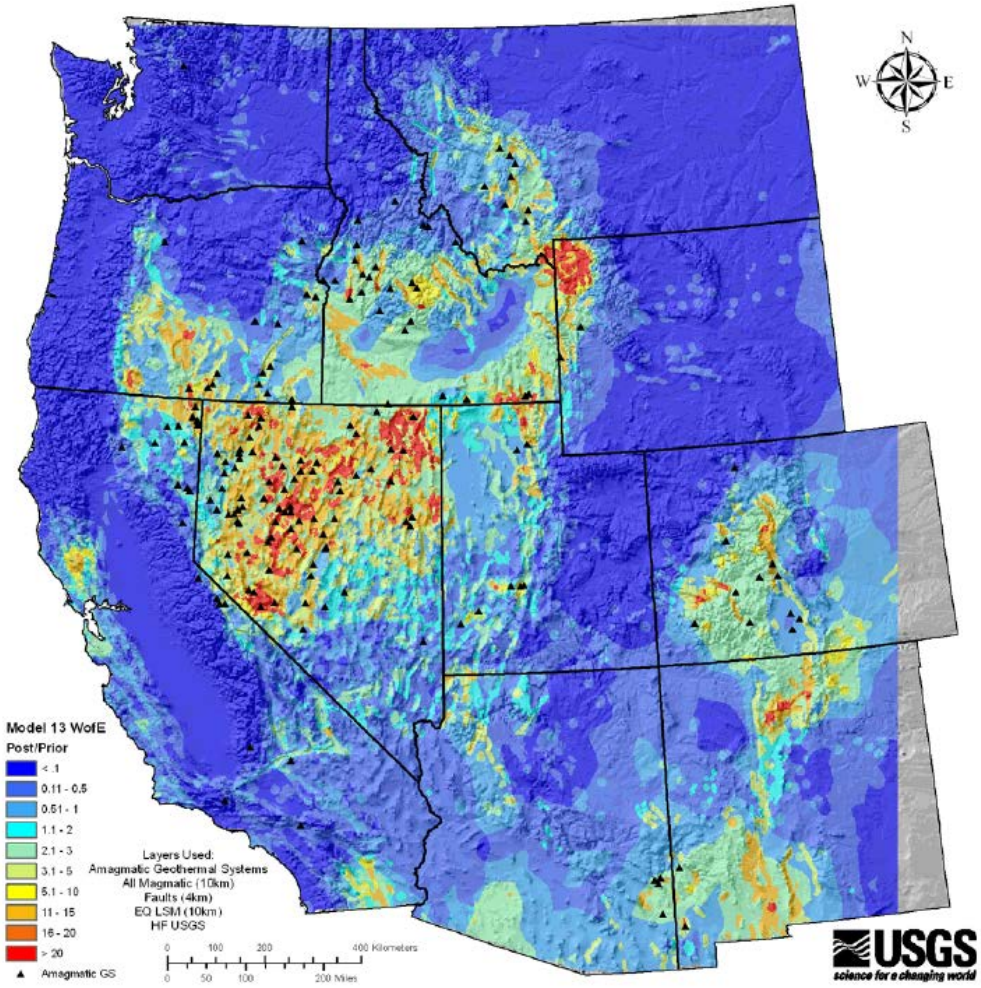

Figure 29. Favorability map of the weights of evidence analysis using a combination of faults, stress, earthquakes, and heat flow evidence layers

From Williams and DeAngelo (2008)

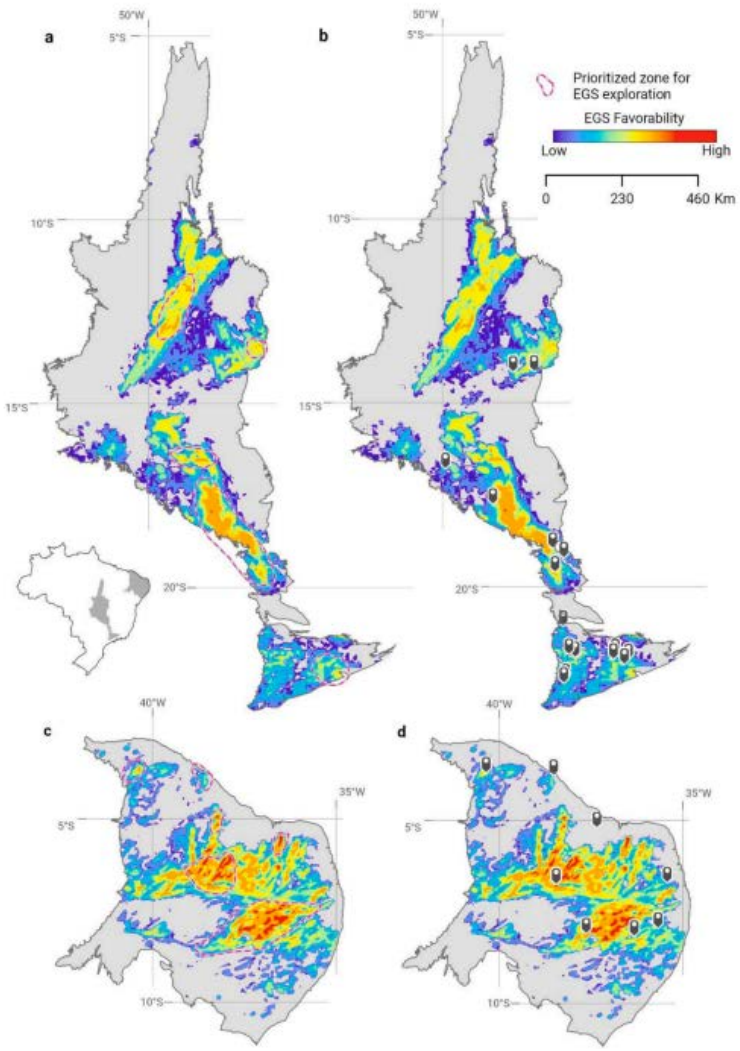

Figure 30. EGS favorability maps in granites with radiogenic high heat production in Brazil

Favorability maps that prioritize zones for further exploration in Tocantins (a-b) and Borborema (c-d).

From Lacasse et al. (2022)

4.4.5 Validation

Data quality and geographical certainty of the existing data points must be addressed to validate the geothermal favorability analysis and identify regions and data gaps where more research and data acquisition will enhance the favorability map (e.g., seismic surveys, magnetotellurics).

PFA methodologies are generally used to identify prospective areas for geothermal development, but the limited subsurface data means that methodologies must address the uncertainty and risk related to data sparsity and/or quality.

PFA favorability maps cannot and should not be used for targeting geothermal wells. Rather, they should be used to identify prospective areas that would warrant more detailed investigations, such as geophysical surveys and/or less costly subsurface investigations such as temperature gradient boreholes shallow temperature probes, or slimholes (designed to gather

important subsurface data and temperature gradient prior to production well targeting (Pauling et al. 2023; in preparation).

4.4.6 Estimating Power and Heat Potential

The power and heat potential of geothermal reservoirs can be evaluated in regions of highest favorability using the Geothermal Resource Portfolio Optimization Reporting Technique (GeoRePORT) Resource Size Assessment Tool (RSAT) developed by NREL (Rubin et al. 2022). GeoRePORT is a geothermal resource reporting tool that reports on the quality of a geothermal resource and the status of the development (Rubin et al. 2021). Resource data entered by the user is ingested by the RSAT module of the GeoRePORT tool to produce preliminary estimates of the size of a geothermal project (MWe or MWth).

The RSAT estimates are simplified results based on established methodologies; they cannot be compared to comprehensive resource studies carried out by engineering experts, nor can they serve as a replacement for comprehensive numerical reservoir modeling. RSAT implements three commonly used methods: the volumetric heat-in-place method (Williams et al. 2008), the power density method (often used by geothermal companies; Wilmarth and Stimac 2015), and estimation of the supplied heat from the fluid flow rate (Rafferty 2004).

For the assessment of GPTs, the USGS volumetric method is likely to be more applicable as it estimates a "heat-in-place" potential based off theoretical heat transfer, rather than other methods relying on empirical relationships from known exploited systems. The USGS volumetric is a simple calculation using the volume of rock (reservoir), the heat energy in the rock, and the lifetime of the plant or heat extraction. The reservoir's gross thermal energy Qr is derived from the reservoir volume, temperature, and heat capacity:

$$Q_r = A \cdot h \cdot [p_r \cdot c_r \cdot (1 - \phi) \cdot (T_{res} - T_{ref})] \quad (4)$$

where ϕ is the reservoir porosity (%), pr is the reservoir rock density (kg/m^3), cr is the reservoir rock specific heat capacity (kJ/kg- °C), A is the reservoir area (m^2), h is the reservoir thickness (m), T_{res} is the reservoir temperature, and T_{ref} is the reference temperature.

$$Q_w = A \cdot h \cdot [\rho_w \cdot c_w \cdot \phi \cdot (T_{res} - T_{ref})] \quad (5)$$

where ρ_w is the fluid density (kg/m^3), and c_w is the fluid specific heat capacity at reservoir conditions (kJ/kg-°C).

Both equations generate a value representative of the total heat stores in the rock. The GeoRePORT RSAT tool implements the equation by Pocasangre and Fujimitsu (2018) for assessing the amount of the available resource base that can be converted to power generation (Rubin et al. 2021):

$$P = (Q_T \cdot R_F \cdot C_e) / (PF \cdot t \cdot 3.154 \cdot 10^{10}) \quad (6)$$

where P is the dimension of the power plant in MWe, R_F is the recovery factor of the reservoir, C_e is the conversion efficiency of the plant, PF is the power factor (capacity factor) of the fraction of time a plant can be functional to generate electricity during a year, and t is the lifetime (years) of the plant. $Q_T = Q_r + Q_w$.

The accessible resource base that can be utilize as heat is estimated by the equation modified from Reed (1982):

$$H = (Q_T \cdot RF \cdot E_e) / (LF \cdot t \cdot 3.154 \cdot 10^{10}) \quad (7)$$

where H is the heat resource MWth, RF is the recovery factor of the reservoir, E_e is the heat conversation efficiency when transferring heat from a brine to the last use application, LF is the load factor, and t is the economic existence of the resource (Rubin et al. 2021).

A range of potential resource size outcomes are determined by the GeoRePORT RSAT tool using probability calculations. Monte Carlo analysis is applied to each of the equations. Each parameter in the equation is given some sort of probability distribution, either chosen by the user or used as a default value, to reflect the uncertainty present in many input values (GeoRePORT RSAT calculates a default of 1,000 iterations; Rubin et al. 2021).

Table 7 shows the level of confidence related to the certainty in estimates for the GeoRePORT tool. The RSAT reports the P10, P50, and P90 estimated from each method in the results label (Rubin et al. 2021).

Table 7. Options to Describe Level of Certainty

Certainty	Probabilistic Outcomes	Deterministic Scenarios
Low	P10 is a value of 10% probability that the correct answer will be P10 or above	Unlikely
Mean	P50 is a value of 50% probability that the correct answer will be lie above P50	More likely that not
High	P90 is a value of 90% probability that the correct answer will be lie above P90	Reasonably certain

Conclusions

The U.S. Department of Energy Geothermal Technologies Office is supporting the Geothermal Heating and Cooling Geospatial Datasets and Analysis project, performed by NREL as part of a broader effort to demonstrate the multifaceted value of integrating geothermal power and geothermal heating and cooling/exchange technologies into national decarbonization plans and community energy plans.

This project takes the approach of classifying low-temperature geothermal resources by GPT. We redefined, updated, and characterized three major classes of low-temperature GPTs: SBGPTs, OBGPTs, and RGPTs. Through our identification and better characterization of plays, this project reveals the potential for widespread assessment of low-temperature geothermal energy from SBGPTs, OBGPTs, and RGPTs as a substitute to current heating sources from fossil fuels.

First, this project focused on collecting baseline data sets and identifying gaps based on the geological key controls of each of the geothermal plays. Then, we developed PFA methodologies for evaluating and analyzing the potential for these low-temperature resources building off the PFA approach to de-risking geothermal exploration and characterization. This PFA approach of low-temperature geothermal resources includes: (1) identifying relevant data (e.g., data sets such as BHT from oil and gas wells, heat flow data, Quaternary faults and stress field data, geophysical data); (2) grouping and weighting of relevant data sets into PFA criteria (e.g., geological, risk, and economic criteria); (3) uncertainty quantification; (4) developing favorability or common risk maps for low-temperature geothermal resources to identify potential locations for more focused data collection and exploration; and (5) estimating electric power generation and heating potential at those locations using the GeoRePORT RSAT. The ultimate objective is assessing geothermal resources of low- temperature that could be used for geothermal heating and cooling, combined heat and power, and geothermal direct use.

The general PFA methodologies suggested by this study for low-temperature resources are similar to other PFA methods suggested for high-temperature hydrothermal resources. However, there is an important distinction in this PFA approach, which is focused on low-temperature resources for applications such as geothermal heating and cooling. For that reason, even though the geological criteria remain the most important in the PFA process, it is critical to include the risk and economic criteria, such as population centers and heat demand and consumption, in order to represent important demand-side factors impacting the feasibility of geothermal direct use for heating and cooling, and other applications of low-temperature geothermal resources (such as small-scale combined heat and power plants).

The relevant data selected and PFA methods suggested in this study could be used in the future as a guide to generate favorability maps and update the low-temperature geothermal resources assessment in the United States, including EGS and AGS resources. However, the input layers and different criteria should be selected depending on data availability of the specific study area and the nature of the GPT and resources (e.g., hydrothermal, EGS, and AGS). This project should facilitate future deployment of geothermal direct use for heating and cooling by providing data, tools, and a workflow applicable to low-temperature geothermal resources.

Future work could consist of utilizing relevant data identified in this study and applying the PFA methodologies described in this study to create favorability maps of low-temperature resources of the different GPT in some regions of the United States (e.g., sedimentary basins, orogenic belts, radiogenic granites) and to identify data gaps where more research and data acquisition will enhance future favorability mapping efforts.

References

Allen, P. A., Homewood, P. and Williams, G. D. 1986. Foreland basins: an introduction. In: Foreland Basins. Eds: P. A. Allen and P. Homewood, Special Publication of the International Association of Sedimentologists, 8, 3-12.

Allen, P.A. and Allen, J.R., 2013. Basin analysis: Principles and application to petroleum play assessment. John Wiley & Sons.

Allen, P.A. and Armitage, J.J., 2011. Cratonic basins. Tectonics of sedimentary basins: Recent advances, pp.602-620.

Allis, R., Moore, J.N., Anderson, T., Deo, M., Kirby, S., Roehner, R. and Spencer, T., 2013. Characterizing the power potential of hot stratigraphic reservoirs in the Western US. In Proceedings (pp. 1463-1473).

Anderson, T.C., 2013, August. Geothermal potential of deep sedimentary basins in the United States. In Unconventional resources technology conference (pp. 1969-1978). Society of Exploration Geophysicists, American Association of Petroleum Geologists, Society of Petroleum Engineers.

Arehart, G.B., Chakurian, A.M., Tretbar, D.R., Christensen, J.N., McInnes, B.A. and Donelick, R.A., 2003. Evaluation of radioisotope dating of Carlin-type deposits in the Great Basin, western North America, and implications for deposit genesis. Economic Geology, 98(2), pp.235-248.

Artemieva, I., 2011. Lithosphere: an interdisciplinary approach. Cambridge University Press.

Artemieva, I.M., Thybo, H., Jakobsen, K., Sørensen, N.K. and Nielsen, L.S., 2017. Heat production in granitic rocks: Global analysis based on a new data compilation GRANITE2017. Earth-Science Reviews, 172, pp.1-26.

Augustine, C., 2013. AASG Wells Data for the EGS Test Site Planning and Analysis Task (No. 252). U.S. DOE Geothermal Data Repository (United States); National Renewable Energy Lab.(NREL), Golden, CO (United States).

Augustine, C., 2014. Analysis of sedimentary geothermal systems using an analytical reservoir model. Geothermal Resources Council Transactions, 38, pp.641-647.

Ballentine, C.J., Burgess, R. and Marty, B., 2002. Tracing fluid origin, transport and interaction in the crust. *Reviews in Minerology and Geochemistry*. https://doi.org/10.2138/rmg.2002.47.13.

Banks, J. and Harris, N.B., 2018. Geothermal potential of Foreland Basins: a case study from the Western Canadian Sedimentary Basin. Geothermics, 76, pp.74-92.

Baranwal, V.C., Sharma, S.P., Sengupta, D., Sandilya, M.K., Bhaumi, B.K., Guin, R., and Saha, S.K., 2006. Anewhigh background radiation area in the Geothermal region of Eastern Ghats Mobile Belt (EGMB) of Orissa, India. Radiation Measurements, 41, pp.602-610.

Basile, C. and Brun, J.P., 1999. Transtensional faulting patterns ranging from pull-apart basins to transform continental margins: an experimental investigation. Journal of Structural Geology, 21(1), pp.23-37.

Batir, J.F., Blackwell, D.D. and Richards, M.C., 2016. Heat flow and temperature-depth curves throughout Alaska: finding regions for future geothermal exploration. Journal of Geophysics and Engineering, 13(3), pp.366-378.

Beardsmore, G.R., and Cull, J.P., 2001. Crustal heat flow: a guide to measurement and modelling. Cambridge university press.

Beckers, K., Kolker, A., Pauling, H., McTigue, J., and Kesseli, D., 2021. Evaluating the feasibility of geothermal deep direct-use in the United States. Energy Conversion and Management, Energy, 243(1), p.114335

Beckers, K.F., Lukawski, M.Z., Anderson, B.J., Moore, M.C. and Tester, J.W., 2014. Levelized costs of electricity and direct-use heat from Enhanced Geothermal Systems. Journal of Renewable and Sustainable Energy, 6(1), p.013141.

Beitollahi, M.M., Ghiassi-Nejad, M., Esmaeli, A. and Dunker, R., 2005, July. Radiological studies in the hot spring region of Mahallat, Central Iran. In Health Physics (Vol. 89, No. 1, pp. S3-S3). 530 Walnut St, Philadelphia, PA 19106-3261 USA: Lippincott Williams & Wilkins.

Berry, G.W., Grim, P.J. and Ikelman, J.A., 1980. Thermal springs list for the United States; National Oceanic and Atmospheric Administration Key to Geophysical Records Documentation No. 12. National Geophysical and Solar-Terrestrial Data Center, Boulder, Colorado; Cooperative Institute for Research in Environmental Sciences, University of Colorado/NOAA, Boulder, Colorado.

Bertani, R., 2016. Geothermal power generation in the world 2010–2014 update report. Geothermics, 60, pp.31-43.

Bilgin, O., 2018. The Importance of Geothermal Energy Resources in Turkey. Open Access Library Journal, 5(2), pp.1-8.

Blackwell, D.D., Negraru, P.T. and Richards, M.C., 2006. Assessment of the enhanced geothermal system resource base of the United States. Natural Resources Research, 15, pp.283-308.

Blackwell, D.D., Negraru, P.T. and Richards, M.C., 2007. Assessment of the enhanced geothermal system resource base of the United States. Natural Resources Research, 15, pp.283-308.

Blume, F. and Sheehan, A.F., 2003. Quantifying seismic hazard in the southern Rocky Mountains through GPS measurements of crustal deformation. Engineering Geology in Colorado: Contributions, Trends, and Case Histories.

Boyd, T.L., Sifford, A. and Lund, J.W., 2015, April. The United States of America country update 2015. In World Geothermal Congress (Vol. 3).

Bradley, D.C., 2008. Passive margins through earth history. Earth-Science Reviews, 91(1-4), pp.1-26.

Brennan, S.T., 2014. The US Geological Survey carbon dioxide storage efficiency value methodology: results and observations. Energy Procedia, 63, pp.5123-5129.

Brennan, S.T., Rivera, J.L., Varela, B.A. and Park, A.J., 2021. National assessment of helium resources within known natural gas reservoirs (No. 2021-5085). US Geological Survey. https://doi.org/10.5066/P92QL79J.

Brugger, J., Long, N., McPhail, D.C. and Plimer, I., 2005. An active amagmatic hydrothermal system: the Paralana hot springs, Northern Flinders Ranges, South Australia. Chemical Geology, 222(1-2), pp.35-64.

Burke, K. and Dewey, J.F., 1973. Plume-generated triple junctions: key indicators in applying plate tectonics to old rocks. The Journal of Geology, 81(4), pp.406-433.

Burkov, A., 2019. The hundred-page machine learning book (Vol. 1, p. 32). Quebec City, QC, Canada: Andriy Burkov.

Carranza, E.J.M., 2008. Geochemical anomaly and mineral prospectivity mapping in GIS. Elsevier.

Cathles, L.M., Erendi, A.H.J. and Barrie, T.J.E.G., 1997. How long can a hydrothermal system be sustained by a single intrusive event? Economic Geology, 92(7-8), pp.766-771.

Christiansen, R.L., Foulger, G.R. and Evans, J.R., 2002. Upper-mantle origin of the Yellowstone hotspot. Geological Society of America Bulletin, 114(10), pp.1245-1256.

Coleman Jr, J.L. and Cahan, S.M., 2012. Preliminary catalog of the sedimentary basins of the United States.

Craw, D., Koons, P.O., Zeitler, P.K. and Kidd, W.S.F., 2005. Fluid evolution and thermal structure in the rapidly exhuming gneiss complex of Namche Barwa–Gyala Peri, eastern Himalayan syntaxis. Journal of Metamorphic Geology, 23(9), pp.829-845.

Crowell, A.M., Ochsner, A.T. and Gosnold, W., 2012. Correcting bottom-hole temperatures in the Denver Basin: Colorado and Nebraska. GRC Transactions, 36(GRC1030229).

Davalos Elizondo, E., Kolker, A. and Warren, I., 2023. Low-Temperature Geothermal Geospatial Datasets: An Example from Alaska (No. NREL/CP-5700-85035). National Renewable Energy Lab (NREL), Golden, CO (United States).

DeCelles, P.G., 2004. Late Jurassic to Eocene evolution of the Cordilleran thrust belt and foreland basin system, western USA. American Journal of Science, 304(2), pp.105-168.

DeCelles, P.G., Carrapa, B., Horton, B.K. and Gehrels, G.E., 2011. Cenozoic foreland basin system in the central Andes of northwestern Argentina: Implications for Andean geodynamics and modes of deformation. Tectonics, 30(6).

Diamond, L.W., Wanner, C. and Waber, H.N., 2018. Penetration depth of meteoric water in orogenic geothermal systems. Geology, 46(12), pp.1063-1066.

Dickinson, W.R., 1974. Plate tectonics and sedimentation.

Dixon, T.H., 1991. An introduction to the Global Positioning System and some geological applications. Reviews of Geophysics, 29(2), pp.249-276.

DOE GTO. https://www.energy.gov/eere/geothermal. Accessed May 2023.

Doughty, C., Dobson, P.F., Wall, A., McLing, T. and Weiss, C., 2018. GeoVision analysis supporting task force report: exploration.

Draut, A.E. and Clift, P.D., 2011. Basins in arc-continent collisions. Tectonics of sedimentary basins: Recent advances, pp.347-368.

Durrance, E.M., 1985. Hydrothermal circulation and isostasy, with particular reference to the granites of southwest England. In High heat production (HHP) granites, hydrothermal circulation and ore genesis. Conference (pp. 71-85).

Eakins, G. R., 1977, Investigations of Alaska's uranium potential, Part I, reconnaissance program, west-central Alaska and Copper River basin, GJBX-28C77), US DOE Grand Junction, CO, 58 p.

Ebinger, C. and Scholz, C.A., 2011. Continental rift basins: the East African perspective. Tectonics of sedimentary basins: Recent advances, pp.183-208.

Erickson, D.C., Kyung, I. and Holdmann, G.P., 2005. Geothermal powered absorption chiller for Alaska Ice Hotel. Geothermal Resources Council Transactions, 29, pp.57-59.

Farndale, H. and Law, R., 2022, February. An Update on the United Downs Geothermal Power Project, Cornwall, UK. In Proceedings of the 47th Workshop on Geothermal Reservoir Engineering, Stanford, CA, USA (pp. 7-9).

Faulds, J. and Hinz, N., 2015, April. Favorable tectonic and structural settings of geothermal systems in the Great Basin region, western USA: Proxies for discovering blind geothermal systems. In Proceedings World Geothermal Congress, Melbourne, Australia, 19-25 April 2015 (No. DOE-UNR-06731-02). Nevada Bureau of Mines and Geology, University of Nevada, Reno.

Faulds, J.E., Coolbaugh, M., Blewitt, G. and Henry, C.D., 2004. Why is Nevada in hot water? Structural controls and tectonic model of geothermal systems in the northwestern Great Basin. Geothermal Resources Council Transactions, 28, pp.649-654.

Faulds, J.E., Hinz, N.H., Coolbaugh, M., Ayling, B., Glen, J., Craig, J.W., McConville, E., Siler, D., Queen, J., Witter, J. and Hardwick, C., 2021. Discovering Blind Geothermal Systems in the Great Basin Region: An Integrated Geologic and Geophysical Approach for Establishing Geothermal Play Fairways: All Phases (No. DOE-UNR-06731-01). Univ. of Nevada, Reno, NV (United States); ATLAS Geosciences, Inc., Reno, NV (United States); US Geological Survey, Menlo Park, CA (United States); Hi-Q Geophysical, Inc., Ponca City, OK (United States); Innovate Geothermal Ltd, Vancouver (Canada); Utah Geological Survey, Salt Lake City, UT (United States).

Fehn, U., 1985. Post-magmatic convection related to high heat production in granites of southwest England: a theoretical study. In High heat production (HHP) granites, hydrothermal circulation and ore genesis. Conference (pp. 99-112).

Forson, C., Czajkowski, J.L., Norman, D.K., Swyer, M.W., Cladouhos, T.T. and Davatzes, N., 2016. Summary of phase 1 and plans for phase 2 of the Washington state geothermal play-fairway analysis. Geothermal Resource Council Transactions, 40.

Foulger, G., 1982. Geothermal exploration and reservoir monitoring using earthquakes and the passive seismic method. Geothermics, 11(4), pp.259-268.

Fournier, R.O., 1981. Application of water geochemistry to geothermal exploration and reservoir engineering; Chap. 4. in. Geothermal systems: principles and case histories, pp.109-143.

Fowler, C.M.R. and Nisbet, E.G., 1985. The subsidence of the Williston Basin. Canadian Journal of Earth Sciences, 22(3), pp.408-415.

Fuller, C.W., Willett, S.D. and Brandon, M.T., 2006. Formation of forearc basins and their influence on subduction zone earthquakes. Geology, 34(2), pp.65-68.

Gallardo, J. and Blackwell, D.D., 1999. Thermal structure of the Anadarko Basin. AAPG bulletin, 83(2), pp.333-361.

Garcia-Castellanos, D. and Cloetingh, S.I.E.R.D., 2011. Modeling the interaction between lithospheric and surface processes in foreland basins. Tectonics of Sedimentary Basins: Recent Advances, pp.152-181.

Grasby, S.E. and Hutcheon, I., 2001. Controls on the distribution of thermal springs in the southern Canadian Cordillera. Canadian Journal of Earth Sciences, 38(3), pp.427-440.

Greene, R., Devillers, R., Luther, J.E. and Eddy, B.G., 2011. GIS-based multiple-criteria decision analysis. Geography compass, 5(6), pp.412-432.

Hamza, V.M., Gomes, A.J.L. and Ferreira, L.E.T., 2005. Status report on geothermal energy developments in Brazil. Natural Gas, 14, pp.7-5.

Hartmann, D.J., Beaumont, E.A. and Coalson, E., 2000. Prediction sandstone reservoir system quality and example of petrophysical evaluation. Search and discovery, 40005.

Haxby, W.F., Turcotte, D.L. and Bird, J.M., 1976. Thermal and mechanical evolution of the Michigan Basin. In Developments in Geotectonics (Vol. 12, pp. 57-75). Elsevier.

Heidbach, O., Rajabi, M., Reiter, K., & Ziegler, M. 2016. WSM-World Stress Map Database Release.

Hein, J.R., Zierenberg, R.A., Maynard, J.B. and Hannington, M.D., 2007. Barite-forming environments along a rifted continental margin, Southern California Borderland. Deep Sea Research Part II: Topical Studies in Oceanography, 54(11-13), pp.1327-1349.

Hervey, C., Beardsmore, G., Moeck, I., Ruter, H. and Bauer, S., 2014. Best practices guide for geothermal exploration. (English). Washington, D.C.: World Bank Group. http://documents.worldbank.org/curated/en/190071480069890732/Best-practices-guide-for-geothermal-exploration.

Hoffman, P., 1974. Shallow and deepwater stromatolites in Lower Proterozoic platform–to–basin facies change, Great Slave Lake, Canada. AAPG Bulletin, 58(5), pp.856-867.

Ingersoll, R.V., 1988. Tectonics of sedimentary basins. Geological Society of America Bulletin, 100(11), pp.1704-1719.

Ingersoll, R.V., 2011. Tectonics of sedimentary basins, with revised nomenclature. Tectonics of sedimentary basins: Recent advances, pp.1-43.

Isaaks, E.H. and Srivastava, R.M., 1989. Applied geostatistics. (No Title).

Jayko, A.S. and Bursik, M., 2011. Active transtensional intracontinental basins: Walker Lane in the western Great Basin. Tectonics of sedimentary basins: Recent advances, pp.226-248.

Johnston, Henry, Amanda Kolker, Greg Rhodes, and Nicole Taverna. 2020. Sedimentary Geothermal Resources in Nevada, Utah, Colorado, and Texas. Golden, CO: National Renewable Energy Laboratory. NREL/TP-5500-76513. https://www.nrel.gov/docs/fy20osti/76513.pdf.

Jordan, T.E., Richards, M.C., Horowitz, F.G., Camp, E., Smith, J.D., Whealton, C.A., Stedinger, J.R., Hornbach, M.J., Frone, Z.S., Tester, J.W. and Anderson, B., 2016. Low Temperature geothermal play fairway analysis for the Appalachian basin: phase 1 revised report November 18, 2016 (No. DE-EE0006726). Cornell Univ., Ithaca, NY (United States).

Kennedy, B.M. and Truesdell, A.H., 1996. The Northwest Geysers high-temperature reservoir: Evidence for active magmatic degassing and implications for the origin of the Geysers geothermal field. Geothermics, 25(3), pp.365-387.

Kennedy, B.M. and Van Soest, M.C., 2007. Flow of mantle fluids through the ductile lower crust: helium isotope trends. Science, 318(5855), pp.1433-1436.

Klingelhoefer, F., Evain, M., Afilhado, A., Rigoti, C., Loureiro, A., Alves, D., Leprêtre, A., Moulin, M., Schnurle, P., Benabdellouahed, M. and Baltzer, A., 2014. Imaging proto-oceanic crust off the Brazilian Continental Margin. Geophysical Journal International, 200(1), pp.471-488.

Kolker, A.M., 2008. Geologic setting of the Central Alaskan Hot Springs Belt: Implications for geothermal resource capacity and sustainable energy production. University of Alaska Fairbanks.

Lacasse, C.M., Prado, E.M.G., Guimarães, S.N.P., de Souza Filho, O.A. and Vieira, F.P., 2022. Integrated assessment and prospectivity mapping of geothermal resources for EGS in Brazil. Geothermics, 100, p.102321.

Lautze, N., Thomas, D., Hinz, N., Apuzen-Ito, G., Frazer, N. and Waller, D., 2017. Play fairway analysis of geothermal resources across the State of Hawaii: 1. Geological, geophysical, and geochemical datasets. Geothermics, 70, pp.376-392.

Lee, T.C. and Henyey, T.L., 1975. Heat flow through the southern California borderland. Journal of Geophysical Research, 80(26), pp.3733-3743.

Legg, M.R., 1991. Developments in understanding the tectonic evolution of the California Continental Borderland.

Liao, Z. and Zhao, P., 1999. Yunnan-Tibet geothermal belt-geothermal resources and case histories. Science, Beijing (in Chinese with English abstract).

Liu, X., Yang, Z., Gluesenkamp, K.R. and Momen, A.M., 2015, December. A technical and economic analysis of an innovative two-step absorption system for utilizing low-temperature geothermal resources to condition commercial buildings. In 41st Workshop on Geothermal Reservoir Engineering.

Lu, X., Zhao, Y., Zhu, J. and Zhang, W., 2018. Optimization and applicability of compound power cycles for enhanced geothermal systems. Applied energy, 229, pp.128-141.

Lund, J.W., 2006. Chena hot springs. Geo-Heat Center Quarterly Bulletin, 27(3), pp.2-4.

Machette, M.N., Haller, K.M., Dart, R.L. and Rhea, S.B., 2003. Quaternary fold and fault database of the United States. United States Geological Survey Open-File Report, https://www.usgs.gov/programs/earthquake-hazards/faults?qtscience_support_page_related_con=4#qt-science_support_page_related_con.

Malczewski, J., 2000. On the use of weighted linear combination method in GIS: common and best practice approaches. Transactions in GIS, 4(1), pp.5-22.

Marjaniemi, D.K. and Basler, A.L., 1972. Geochemical investigations of plutonic rocks in the western United States for the purpose of determining favorability for vein-type uranium deposits (No. GJO-912-16). Pitkin (Lucius), Inc., Grand Junction, Colo.(USA). Western Uranium Project.

McKenzie, D., 1978. Some remarks on the development of sedimentary basins. Earth and Planetary science letters, 40(1), pp.25-32.

McLaren, S. and Powell, R., 2014. Magmatism, orogeny and the origin of high-heat-producing granites in Australian Proterozoic terranes. Journal of the Geological Society, 171(2), pp.149-152.

McLaren, S. Sandiford, M., Powell, R., Neumann, N. and Woodhead, J., 2006. Palaeozoic intraplate crustal anatexis in the Mount Painter Province, South Australia: timing, thermal budgets and the role of crustal heat production. Journal of Petrology, 47(12), pp.2281-2302.

Meissner, R. and Mooney, W., 1998. Weakness of the lower continental crust: a condition for delamination, uplift, and escape. Tectonophysics, 296(1-2), pp.47-60.

Middleton, M.F., 1989. A model for the formation of intracratonic sag basins. Geophysical Journal International, 99(3), pp.665-676.

Miller, T.P. and Barnes, I., 1976. Potential for Geothermal-Energy Development in Alaska--Summary: Geothermal Energy.

Miller, T.P. and Bunker, C.M., 1976. Southeastern Seward Peninsula, Alaska. Journal of Research of the US Geological Survey, 4(3), pp.367-377.

Miller, T.P., Barnes, I. and Patton Jr, W.W., 1975. Geologic setting and chemical characteristics of hot springs in west-central Alaska. J. Res. US Geol. Surv, 3(2), pp.149-162.

Moeck, I.S., 2014. Catalog of geothermal play types based on geologic controls. Renewable and Sustainable Energy Reviews, 37, pp.867-882.

Mordensky, S.P., Lipor, J.J., Deangelo, J., Burns, E.R. and Lindsey, C.R., 2022, February. Predicting Geothermal Favorability in the Western United States by Using Machine Learning: Addressing Challenges and Developing Solutions. In Proceedings: Forty Seventh Workshop on Geothermal Reservoir Engineering.

Motyka, R.J., Moorman, M.A., and Liss, S.A. 1983. Geothermal resources of Alaska: Alaska Division of Geological & Geophysical Surveys Miscellaneous Publication, 8, 1 sheet, scale 1:2,500,000. https://doi.org/10.14509/671.

Muffler, L.J., 1979. Assessment of geothermal resources of the United States, 1978 (No. USGS-CIRC-790). Geological Survey, Reston, VA (USA). Geologic Div.

Mullane, M., Gleason, M., McCabe, K., Mooney, M., Reber, T. and Young, K.R., 2016. An estimate of shallow, low-temperature geothermal resources of the United States (No. NREL/CP-6A20-66461). National Renewable Energy Lab.(NREL), Golden, CO (United States).

Nelson, P.H. and Kibler, J.E., 2003. A catalog of porosity and permeability from core plugs in siliciclastic rocks (pp. 03-420). US Department of the Interior, US Geological Survey.

Nicholson, K. 1993. Geothermal systems. Geothermal Fluids: Chemistry and Exploration Techniques, pp.1-18.

Nimz, G., Janik, C., Goff, F., Dunlap, C., Huebner, M., Counce, D. and Johnson, S.D., 1999. Regional hydrology of the Dixie Valley geothermal field, Nevada: preliminary interpretations of chemical and isotopic data. Lawrence Livermore National Laboratory, Tech Inf Dep Digital Library; 1999. [cited 2012 Dec] [11 p]. Available from: http://www.llnl.gov./tid/Library.html.

Oh, H. and Beckers, K., 2023. Geospatial Characterization of Low-Temperature Heating and Cooling Demand in the United States (No. NREL/CP-5700-84708). National Renewable Energy Lab.(NREL), Golden, CO (United States).

Oxburgh, E.R. and O'Nions, R.K., 1987. Helium loss, tectonics, and the terrestrial heat budget. Science, 237(4822), pp.1583-1588.

Oyepeju, A.O., 2013. Origin of Rifted Cratonic Basins: Testing the Slow Stretching Model (Doctoral dissertation).

Palmer-Wilson, K., Banks, J., Walsh, W. and Robertson, B., 2018. Sedimentary basin geothermal favourability mapping and power generation assessments. Renewable Energy, 127, pp.1087-1100.

Pauling, H., Taverna, N., Trainor-Guitton, W., Witter, E., Kolker, A., Warren, I., Robins, J., and Rhodes, G. 2023 (In preparation). Geothermal PFA Best Practice: A Review of DOE PFA Projects. National Renewable Energy Lab (NREL), Golden, CO (United States).

Pleitavino, M., Carro Pérez, M.E., García Aráoz, E. and Cioccale, M.A., 2021. Radiogenic heat production in granitoids from the Sierras de Córdoba, Argentina. Geothermal Energy, 9(1), p.16.

Pocasangre, C. and Fujimitsu, Y., 2018. A Python-based stochastic library for assessing geothermal power potential using the volumetric method in a liquid-dominated reservoir. Geothermics, 76, pp.164-176.

Pollack, H.N. and Chapman, D.S., 1977. On the regional variation of heat flow, geotherms, and lithospheric thickness. Tectonophysics, 38(3-4), pp.279-296.

Poreda, R.J., Cerling, T.E. and Salomon, D.K., 1988. Tritium and helium isotopes as hydrologic tracers in a shallow unconfined aquifer. Journal of hydrology, 103(1-2), pp.1-9.

Porro, C., Esposito, A., Augustine, C. and Roberts, B., 2012. An estimate of the geothermal energy resource in the major sedimentary basins in the United States. Geothermal Resources Council Transactions, 36, pp.1359-1369.

Rafferty, K.D., 2004. Water chemistry issues in geothermal heat pump systems. ASHRAE Transactions, 110, p.550.

Reed, M.J., 1982. Assessment of low-temperature geothermal resources of the United States-1982 (No. USGS-CIRC-892). Geological Survey, Menlo Park, CA (USA).

Robins, J.C., Kolker, A., Flores-Espino, F., Pettitt, W., Schmidt, B., Beckers, K., Pauling, H. and Anderson, B., 2021. 2021 US Geothermal Power Production and District Heating Market Report (No. NREL/TP-5700-78291). National Renewable Energy Lab.(NREL), Golden, CO (United States).

Rosendahl, B.R., 1987. Architecture of continental rifts with special reference to East Africa. Annual Review of Earth and Planetary Sciences, 15(1), pp.445-503.

Rubin, R., Kolker, A., Witter, E. and Levine, A., 2022. GeoRePORT Protocol Volume VI: Resource Size Assessment Tool (No. NREL/TP-5700-81820). National Renewable Energy Lab.(NREL), Golden, CO (United States).

Rubin, R., Vraa, H., Badgett, A., Kolker, A., Wilmarth, M. and Young, K., 2021. Introducing the GeoRePORT Resource Size Tool: Reporting on Geothermal Resource Size Estimations Using the Geothermal Resource Portfolio Optimization and Reporting Technique (GeoRePORT) (No. NREL/CP-5500-75267). National Renewable Energy Lab.(NREL), Golden, CO (United States).

Rybach, L. and Muffler, L.J.P., 1981. Geothermal systems: principles and case histories. Chichester.

Rybach, L., 1981. Geothermal systems, conductive heat flow, geothermal anomalies. Geothermal Systems: Principles and case histories, pp.3-36.

Saintot, A., Stephenson, R.A., Stovba, S., Brunet, M.F., Yegorova, T. and Starostenko, V., 2006. The evolution of the southern margin of Eastern Europe (Eastern European and Scythian platforms) from the latest Precambrian-Early Palaeozoic to the Early Cretaceous. Geological Society, London, Memoirs, 32(1), pp.481-505.

Schindler, C.S., 2010. 3D fault geometry and basin evolution in the northern Continental Borderland offshore Southern California. unpublished MS thesis, California State Univ., Bakersfield.

Schweitzer, P.N., 2011. Combined geologic map data for the conterminous US derived from the USGS state geologic map compilation.: U.S. Geological Survey, available at https://mrdata.usgs.gov/geology/state/geol_poly.zip.

Sdrolias, M. and Müller, R.D., 2006. Controls on back-arc basin formation. Geochemistry, Geophysics, Geosystems, 7(4).

Sengör, A.C. and Burke, K., 1978. Relative timing of rifting and volcanism on Earth and its tectonic implications. Geophysical Research Letters, 5(6), pp.419-421.

Siler, D.L., Hinz, N.H. and Faulds, J.E., 2018. Stress concentrations at structural discontinuities in active fault zones in the western United States: Implications for permeability and fluid flow in geothermal fields. Bulletin, 130(7-8), pp.1273-1288.

Simiyu, S.M., 2009. Application of micro-seismic methods to geothermal exploration: Examples from the Kenya Rift. Proceedings of the Short Course VIII on Exploration for Geothermal Resources, Lake Naivasha, Kenya, 31.

Sorey, M.L., Kennedy, B.M., Evans, W.C., Farrar, C.D. and Suemnicht, G.A., 1993. Helium isotope and gas discharge variations associated with crustal unrest in Long Valley Caldera, California, 1989–1992. Journal of Geophysical Research: Solid Earth, 98(B9), pp.15871-15889.

Stone, M. and Exley, C.S., 1985. High Heat Production (HHP) Granites, Hydrothermal Circulation and Ore Genesis.

Taylor, S.R. and McLennan, S.M., 1986. The chemical composition of the Archaean crust. Geological Society, London, Special Publications, 24(1), pp.173-178.

Thompson, J.F. and Newberry, R.J., 2000. Gold deposits related to reduced granitic intrusions.

Tóth, J., 2009. Gravitational systems of groundwater flow: theory, evaluation, utilization. Cambridge University Press.

Trainor-Guitton, W., Jreij, S., Guitton, A. and Simmons, J., 2018, October. Fault classification from 3D imaging of vertical DAS profile. In 2018 SEG International Exposition and Annual Meeting. OnePetro.

Trainor-Guitton, W., Siler, D. and Ayling, B., (under review) Temperature Uncertainty Modeling with Proxy Structural Data as Geostatistical Constraints for Well Siting: An Example Applied to Granite Springs Valley, NV, USA.

Truesdell, A.H., 1984. Chemical geothermometors for geothermal exploration. Fluid-mineral equilibria in hydrothermal systems. Reviews in Econ. Geol., 1, pp.31-43.

Turner, D.L., Swanson, S.E. and Wescott, E., 1981. Continental rifting: a new tectonic model for geothermal exploration of the Central Seward Peninsula, Alaska. Trans.-Geotherm. Resour. Counc.;(United States), 5(CONF-811015-).

Vogt, W.C., Shen, H., Wang, G. and Rylander, C.G., 2010. Parametric study of tissue optical clearing by localized mechanical compression using combined finite element and Monte Carlo simulation. Journal of innovative optical health sciences, 3(03), pp.203-211.

Wang, B., Klemeš, J.J., Varbanov, P.S., Shahzad, K. and Kabli, M.R., 2021. Total Site Heat Integration benefiting from geothermal energy for heating and cooling implementations. Journal of Environmental Management, 290, p.112596.

Wang, C., Wu, J., Lou, H., Zhou, M. and Bai, Z., 2003. P-wave crustal velocity structure in western Sichuan and eastern Tibetan region. Science in China Series D: Earth Sciences, 46, pp.254-265.

Welhan, J.A., 1988. Origins of methane in hydrothermal systems. Chemical Geology, 71(1-3), pp.183-198.

Wellmann, J.F., Lindsay, M., Poh, J. and Jessell, M., 2014. Validating 3-D structural models with geological knowledge for improved uncertainty evaluations. Energy Procedia, 59, pp.374-381.

Williams, C.F. and DeAngelo, J., 2008. Mapping geothermal potential in the western United States. Geothermal Resources Council Transactions, 32, p.181.

Williams, C.F. and DeAngelo, J., 2011. Evaluation of approaches and associated uncertainties in the estimation of temperatures in the upper crust of the Western United States. GRC Transactions, 35, pp.1599-1605.

Williams, C.F., Reed, M. and Mariner, R.H., 2008. A Review of Methods Applied by the US Geological Survey in the Assessment If Identified Geothermal Resources (p. 27). US Department of Interior, US Geological Survey.

Wilmarth, M. and Stimac, J., 2015. Power density in geothermal fields. Power, 19, p.25.

Witter, J.B., Trainor-Guitton, W.J. and Siler, D.L., 2019. Uncertainty and risk evaluation during the exploration stage of geothermal development: A review. Geothermics, 78, pp.233-242.

Wolfgramm, M., Obst, K., Beichel, K., Brandes, J., Koch, R., Rauppach, K. and Thorwart, K., 2009. Produktivitätsprognosen geothermischer aquifere in Deutschland. Der Geothermiekongress, pp.17-19.

Yang, W.C., Jin, S., Zhang, L.L., et al., 2020. The three-dimensional resistivity structures of the lithosphere beneath the Qinghai-Tibet Plateau. Chin. J. Geophys. 63 (3), 817–827 (in Chinese with English abstract).

Yi, L., Qi, J., Li, X., Xu, M., Zhang, X., Zhang, Q. and Tang, Y., 2021. Geochemical characteristics and genesis of the high-temperature geothermal systems in the north section of the Sanjiang Orogenic belt in southeast Tibetan Plateau. Journal of Volcanology and Geothermal Research, 414, p.107244.

Yuan, H. and Romanowicz, B., 2010. Lithospheric layering in the North American craton. Nature, 466(7310), pp.1063-1068.

Zhang, C., Hu, S., Zhang, S., Li, S., Zhang, L., Kong, Y., Zuo, Y., Song, R., Jiang, G. and Wang, Z., 2020. Radiogenic heat production variations in the Gonghe basin, northeastern Tibetan Plateau: Implications for the origin of high-temperature geothermal resources. Renewable Energy, 148, pp.284-297.

Zhang, X.Z., Wang, Q., Wyman, D., Kerr, A.C., Dan, W. and Qi, Y., 2022. Tibetan Plateau insights into> 1100° C crustal melting in the Quaternary. Geology, 50(12), pp.1432-1437.

Zhou, Z.M., Ma, C.Q., Qi, S.H., Xi, Y.F. and Liu, W., 2020. Late Mesozoic high-heat-producing (HHP) and high-temperature geothermal reservoir granitoids: The most significant geothermal mechanism in South China. Lithos, 366, p.105568.

Zimmermann, G., Reinicke, A., Blöcher, G., Milsch, H., Gehrke, D., Holl, H.G., Moeck, I., Brandt, W., Saadat, A. and Huenges, E., 2007, January. Well path design and stimulation treatments at the geothermal research well GtGrSk4/05 in Groß Schönebeck. In Proceedings Thirty-Second Workshop on Geothermal Reservoir Engineering (pp. 22-24). Stanford University Stanford, California.

Zody, Z.J. and Gisladottir, V.R., 2023. Shallow geothermal technology, opportunities in cold regions, and related data for deployment at Fort Wainwright.